Separation and Purification Technology 76 (2011) 325–330

Contents lists available at ScienceDirect

Separation and Purification Technology

journal homepage: www.elsevier.com/locate/seppur

Entropy-based separation of linear chain molecules by exploiting differences in the saturation capacities in cage-type zeolites

Rajamani Krishna[a,b,*], Jasper M. van Baten[a]

[a] Van 't Hoff Institute for Molecular Sciences, University of Amsterdam, Science Park 904, 1098 XH Amsterdam, The Netherlands
[b] Department of Chemical & Biomolecular Engineering, University of California, Berkeley, Berkeley, CA 94720, USA

ARTICLE INFO

Article history:
Received 31 August 2010
Received in revised form 26 October 2010
Accepted 27 October 2010

Keywords:
Linear alcohols
Linear alcohols
Adsorption selectivity reversal
Cage-type zeolites
Saturation capacity

ABSTRACT

For zeolites such as CHA, LTA, DDR, ERI, AFX, and TSC that consist of cages separated by narrow windows, the saturation capacities expressed as molecules per cage, $\Theta_{i,sat}$, of linear alcohols and alkanes have integer values in a certain range of C numbers. In this range, the $\Theta_{i,sat}$ decreases in a step-wise manner with increasing chain length. Using Configurational-Bias Monte Carlo simulations, we demonstrate the potential of separation of binary mixtures of linear chain molecules that exploits the differences in the $\Theta_{i,sat}$. This separation principle can lead to an almost total exclusion of the longer molecule in preference to the shorter one, as cage saturation conditions are approached.

1. Introduction

Adsorption of guest molecules within ordered crystalline materials such as zeolites (crystalline aluminosilicates), metal–organic frameworks (MOFs), and zeolitic imidazolate frameworks (ZIFs) opens up the possibility of separations that are entropy-based. Many recent publications have shown that mixtures of alkane isomers can be separated by exploiting differences in the packing efficiency of molecules within zeolites and MOFs [1–10]. For example, within the *intersecting channel* structure of MFI zeolite, linear alkanes can be packed more efficiently and at high loadings branched isomers can be virtually excluded from the zeolite [1]. In *one-dimensional channel* structures of AFI, and MOR zeolites, the branched alkanes have a higher packing efficiency due to their smaller "footprint" and the linear alkanes can be excluded at high loadings [11,12]. Within the box-like channels of MIL-47, the differences in the packing efficiencies of xylene isomers can be exploited to achieve separation [13].

The focus in this paper is on separation of mixtures of linear chain molecules such as alkanes or alcohols; such separations are important in several contexts in the petroleum and petrochemical industries. For adsorption in cage-type zeolites, or its ZIF analogs, the number of molecules that can be accommodated within a single cage is limited. The principle of separation is best understood by examination of the data presented in Fig. 1 on the saturation capacities for adsorption of linear alkanes in all-silica zeolites CHA, ERI, AFX, and LTA-Si, that have cage volumes of 316, 409, 490, and 743 Å^3, respectively. We note that for the range of C numbers considered the saturation loading, $\Theta_{i,sat}$, decreases in a step-wise manner with increasing chain length. Configurational-Bias Monte Carlo (CBMC) simulations have been recently used to demonstrate the possibility of separating mixtures of linear alkanes, with 3–6 C atoms, by exploiting *differences* in the saturation capacities within the cages of CHA, AFX, and ERI zeolites [14]. This is an entropy-based separation that favors the shorter molecule in the mixture because of a higher efficiency of packing within the cages of the zeolites.

The primary objective of the present communication is to demonstrate the application of the same entropy-based principle to the separation of linear *alcohols* in the 1–6 C atom range using CHA zeolite. We aim to show that experimental data of Daems et al. [15] on ethanol–*n*-hexanol separation using CHA zeolite has a wider application potential.

The second objective is to extend the separation principle to longer linear chain molecules by appropriate, larger, choice of the cage size using say LTA or TSC zeolites.

The CBMC simulation methodology used in the present work, along with specification of force fields, structural information (unit cell sizes, pore volumes, cage volumes), and snapshots showing the location of equilibrated molecules is provided in Supplementary data accompanying this publication.

* Corresponding author at: Van 't Hoff Institute for Molecular Sciences, University of Amsterdam, Science Park 904, 1098 XH Amsterdam, The Netherlands.
Tel.: +31 20 6270990; fax: +31 20 5255604.
E-mail address: r.krishna@uva.nl (R. Krishna).

1383-5866/$ – see front matter © 2010 Elsevier B.V. All rights reserved.
doi:10.1016/j.seppur.2010.10.023

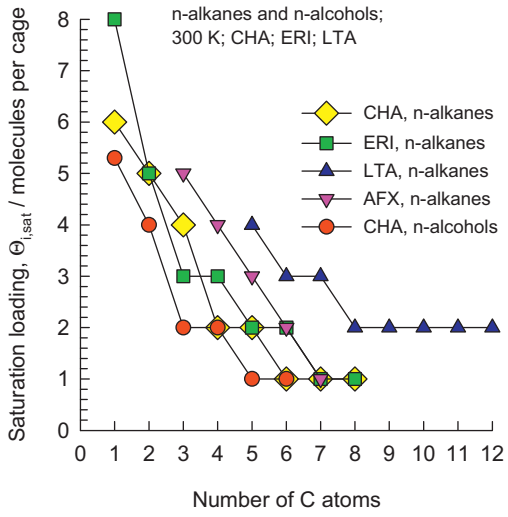

Fig. 1. Saturation capacities for adsorption of *n*-alkanes and *n*-alcohols in CHA, ERI, AFX, and LTA, at 300 K. The data for *n*-alkanes in CHA, ERI, and AFX are from Krishna and van Baten [14]. The data for *n*-alcohols in CHA are from Fig. 2 of this work. The data for *n*-alkanes in LTA are from Fig. 5 of this work.

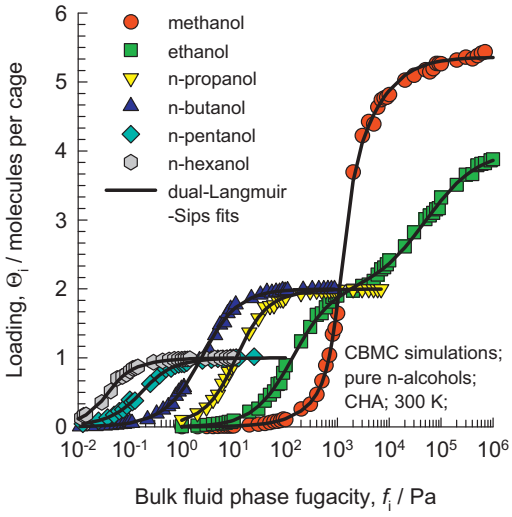

Fig. 2. CBMC simulations of pure component adsorption isotherms for *n*-alcohols in CHA at 300 K.

2. Adsorption of pure *n*-alcohols in CHA zeolite

We first investigate the potential of CHA for separation of *n*-alcohols by performing CBMC simulations of the pure component isotherms for *n*-alcohols in the 1–6 C atom range; see Fig. 2. The continuous solid lines in Fig. 2 are fits using the dual-Langmuir–Sips isotherm [5,16–18] that relates the loadings Θ_i to the bulk fluid phase fugacity f_i:

$$\Theta_i = \Theta_{i,A,sat}\frac{b_{i,A}f_i^{\nu_{i,A}}}{1+b_{i,A}f_i^{\nu_{i,A}}} + \Theta_{i,B,sat}\frac{b_{i,B}f_i^{\nu_{i,B}}}{1+b_{i,B}f_i^{\nu_{i,B}}} \quad (1)$$

All the six constants in Eq. (1) were fitted to match the CBMC simulated isotherms. As can be seen the fitted isotherms represent the CBMC data extremely well over the entire range of fluid phase fugacities. For any molecule the simulations were carried out to sufficiently high fugacities, up to 1 MPa, till the component loadings attained a constant plateau in the loadings indicating that saturation conditions were reached. The saturation capacities, $\Theta_{i,sat}$, decreases from 5.5 molecules per cage for methanol to 1 molecule per cage for *n*-hexanol; see data in Fig. 1. Except for methanol, the cage capacity at saturation has an integer value because no *n*-alcohol or *n*-alkane molecule can locate at the window region. A close examination of the CBMC data show that perhaps the loading for methanol would approach 6 per

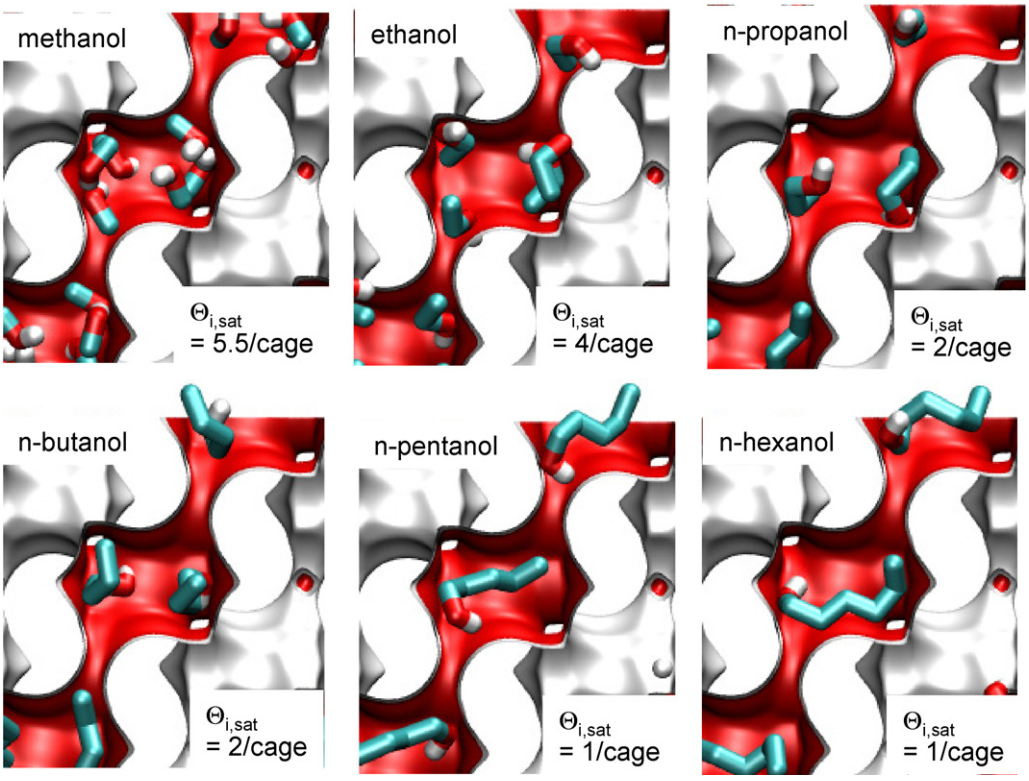

Fig. 3. Comparison of the snapshots showing the conformations of *n*-alcohols in CHA at saturation conditions.

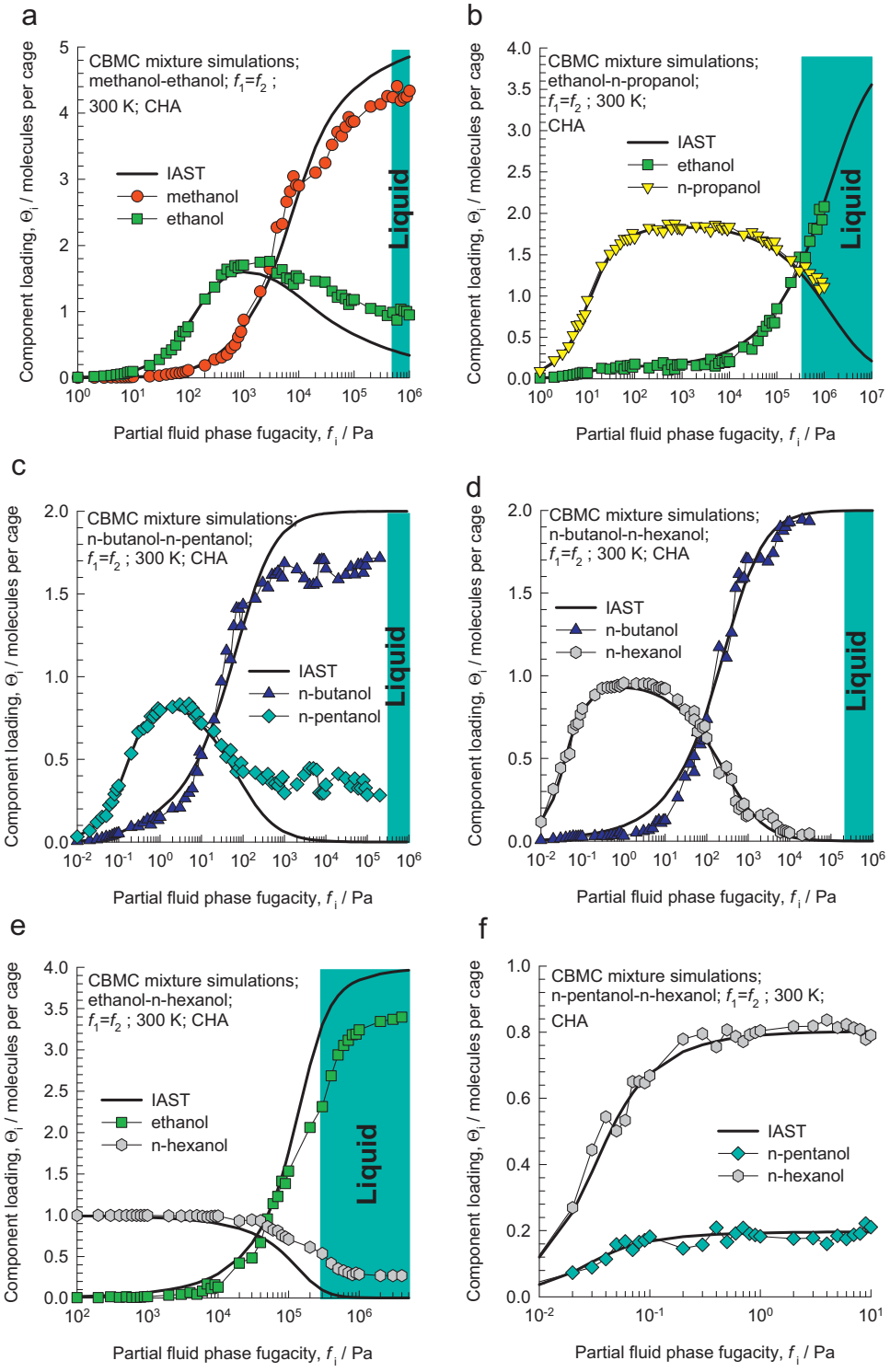

Fig. 4. Comparison of CBMC mixture simulations for (a) methanol–ethanol, (b) ethanol–*n*-propanol, (c) *n*-butanol–*n*-pentanol, (d) *n*-butanol–*n*-hexanol, (e) ethanol–*n*-hexanol, and (f) *n*-pentanol–*n*-hexanol in CHA at 300 K. The partial fugacities in the bulk fluid phase are taken to be equal, i.e. $f_1 = f_2$. The continuous solid lines represent calculations of the IAST [19] using dual-Langmuir–Sips fits of pure component isotherms. The range of liquid phase operation is indicated by the shaded region; the transition between vapor and liquid bulk phase is determined using the Peng–Robinson equation of state.

cage, had the simulations been performed to fugacties exceeding 1 MPa. Fig. 3 presents snapshots of the location, and conformation, of the *n*-alcohols within the cages of CHA at saturation conditions.

3. Adsorption of binary mixtures of *n*-alcohols in CHA

Consider adsorption of a fluid mixture of methanol and ethanol in CHA. The saturation capacities are 5.5 and 4 molecules per cage,

respectively. CBMC simulations on the component loadings in equilibrium with an equimolar methanol–ethanol mixture is shown in Fig. 4a for varying fluid phase partial fugacities, f_i. At $f_i < 5$ kPa, the selectivity is in favor of the component with the longer chain length, ethanol; this is "normal" behavior for mixture adsorption. However, for $f_i > 5$ kPa selectivity reversal occurs and methanol is preferentially adsorbed due to its higher packing efficiency. An analogous selectivity reversal is found for ethanol–*n*-propanol and *n*-butanol–*n*-pentanol mixtures; see Fig. 4b and c.

The shaded regions in Fig. 4 indicate that the bulk fluid phase is in the liquid phase for the range of fugacities, f_i. This region has been estimated using the Peng–Robinson equation of state. The data indicates that selectivity reversal is ensured when adsorption is from the *liquid* phase mixture.

For some mixtures, the entropy based separation principle can lead to total exclusion of the longer molecule in preference to the shorter one, when adsorbing from the liquid phase. To illustrate this Fig. 4d shows CBMC simulations for *n*-butanol ($\Theta_{i,sat} = 2$)–*n*-hexanol ($\Theta_{i,sat} = 1$) mixtures. For bulk fluid phase fugacities $f_i > 50$ kPa, the adsorption selectivity in favor of the shorter alcohol and the longer alcohol is virtually excluded from the cages of CHA. Exclusion is guaranteed when adsorption is from the *liquid* phase mixture, shown as the shaded region in Fig. 4d. It is also interesting to note that the IAST calculations are in almost perfect agreement with the CBMC simulation data over the entire range of fugacities.

Selectivity reversal for ethanol ($\Theta_{i,sat} = 4$)–*n*-hexanol ($\Theta_{i,sat} = 1$) mixtures occurs at slightly higher fugacties $f_i > 100$ kPa; see Fig. 4e. Further increase in f_i progressively favors adsorption of the shorter ethanol molecule and the longer *n*-hexanol is virtually excluded at pressures $f_i \approx 1$ MPa, corresponding to adsorption from the liquid phase. The results presented in Fig. 4e are in broad agreement with Daems et al. [15] who have presented experimental data on ethanol–*n*-hexanol that demonstrate total exclusion of the longer alcohol when the following two conditions are satisfied: (1) the adsorption is from a bulk liquid mixture and (2) the liquid mixture contains more than 80% of the longer molecule. A quantitative agreement is not to be expected because in the experimental work of Daems et al. [15], the CHA that they used had a Si/Al ratio of 2.59; the presence of cations will have a significant effect on the adsorption loadings.

For mixtures of *n*-pentanol ($\Theta_{i,sat} = 1$)–*n*-hexanol ($\Theta_{i,sat} = 1$), there is no difference in the saturation capacities and we should not expect selectivity reversal to occur; the CBMC simulation data presented in Fig. 4f confirms this expectation.

The continuous solid lines in Fig. 4 are the predictions of the Ideal Adsorbed Solution Theory (IAST) of Myers and Prausnitz [19] using pure component isotherm fits using Eq. (1) as input data. The IAST calculations have been presented here to demonstrate that selectivity reversal is not an unexpected phenomenon, but is a natural result that is obtained for a mixture of two species having (1) lower adsorption strength, but higher saturation capacity and (2) higher adsorption strength, but lower saturation capacity. When saturation conditions are approached the component with the higher saturation capacity is invariably preferred. This is due to the fact that vacant "sites" are more easily filled by the smaller molecule at near-saturation conditions. Though the predictions of the IAST are in general qualitative agreement with CBMC simulations, the agreement is not quantitatively good in all case. The reason for this is that the IAST assumes a homogeneous adsorbed phase composition throughout the zeolite, which is not realized in practice. The failure of the IAST due to segregated mixture adsorption has been stressed in the literature for adsorption in MFI, MOR, and cage-type zeolites [14,20–22].

A further point to note is that the data in Fig. 4 are analogous to that for binary mixtures of *n*-alkanes in CHA; the phenomenon

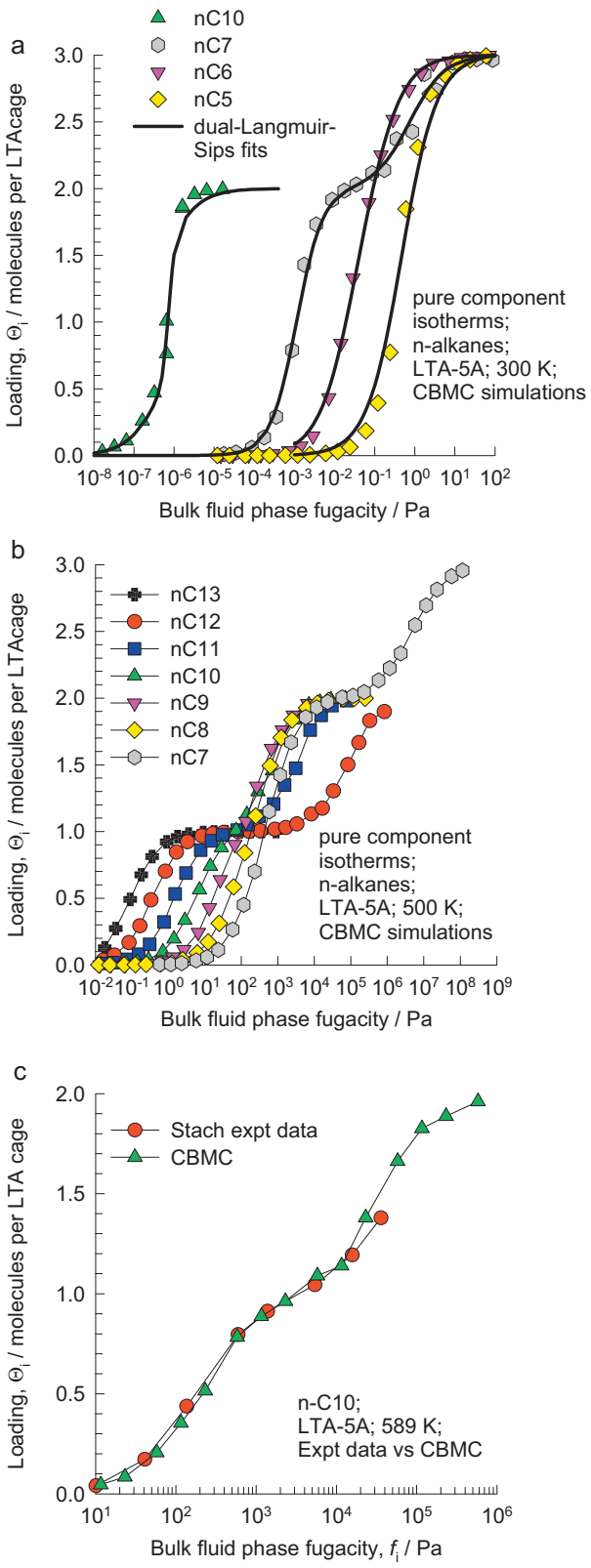

Fig. 5. (a–c) CBMC simulations of pure component adsorption isotherms for *n*-alkanes in LTA-5A at (a) 300 K, (b) 500 K, and 589 K. Also shown in (c) are the experimental data of Stach and Fiedler [24].

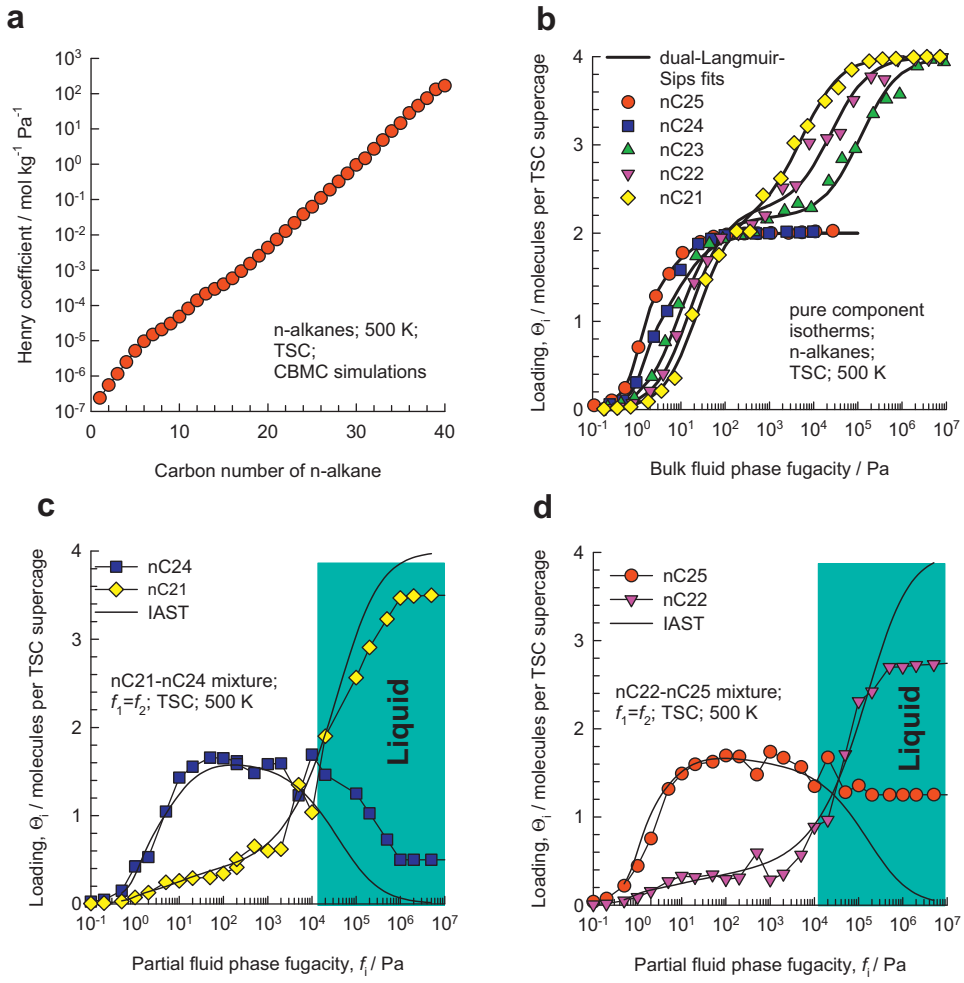

Fig. 6. (a) CBMC simulations of Henry coefficients for *n*-alkanes in TSC at 500 K, (b) CBMC simulations of pure component adsorption isotherms for *n*-alkanes in TSC at 500 K. Then continuous solids lines are the dual-Langmuir–Sips fits of the isotherms, (c and d) CBMC simulations of (c) nC21–nC24, and (d) nC22–nC25 alkane mixtures in TSC at 500 K. The partial fugacities in the bulk fluid phase, $f_1 = f_2$. The continuous solid lines represent calculations of the IAST [19] using dual-Langmuir–Sips fits of pure component isotherms. The range of liquid phase operation is indicated by the shaded region; the transition between vapor and liquid bulk phase is determined using the Peng–Robinson equation of state.

of selectivity reversal and exclusion of the longer molecule is valid for both linear alkanes and alcohols.

4. Extension of entropy concept to higher chain lengths

The same concept can be applied to mixtures of linear alkanes, and linear alcohols, with chain length considerably larger than 6, as considered above. For this purpose, we need to choose a zeolite with the appropriate, higher, capacity. Daems et al. [23] have investigated in quite considerable detail the potential of LTA-5A, whose cages are larger in size than for CHA, for separation of *n*-alkanes in the 5–24 C atom range. To demonstrate the separation potential, let us consider the pure component adsorption isotherms for *n*-alkanes with C numbers in the 5–13 range in LTA-5A; see Fig. 5a–c. The first point to note is that the saturation capacities for a given molecule is the same at 300 K and at 500 K; the saturation capacities are shown in Fig. 1. In Fig. 5c, the experimental data of Stach and Fiedler [24] are compared with the CBMC simulations of nC10 isotherm at 589 K. The agreement is found to be very good. In particular, it is to be noted that the inflection in the isotherm at a loading of $\Theta_i = 1$ per cage is well reproduced by the CBMC simulations. On the basis of this information, it appears feasible that for adsorption of binary mixtures of nC7 and nC10, nC11, or nC12 alkanes, the shorter molecule will be favored near saturation conditions. The experimental data of Sundstrom and Krautz [25], confirms this expectation.

In the event a linear molecule cannot locate comfortably within a cage, the fingerprint of this would be found in a maximum value of the Henry coefficient for the C number, beyond which the Henry coefficient would decrease [26]. For LTA-5A, *n*-alkanes considerably longer than 25 C atoms cannot fit into one cage. Therefore, if it is required to separate longer linear alkanes, as is often required in the petroleum industry in lube oil processing, we must choose zeolites with considerably larger cage capacity. The all-silica TSC zeolite, with a Tschörtnerite framework, has the largest cage volume of any known zeolite [27]. Each unit cell of TSC has four "LTA type cages" of 743 Å^3, and four "TSC supercages" of 2553 Å^3. One indication of the length of the longest chain molecule that can be accommodated within a single TSC supercage is to examine the data on the Henry coefficients; see Fig. 6a. The variation of the Henry coefficient versus chain length is monotonous till 40 C atoms. This indicates that nC40 molecules can locate comfortably within a single TSC supercage. Simulations were also carried out to determine the Henry coefficients for linear alkanes with more than 40 C atoms. These data, available in Supplementary data accompanying this publication, show that the Henry coefficient shows a tendency to decrease in value for chain lengths longer than 60.

Fig. 6b presents CBMC simulations of pure component isotherms for *n*-alkanes in the 21–25 C atom range in TSC at 500 K. The loadings are expressed as molecules per TSC supercage, because the LTA-type cages are too small to accommodate these long chain alkanes. Generally speaking, the adsorption separation selectivity for mixtures will be higher when the differences in the saturation capacities on the constituent species is larger. From the data in Fig. 6b it will be clear that it is not possible to separate nC24 and nC25 on the basis of the entropy principle. The data also indicate that it is possible to separate nC24 and nC25 from mixtures with nC21, nC22, and nC23 because the differences in saturation capacities are two molecules per TSC supercage in each case. To demonstrate this separation potential, in which the shorter chain is preferred, we carried out CBMC simulations for nC21–nC24, and nC22–nC25 mixtures. The simulation results are presented in Fig. 6c and d, respectively. For both mixtures, as anticipated, adsorption from a liquid phase will yield adsorbate compositions that are considerably richer in the shorter *n*-alkane. Also shown in Fig. 6c and d are the predictions of the IAST for the component loadings using the pure component isotherm fits. The IAST anticipates the correct trends in the loading, especially the pressures at which selectivity reversal occurs. Generally speaking the IAST predicts a higher separation selectivity than obtained on the basis of molecular simulations. The reason for the deviations of IAST and CBMC simulations is ascribable to the breakdown in the assumption of homogeneous distribution of the components in the mixture in all cages. Due to the long chains involved, some cages will have either one or other component in the mixture.

5. Conclusions

We have used CBMC simulations to show that for adsorption within the cages of CHA zeolite from liquid phase mixtures of methanol–ethanol, ethanol–*n*-propanol, *n*-butanol–*n*-hexanol, and ethanol–*n*-hexanol is in favor of the shorter alcohol. For the last two mixtures there is virtual exclusion of the longer alcohol.

The entropy based principle can be extended to longer chain molecules by choosing appropriate zeolites, such as LTA-5A and TSC that have higher cage capacities.

The experimental data presented by Daems et al. [15] and Denayer et al. [28] for separation of linear alkanes and linear alcohols using CHA provide direct confirmation that the separation principle discussed in this paper can be realized in practice. Cage-type zeolites such as CHA, AFX, and ERI could be applied in purification processes in which traces of smaller linear molecules have to be removed from mixtures with longer chain molecules. Such separations are very difficult to realize by conventional separation techniques such as distillation. Our simulation results for TSC zeolite show that this separation principle can be applied in lube oil refining.

Though the emphasis of this paper has been on *separation*, the differences in the cage capacity of *n*-alkanes have implications in catalytic *conversion* processes as well [29]. Preferentially adsorbing shorter chains over longer ones offers perspectives with respect to selective separation processes and chain length selective cracking reactions [28].

Acknowledgements

This material is based upon work supported as part of the Center for Gas Separations Relevant to Clean Energy Technologies, an Energy Frontier Research Center funded by the U.S. Department of Energy, Office of Science, Office of Basic Energy Sciences under Award Number DE-SC0001015.

Appendix A. Supplementary data

Supplementary data associated with this article can be found, in the online version, at doi:10.1016/j.seppur.2010.10.023.

References

[1] T.J.H. Vlugt, R. Krishna, B. Smit, Molecular simulations of adsorption isotherms for linear and branched alkanes and their mixtures in silicalite, J. Phys. Chem. B 103 (1999) 1102–1118.
[2] R. Krishna, B. Smit, S. Calero, Entropy effects during sorption of alkanes in zeolites, Chem. Soc. Rev. 31 (2002) 185–194.
[3] M. Schenk, S.L. Vidal, T.J.H. Vlugt, B. Smit, R. Krishna, Separation of alkane isomers by exploiting entropy effects during adsorption on silicalite-1: a configurational-bias Monte Carlo simulation study, Langmuir 17 (2001) 1558–1570.
[4] R. Krishna, J.M. van Baten, Screening of zeolite adsorbents for separation of hexane isomers: a molecular simulation study, Sep. Purif. Technol. 55 (2007) 246–255.
[5] R. Krishna, J.M. van Baten, Highlighting a variety of unusual characteristics of adsorption and diffusion in microporous materials induced by clustering of guest molecules, Langmuir 26 (2010) 8450–8463.
[6] J. Jiang, S.I. Sandler, Monte Carlo simulation for the adsorption and separation of linear and branched alkanes in IRMOF-1, Langmuir 22 (2006) 5702–5707.
[7] R. Babarao, Y.H. Tong, J. Jiang, Molecular insight into adsorption and diffusion of alkane isomer mixtures in metal–organic frameworks, J. Phys. Chem. B 113 (2009) 9129–9136.
[8] J. Jiang, Pore size or geometry: which determines the shape and inverse-shape selective adsorption of alkane isomers? J. Phys. Chem. B 110 (2006) 8670–8673.
[9] M. Schenk, S. Calero, T.L.M. Maesen, T.J.H. Vlugt, L.L. van Benthem, M.G. Verbeek, B. Schnell, B. Smit, Shape selectivity through entropy, J. Catal. 214 (2003) 88–99.
[10] B. Smit, T.L.M. Maesen, Molecular simulations of zeolites: adsorption, diffusion, and shape selectivity, Chem. Rev. 108 (2008) 4125–4184.
[11] M. Schenk, B. Smit, T.J.H. Vlugt, T.L.M. Maesen, Shape selectivity in hydrocarbon conversion, Angew. Chem.-Int. Ed. 40 (2001) 736–739.
[12] J.M. van Baten, R. Krishna, Entropy effects in adsorption and diffusion of alkane isomers in mordenite: an investigation using CBMC and MD simulations, Micropor. Mesopor. Mater. 84 (2005) 179–191.
[13] J.M. Castillo, T.J.H. Vlugt, S. Calero, Molecular simulation study on the separation of xylene isomers in MIL-47 metal–organic frameworks, J. Phys. Chem. C 113 (2009) 20869–20874.
[14] R. Krishna, J.M. van Baten, Separating *n*-alkane mixtures by exploiting differences in the adsorption capacity within cages of CHA, AFX and ERI zeolites, Sep. Purif. Technol. 60 (2008) 315–320.
[15] I. Daems, R. Singh, G.V. Baron, J.F.M. Denayer, Length exclusion in the adsorption of chain molecules on chabazite type zeolites, Chem. Commun. (2007) 1316–1318.
[16] C. Chmelik, J. Kärger, M. Wiebcke, J. Caro, J.M. van Baten, R. Krishna, Adsorption and diffusion of alkanes in CuBTC crystals investigated using infrared microscopy and molecular simulations, Micropor. Mesopor. Mater. 117 (2009) 22–32.
[17] R. Krishna, J.M. van Baten, Investigating cluster formation in adsorption of CO_2, CH_4, and Ar in zeolites and metal organic frameworks at sub-critical temperatures, Langmuir 26 (2010) 3981–3992.
[18] R Krishna, J.M. van Baten, Hydrogen bonding effects in adsorption of water–alcohol mixtures in zeolites and the consequences for the characteristics of the Maxwell–Stefan diffusivities, Langmuir 26 (2010) 10854–10867.
[19] A.L. Myers, J.M. Prausnitz, Thermodynamics of mixed gas adsorption, AIChE J. 11 (1965) 121–130.
[20] R. Krishna, D. Paschek, Molecular simulations of adsorption and siting of light alkanes in silicalite-1, Phys. Chem. Chem. Phys. 3 (2001) 453–462.
[21] M. Murthi, R.Q. Snurr, Effects of molecular siting and adsorbent heterogeneity on the ideality of adsorption equilibria, Langmuir 20 (2004) 2489–2497.
[22] R. Krishna, J.M. van Baten, Segregation effects in adsorption of CO_2 containing mixtures and their consequences for separation selectivities in cage-type zeolites, Sep. Purif. Technol. 61 (2008) 414–423.
[23] I. Daems, G.V. Baron, S. Punnathanam, R.Q. Snurr, J.F.M. Denayer, Molecular cage nestling in the liquid-phase adsorption of *n*-alkanes in 5A zeolite, J. Phys. Chem. C 111 (2007) 2191–2197.
[24] H. Stach, K. Fiedler, Vergleich der adsorption von *n*-Dekan an verschiedenen Zeolithen von Faujasittyp, Z. Phys. Chem., Leipzig 261 (1980) 246–257.
[25] D.W. Sundstrom, F.G. Krautz, Equilibrium adsorption of liquid phase normal paraffins on type 5A molecular sieves, J. Chem. Eng. Data 13 (1968) 223–226.
[26] D. Dubbeldam, B. Smit, Computer simulation of incommensurate diffusion in zeolites: understanding window effects, J. Phys. Chem. B 107 (2003) 12138–12152.
[27] M.D. Foster, I. Rivin, M.M.J. Treacy, O.D. Friedrichs, A geometric solution to the largest-free-sphere problem in zeolite frameworks, Micropor. Mesopor. Mater. 90 (2006) 32–38.
[28] J.F.M. Denayer, L.I. Devriese, S. Couck, J.A. Martens, R. Singh, P.A. Webley, G.V. Baron, Cage and window effects in the adsorption of *n*-alkanes on chabazite and SAPO-34, J. Phys. Chem. C 112 (2008) 16593–16599.
[29] T.L.M. Maesen, E. Beerdsen, S. Calero, D. Dubbeldam, B. Smit, Understanding cage effects in the *n*-alkane conversion on zeolites, J. Catal. 231 (2006) 278–290.

Supporting Information to accompany:

Entropy-based separation of linear chain molecules by exploiting differences in the saturation capacities in cage-type zeolites

Rajamani Krishna[a,b,*] and Jasper M. van Baten[a]

[a]Van 't Hoff Institute for Molecular Sciences, University of Amsterdam, Science Park 904, 1098 XH Amsterdam, The Netherlands

[b]Department of Chemical & Biomolecular Engineering, University of California, Berkeley, Berkeley CA 94720, U.S.A.

*CORRESPONDING AUTHOR Tel +31 20 6270990; Fax: + 31 20 5255604;

email: r.krishna@uva.nl

1. Structural data, force fields used, and simulation methodology

In this work three different types of cage-type zeolites have been investigated.

CHA

The synthesis of the all-silica CHA structure is described in the paper by Olson et al. [1]

LTA-5A (96 Si, 96 Al, 32 Na^+, 32 Ca^{++}, Si/Al=1)

Zeolite LTA-5A is obtained by replacing 64 sodium monovalent cations from the LTA 4A by 32 bivalent calcium ions in an exchange after synthesis. These cations are preferentially located in 4 crystallographic positions; in the window formed by 8 member ring; in the window of the 6-member ring; displaced inside α-cage; or in the sodalites displaced into the center of 6-member ring. In this structure there are no cations inside the windows of the eight-member ring [2]. The cations do not hinder the inter-cage hopping of guest molecules and MD simulations can be used to determine diffusivities.

TSC

This all-silica structure, with a Tschörtnerite framework, has the largest cage volume of any known zeolite [3]. The diameter of the TSC supercage is 17 Å.

Table 1 gives salient information on the zeolites. The unit cell volume, pore volume fraction, and pore volume are summarized in Table 2. Table 3 gives information on the cage volumes.

For simulations of adsorption of alcohols in all-silica CHA, the force field implementation follows that of Kuhn et al.[4], as used in our earlier work [5]. The alcohols are described with the TraPPE force field [6]. Intramolecular potentials are included to describe the flexibility of alcohols. The bond lengths are fixed for all molecules. Bond bending, and torsion potentials are taken into consideration [6].

For simulations with linear alkanes with two or more C atoms, the beads in the chain are connected by harmonic bonding potentials. A harmonic cosine bending potential models the bond bending between three neighboring beads, a Ryckaert-Bellemans potential controls the torsion angle. The force fields of Dubbeldam et al. was used for the variety of potentials. The force fields information for the simulations with cations, as for LTA-5A, are taken from Calero et al. [7-10].

The Lennard-Jones potentials are shifted and cut at 12 Å. The CHA frameworks were considered to be rigid in all the simulation results reported in this article.

The Configurational-Bias Monte Carlo (CBMC) simulation technique used is identical to that used in earlier publications [4, 7-11], and is described in detail by Frenkel and Smit[12].

The pore volumes were determined using the helium insertion technique of Talu and Myers [13]. Table 4 gives the force field for interaction of He with the O atoms in the zeolite structure required in these simulations.

2. Determination of pore volume fraction

The pore volume is determined using a simulation of a single helium molecule at the reference temperature T [14-16]. The simulation details are provided in the Supporting Information accompanying our earlier publication [5].

3. Snapshots and Simulation results

The Figures following this Supporting Information document contain: pore landscapes, and snapshots showing the location of alcohol, and alkane molecules within the cages of CHA, LTA-5A, and TSC. Also presented are the CBMC simulation data for pure components and mixtures.

4. Acknowledgements

We are grateful to T.J.H. Vlugt, Delft, for providing the BIGMAC code. This code was modified to handle rigid molecular structures and charges, with generous assistance and technical inputs from S. Calero, Seville.

The calculation of the accessible pore volume using the Widom insertion of He probe atoms is implemented within the BIGMAC code.

5. References

[1] D.H. Olson, M.A. Camblor, L.A. Vallaescusa, G.H. Kuehl, Light hydrocarbon sorption properties of pure silica Si-CHA and ITQ-3 and high silica ZSM-58, Microporous Mesoporous Mater. 67 (2004) 27-33.

[2] R.L. Firor, K. Seff, Near Zero Coordinate Ca^{2+} and Sr^{2+} in Zeolite A. Crystal Structures of Dehydrated Ca_6-A and Sr_6-A, J. Am. Chem. Soc. 100 (1978) 3091-3096.

[3] M.D. Foster, I. Rivin, M.M.J. Treacy, O.D. Friedrichs, A geometric solution to the largest-free-sphere problem in zeolite frameworks, Microporous Mesoporous Mater. 90 (2006) 32-38.

[4] J. Kuhn, J.M. Castillo-Sanchez, J. Gascon, S. Calero, D. Dubbeldam, T.J.H. Vlugt, F. Kapteijn, J. Gross, Adsorption and Diffusion of Water, Methanol, and Ethanol in All-Silica DD3R: Experiments and Simulation, J. Phys. Chem. C 113 (2009) 14290-14301.

[5] R. Krishna, J.M. van Baten, Hydrogen bonding effects in adsorption of water-alcohol mixtures in zeolites and the consequences for the characteristics of the Maxwell-Stefan diffusivities, Langmuir 26 (2010) 10854-10867.

[6] B. Chen, J.J. Potoff, J.I. Siepmann, Monte Carlo Calculations for Alcohols and Their Mixtures with Alkanes. Transferable Potentials for Phase Equilibria. 5. United-Atom Description of Primary, Secondary, and Tertiary Alcohols, J. Phys. Chem. B 105 (2001) 3093-3104.

[7] S. Calero, D. Dubbeldam, R. Krishna, B. Smit, T.J.H. Vlugt, J.F.M. Denayer, J.A. Martens, T.L.M. Maesen, Understanding the role of sodium during adsorption. A force field for alkanes in sodium exchanged faujasites, J. Am. Chem. Soc. 126 (2004) 11377-11386.

[8] E. García-Pérez, D. Dubbeldam, T.L.M. Maesen, S. Calero, Influence of cation Na/Ca ratio on adsorption in LTA 5A: A systematic molecular simulations study of alkane chain length, J. Phys. Chem. B 110 (2006) 23968-23976.

[9] A. García-Sánchez, E. García-Pérez, D. Dubbeldam, R. Krishna, S. Calero, A Simulation Study of Alkanes in Linde Type A Zeolites, Adsorpt. Sci. Technol. 25 (2007) 417-427.

[10] S. Calero, M.D. Lobato, E. García-Pérez, J.A. Mejías, S. Lago, T.J.H. Vlugt, T.L.M. Maesen, B. Smit, D. Dubbeldam, A coarse-graining approach for the proton complex in protonated aluminosilicates, J. Phys. Chem. B 110 (2006) 5838-5841.

[11] D. Dubbeldam, S. Calero, T.J.H. Vlugt, R. Krishna, T.L.M. Maesen, B. Smit, United Atom Forcefield for Alkanes in Nanoporous Materials, J. Phys. Chem. B 108 (2004) 12301-12313.

[12] D. Frenkel, B. Smit, Understanding molecular simulations: from algorithms to applications, Academic Press, 2nd Edition, San Diego, 2002.

[13] O. Talu, A.L. Myers, Molecular Simulation of Adsorption: Gibbs Dividing Surface and Comparison with Experiment, A.I.Ch.E.J. 47 (2001) 1160-1168.

[14] A.L. Myers, P.A. Monson, Adsorption in Porous Materials at High Pressure: Theory and Experiment, Langmuir 18 (2002) 10261-10273.

[15] R. Babarao, Z. Hu, J. Jiang, S. Chempath, S.I. Sandler, Storage and separation of CO_2 and CH_4 in silicalite, C_{168} schwarzite, and IRMOF-1: A comparative study from Monte Carlo simulation, Langmuir 23 (2007) 659-666.

[16] R. Babarao, J. Jiang, Exceptionally high CO_2 storage in covalent-organic frameworks: Atomistic simulation study, Energy Environ. Sci. 1 (2008) 139-143.

[17] C. Baerlocher, L.B. McCusker, Database of Zeolite Structures, International Zeolite Association, http://www.iza-structure.org/databases/, 10 January 2002.

Table 1. Salient information on zeolite structures. The channel and window sizes that are quoted here are taken from the IZA website [17]. Please note that these sizes are for indicative purposes only. For cage-type zeolites the cage sizes were calculated after determining the pore volume from molecular simulations; these values are not available in the IZA atlas.

Zeolite	**Channel or window size/ Å**
LTA-Si	743.05 $Å^3$ size cages separated by 4.11 Å × 4.47 Å size windows. The sodalite cages are blocked in simulations and are not accessible to guest molecules.
CHA	316.4 $Å^3$ size cages separated by 3.77 Å × 4.23 Å size windows.
LTA-5A	703 $Å^3$ size cages separated by 4 Å × 4.58 Å size windows. The sodalite cages are blocked in simulations and are not accessible to guest molecules.
ERI	408.7 $Å^3$ size cages separated by 3.8 Å × 4.9 Å size windows
AFX	490 $Å^3$ size cages connected to pockets of 98 $Å^3$ in size. Cages are separated by 3.4 Å × 3.9 Å size windows.
TSC	Two types of cages: LTA-type of 743.05 $Å^3$ and TSC-supercage of 2552.6 $Å^3$size. Two types of 8-ring windows: 4.02 Å × 4.17 Å and 3.1 Å × 5.41 Å. The sodalite cages are blocked in simulations and are not accessible to guest molecules; these are excluded for pore volume determination.

Table 2. Unit cell dimensions, unit cell volumes, pore volumes of various all-silica zeolites. Also indicated are the framework density, ρ (expressed as kg per m^3 framework), the factor to convert from molecules per unit cell to kmol/m^3 of accessible pore volume. Please also note that for all the structures listed here below have orthorhombic unit cells, i.e. with the angles $\alpha = 90^o$, $\beta = 90^o$, $\gamma = 90^o$. For CHA the original structure is monoclinic. We use orthorhombic re-constructs with different unit cell sizes (i.e. larger). The unit cell sizes therefore do not correspond in all cases to those reported in the IZA atlas website[17].

Structure	*a* / Å	*b* / Å	*c* / Å	Unit cell volume/ $Å^3$	Pore volume per unit cell/ $Å^3$	Fractional pore volume, ϕ	Pore volume/ cm^3/g	Framework density/ kg/m^3	Conversion factor
CHA	15.08	23.91	13.80	4974.57	1898.40	0.382	0.264	1444.10	0.8747
LTA-5A	24.56	24.56	24.56	14805.39	5620.41	0.38	0.25	1508.38	0.2955
TSC	30.74	30.74	30.74	29053.36	13182.60	0.454	0.344	1318.73	0.1260

Table 3. Cage volume for cage-type zeolites. The cage sizes were calculated after determining the pore volume from molecular simulations; these values are not available in the IZA atlas. Also indicated is the diameter of a equivalent sphere with the same cage volume.

Structure	Pore volume per unit cell/ Å^3	Volume per cage/ Å^3	Cage diameter/ Å
LTA-Si (all silica)	5944.38	743.05	11.23
LTA-5A	5620.4	702.56	11.03
CHA	1898.40	316.4	8.45
ERI	1635.01	408.7	9.21
AFX	2352.45	490 Pockets are 98 Å^3 in size	
TSC = 4 “LTA-cages” and 4 “TSC-supercages”	13182.60	2552.6	16.96

Table 4. Lennard-Jones parameters used to determine the pore volume in CHA. The He-He parameters are from Table 1 of the paper by Talu and Myers [13]. The interaction parameters for interaction of He with the O atoms of zeolite frameworks is from Table 1 of Talu and Myers [13]

(pseudo-) atom	**Atom-atom** σ **/ Å**	**Atom-atom** ε/k_B **/ K**
He - He	2.64	10.9
He - O	2.952	28

All-silica
CHA

CHA

To convert from molecules per unit cell to mol kg^{-1}, multiply by 0.2311.
The pore volume is 0.264 cm^3/g.

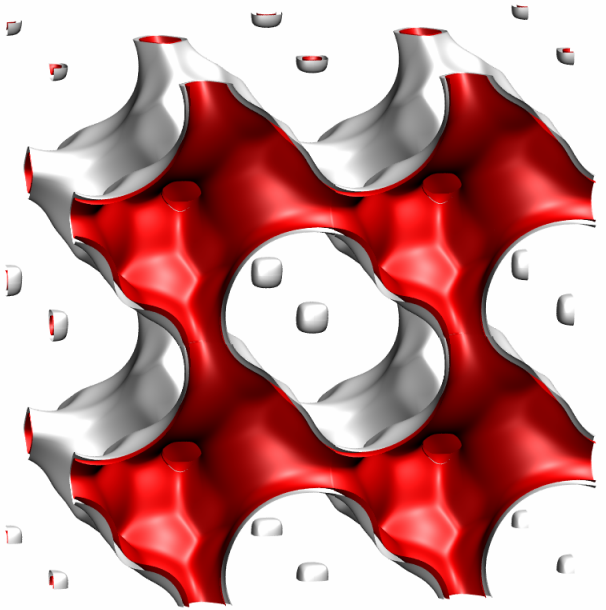

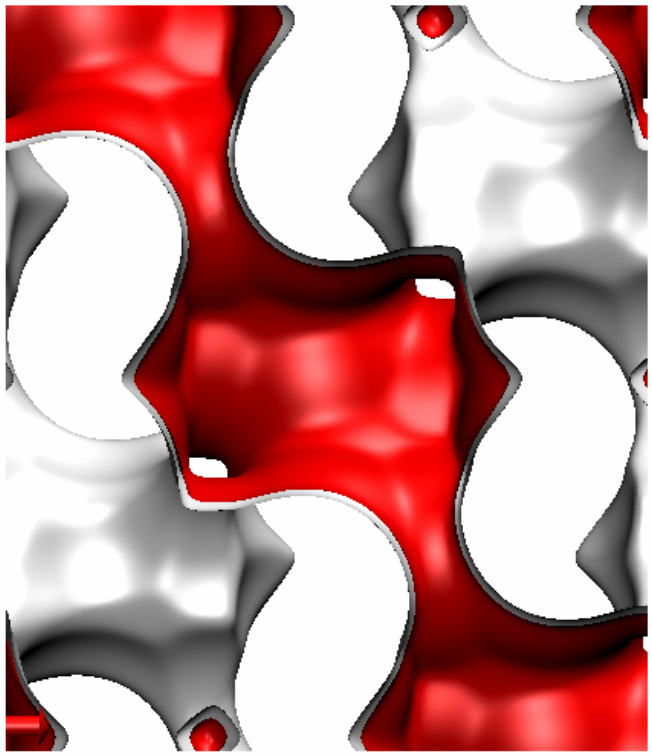

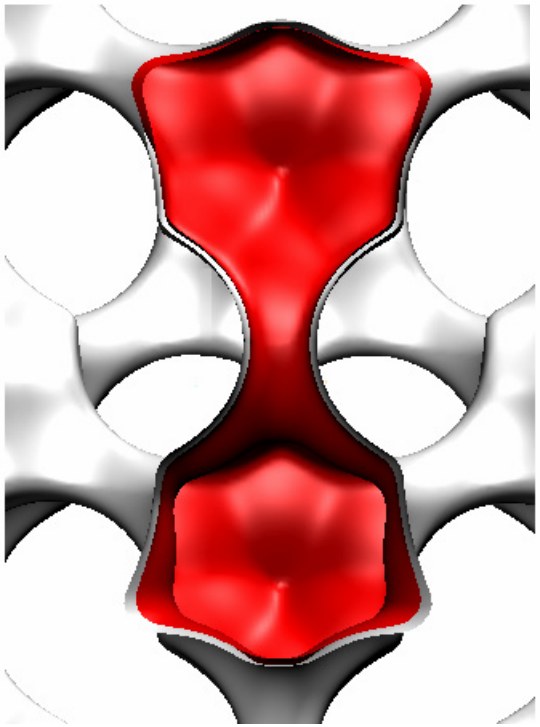

Snapshot of CH_4

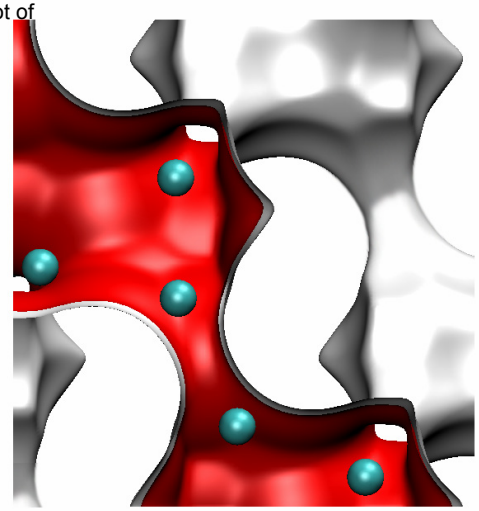

CHA window dimensions

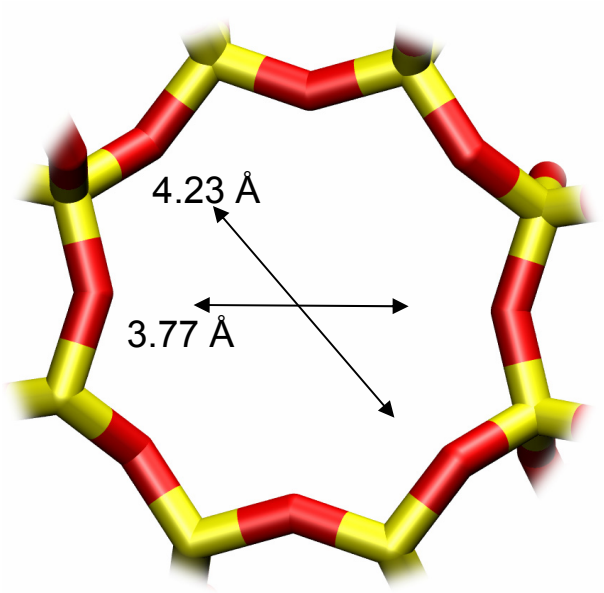

CHA

The window dimensions calculated using the van der Waals diameter of framework atoms = 2.7 Å are indicated above by the arrows.

CHA CBMC simulation of methanol isotherm at 300 K

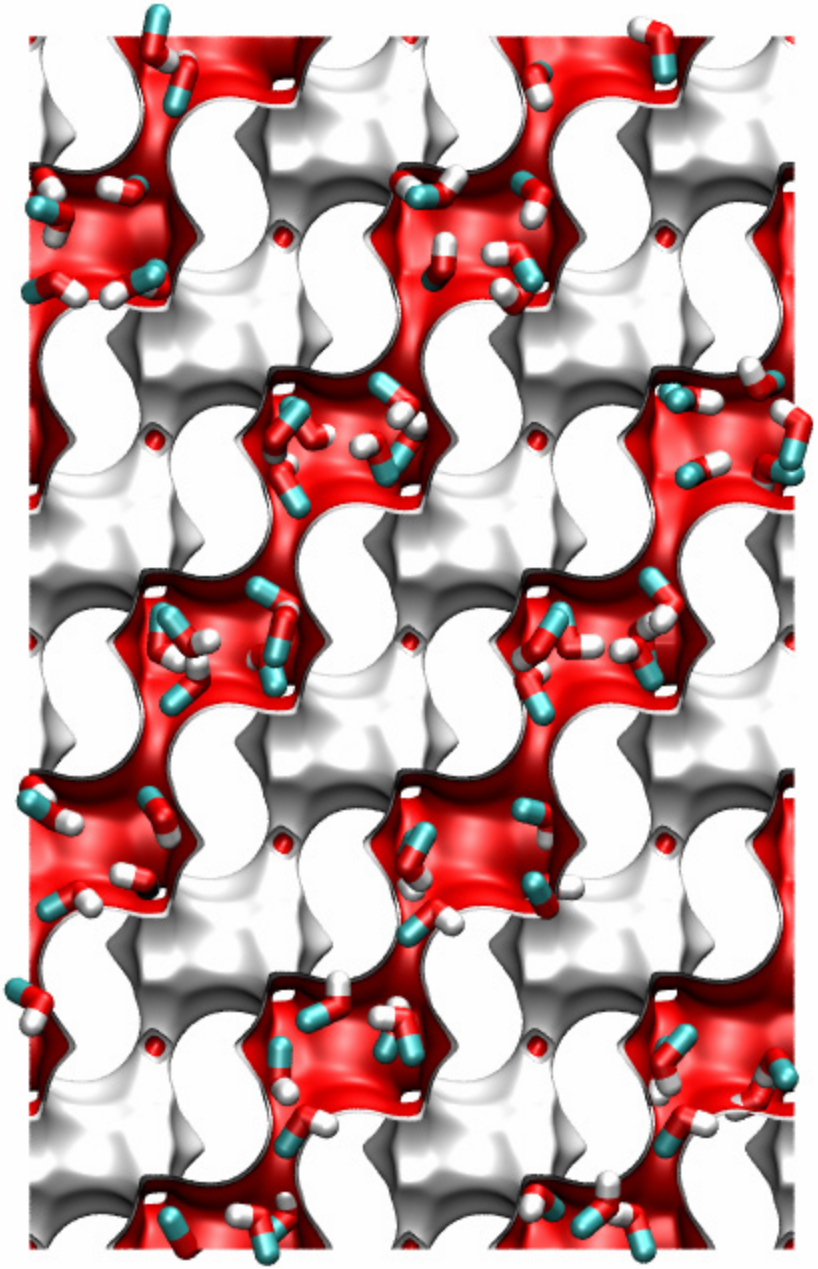

Snapshot of methanol in CHA
$f = 10^6$ Pa, $T = 300$ K

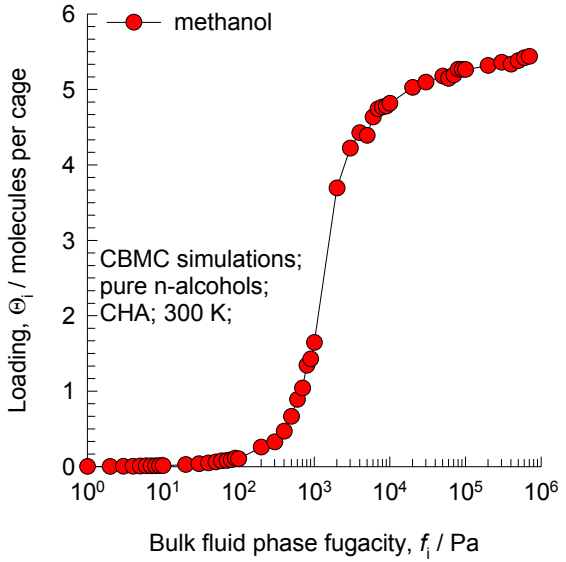

CHA CBMC simulation of ethanol isotherm at 300 K

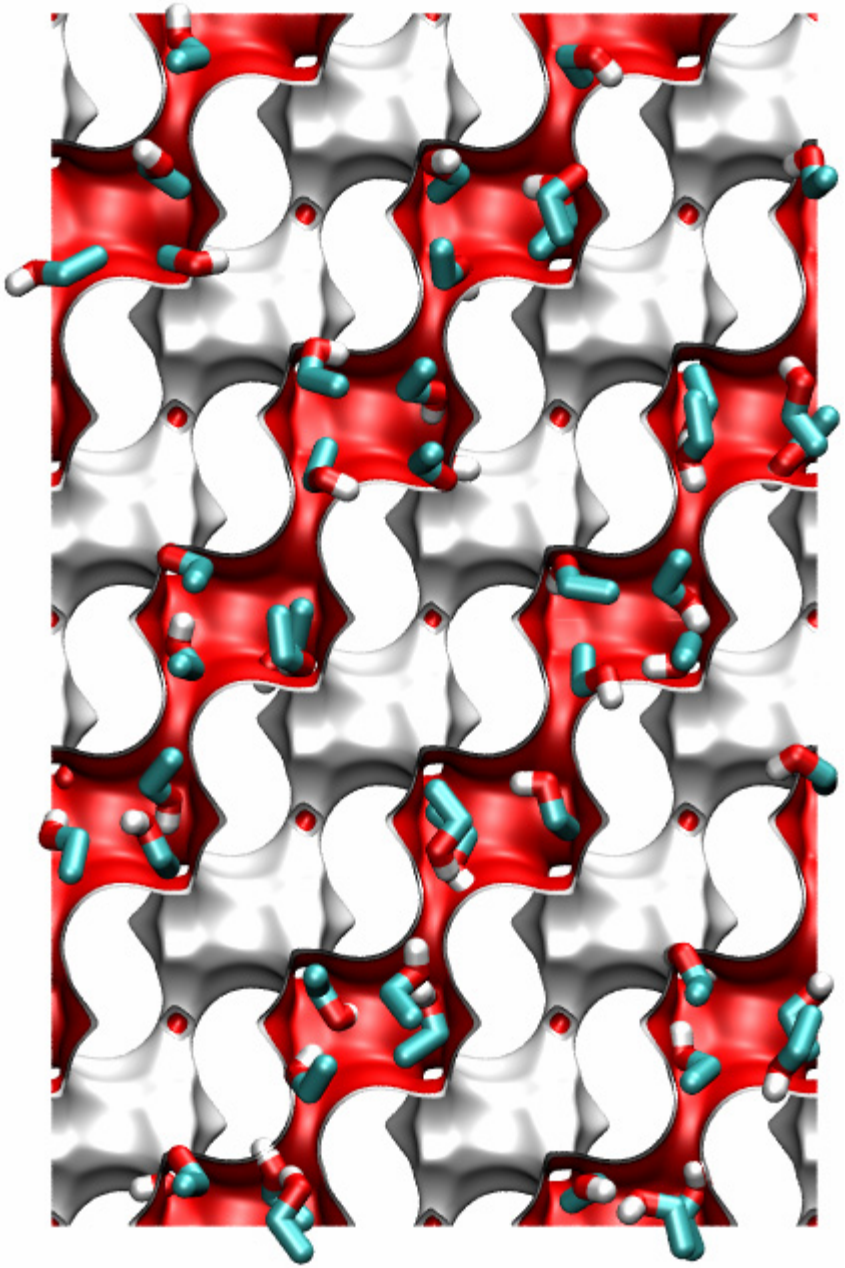

Snapshot of ethanol in CHA
f = 1x10^6 Pa, T = 300 K

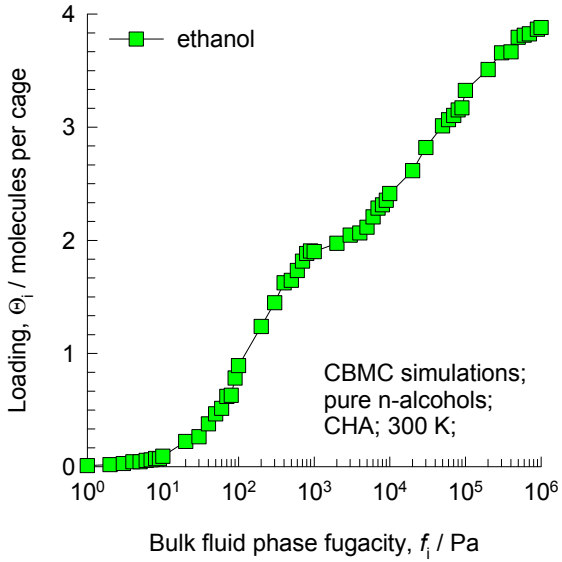

CHA CBMC simulation of n-propanol isotherm at 300 K

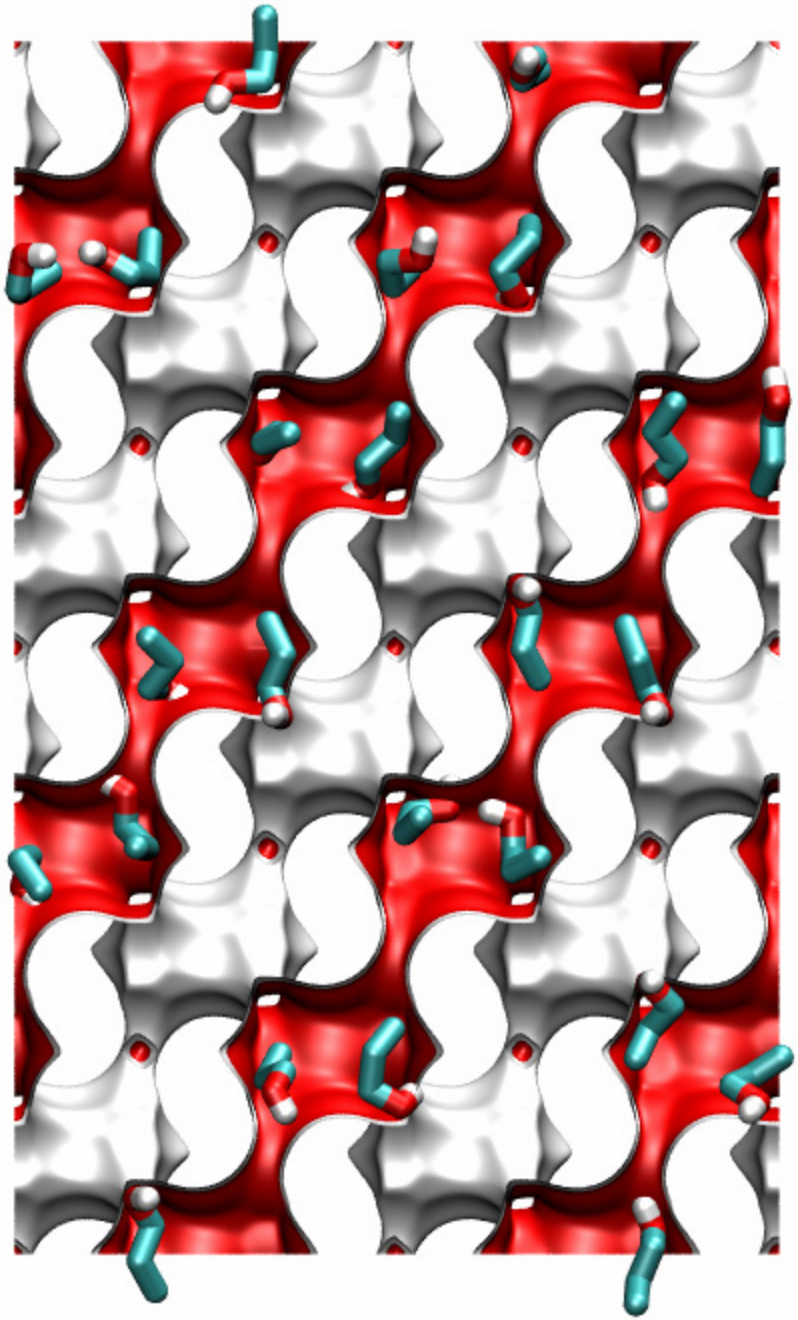

Snapshot of n-propanol in CHA
f = 1x10^3 Pa, T = 300 K

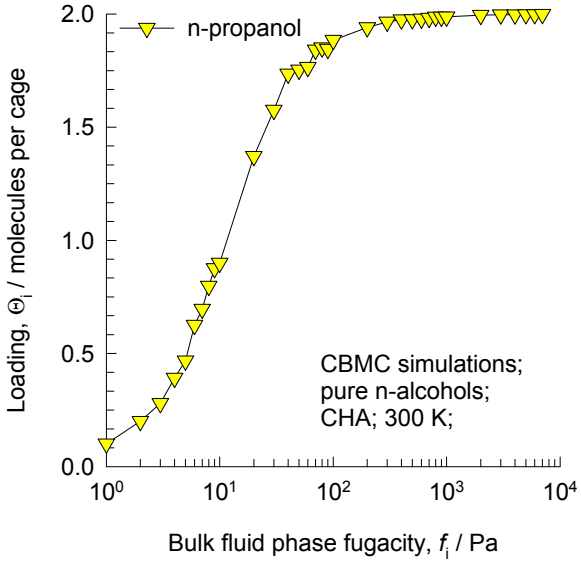

CHA CBMC simulation of n-butanol isotherm at 300 K

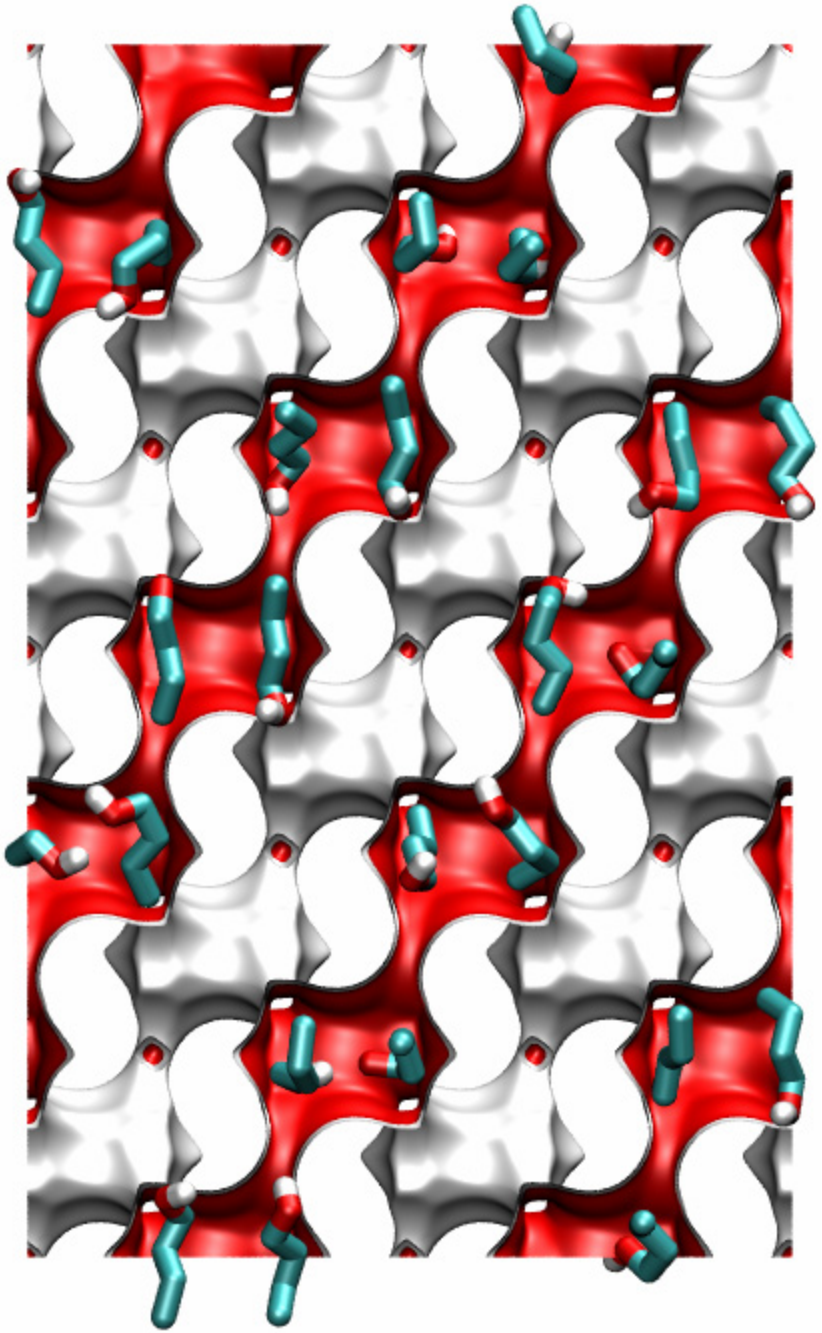

Snapshot of n-butanol in CHA
f = 1x10^3 Pa, T = 300 K

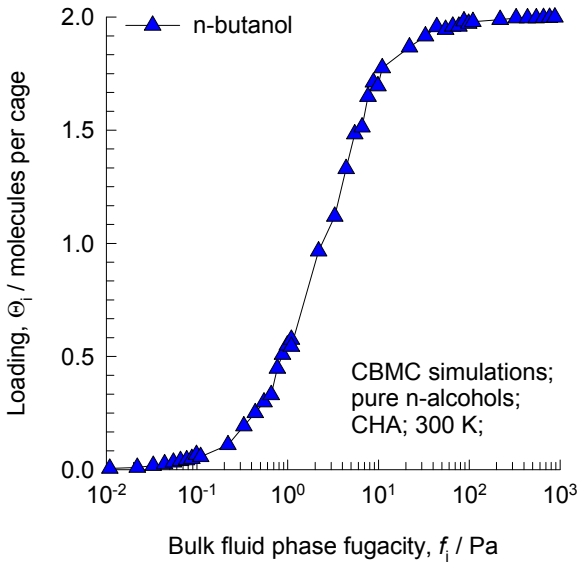

CHA CBMC simulation of n-pentanol isotherm at 300 K

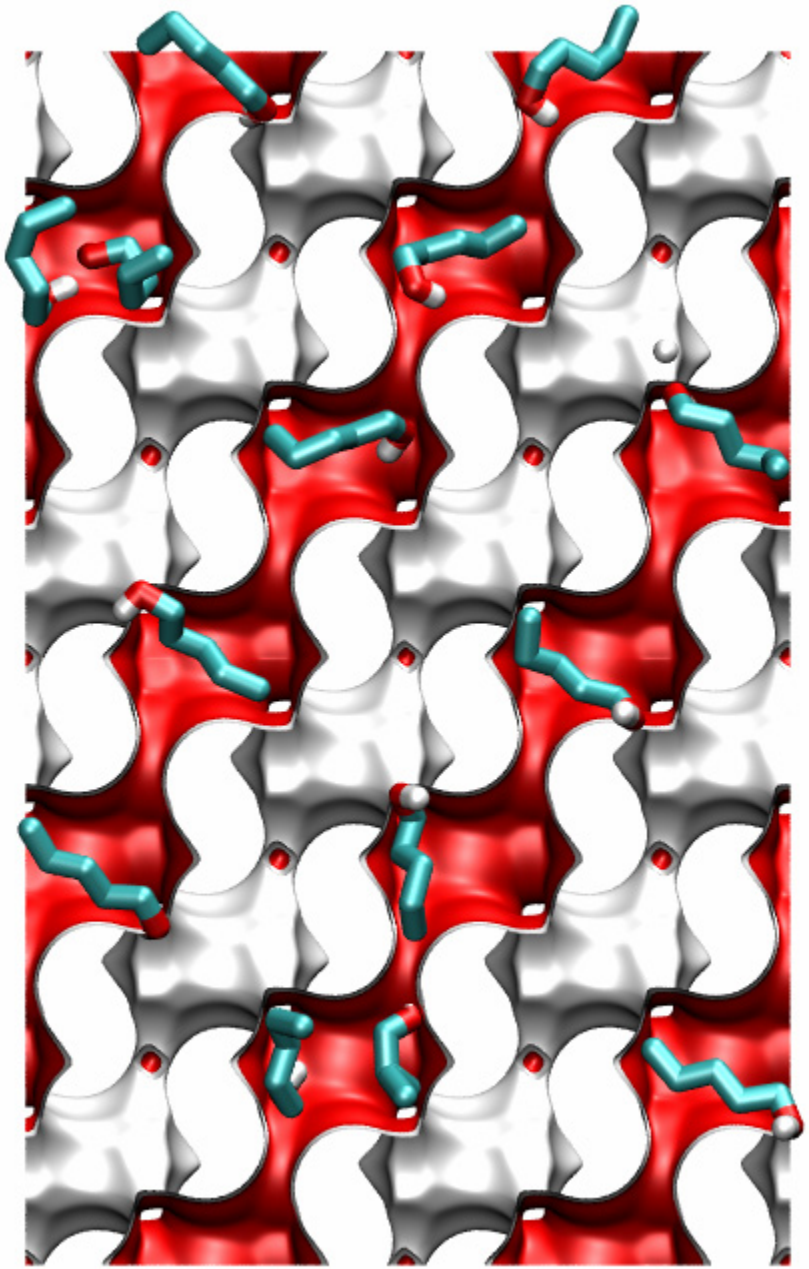

Snapshot of n-pentanol in CHA
f = 5 Pa, T = 300 K

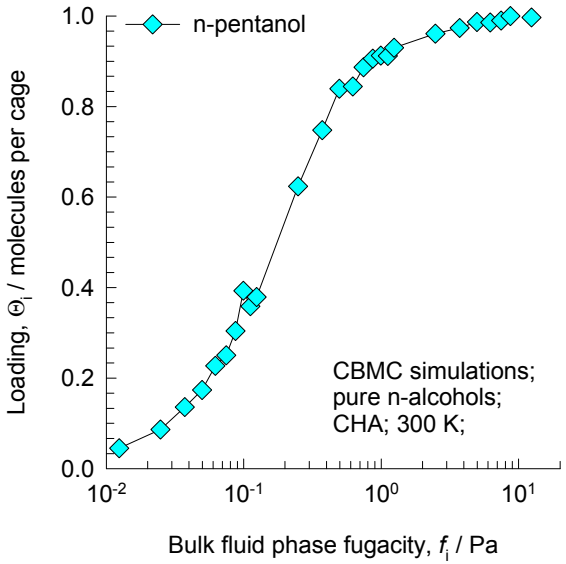

CHA CBMC simulation of n-hexanol isotherm at 300 K

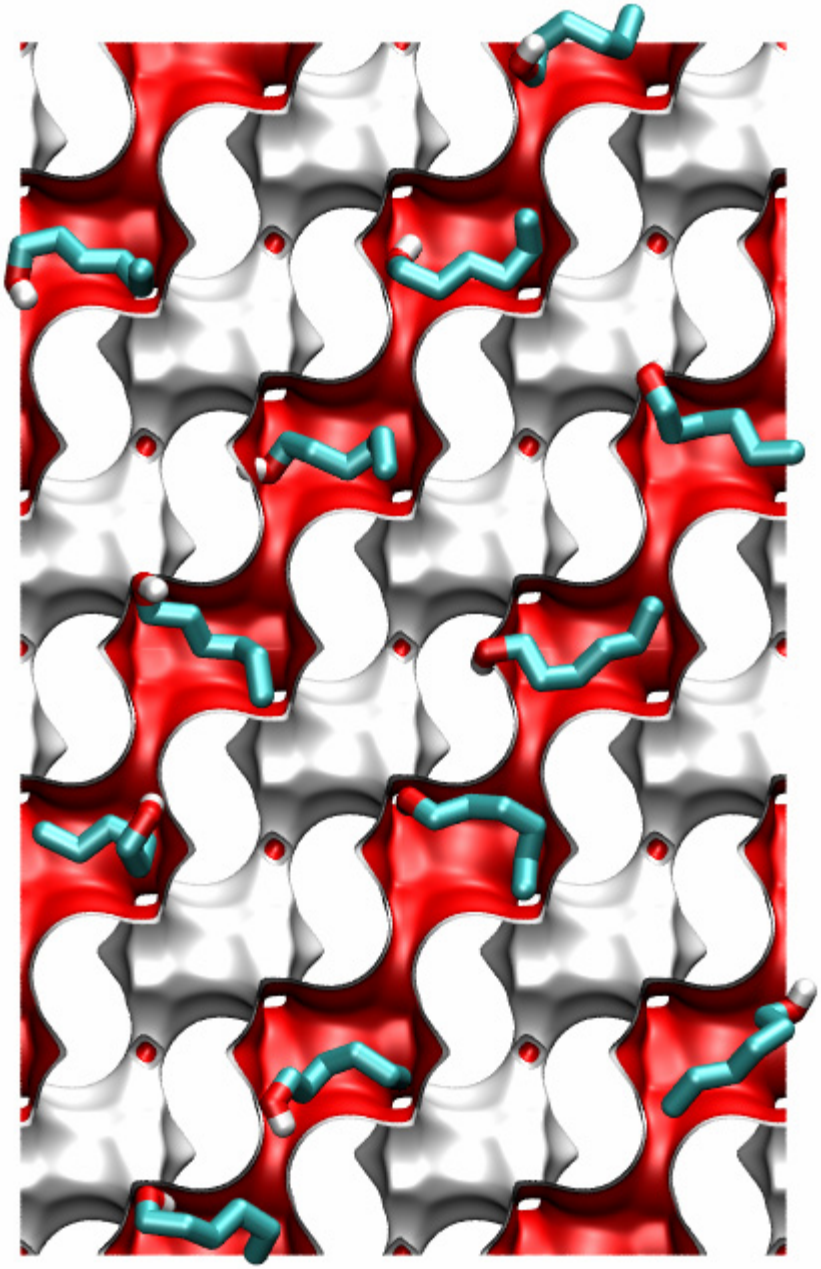

Snapshot of n-hexanol in CHA
f = 10 Pa, T = 300 K

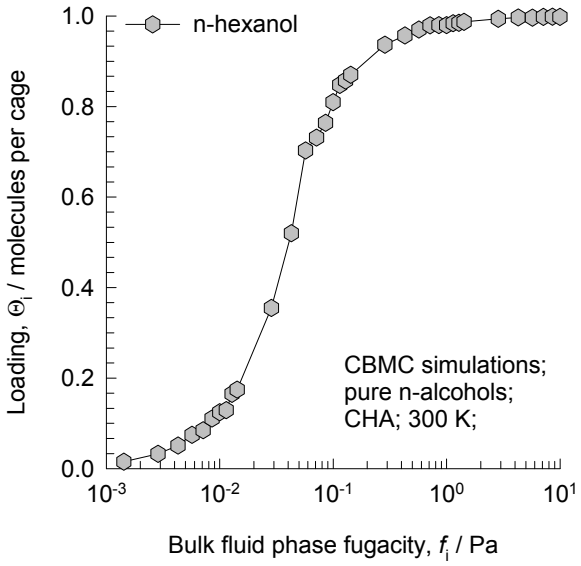

CHA CBMC simulations for methanol-ethanol mixture

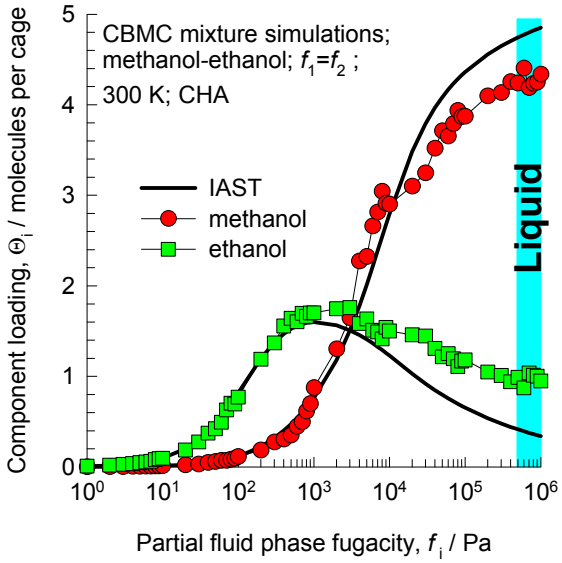

CHA CBMC simulations for ethanol-n-propanol mixture

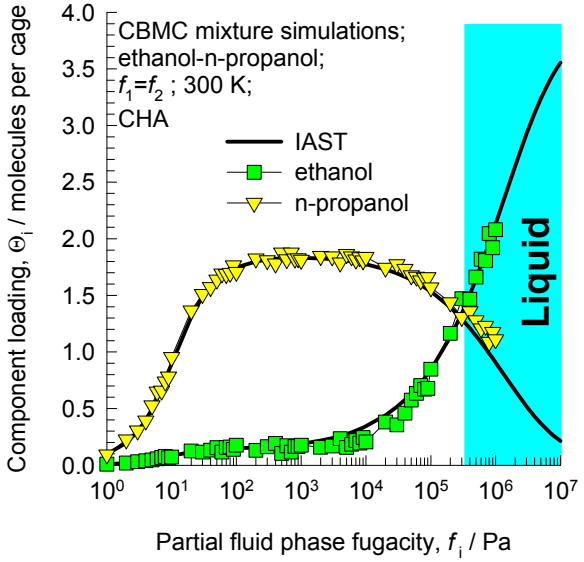

CHA CBMC simulations for butanol-n-pentanol mixture

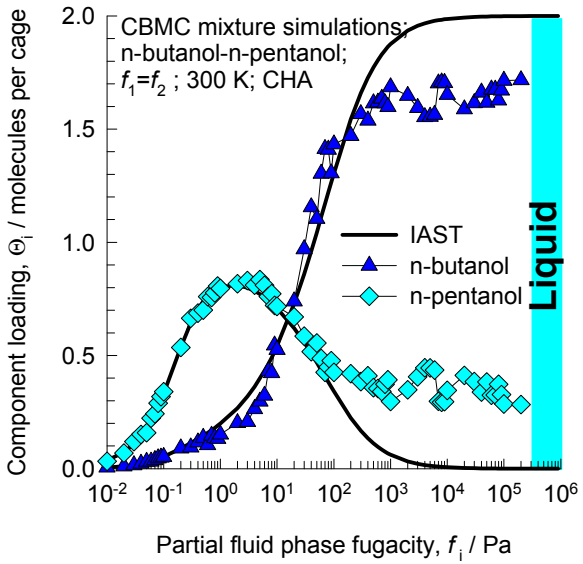

CHA CBMC simulations for butanol-n-hexanol mixture

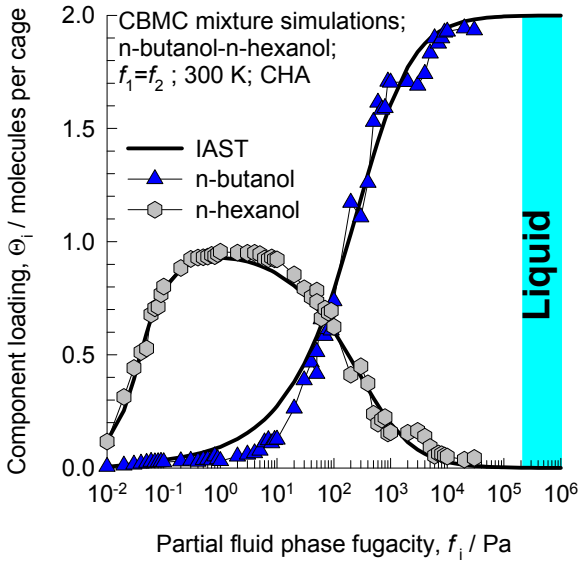

CHA CBMC simulations for ethanol-n-hexanol mixture

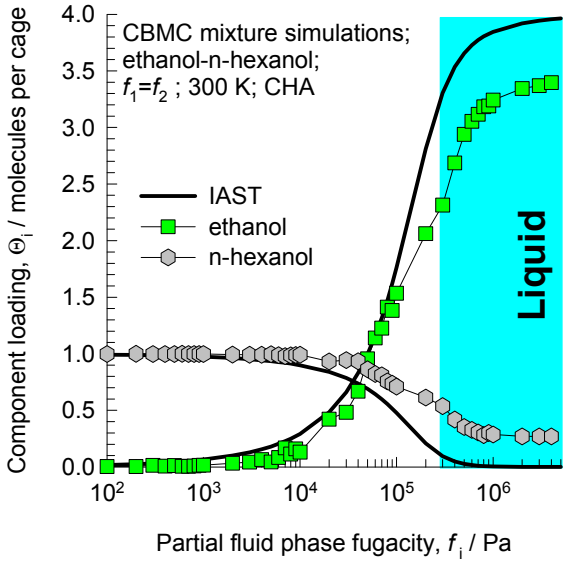

CHA CBMC simulations for pentanol-n-hexanol mixture

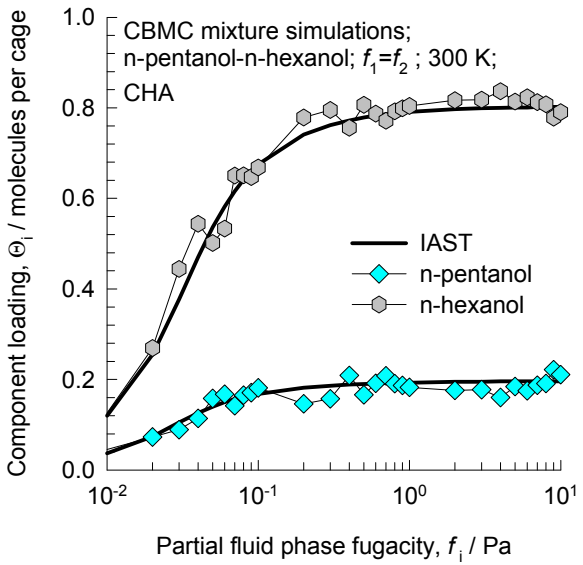

LTA-5A
with cations

LTA-5A

To convert from molecules per unit cell to mol kg^{-1}, multiply by 0.074358.
The pore volume is 0.252 cm^3/g.

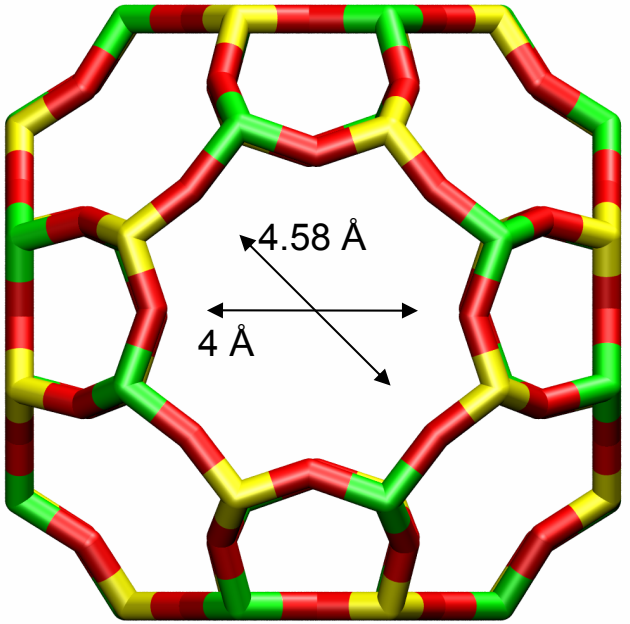

LTA-5A

The window dimension calculated using the van der Waals diameter of framework atoms = 2.7 Å is indicated above by the arrow.

LTA-5A (32 Na^+, 32 Ca^{++})

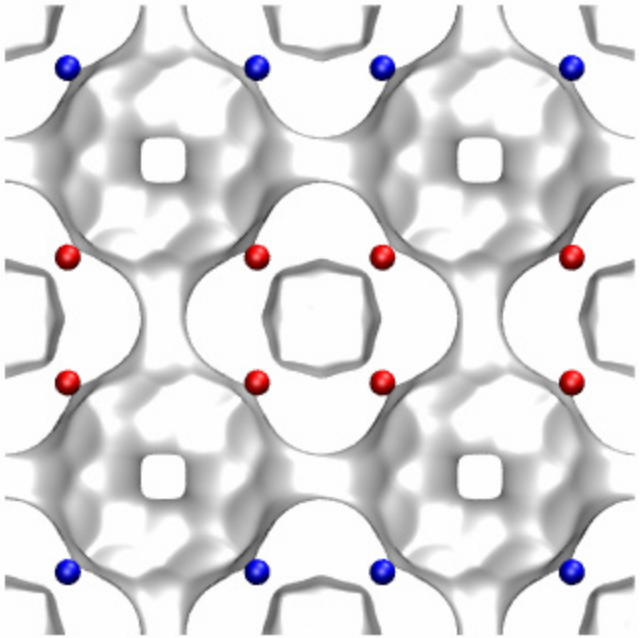

LTA-5A, snapshots of single n-alkane molecules

nC8

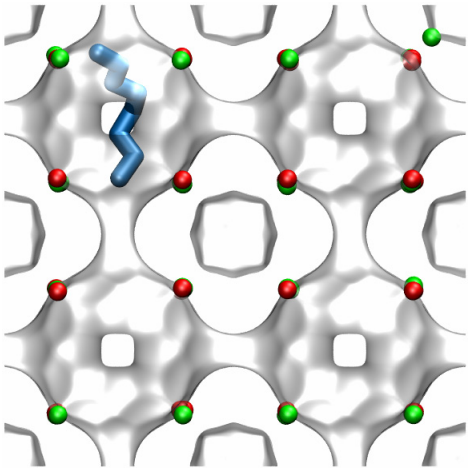

nC9

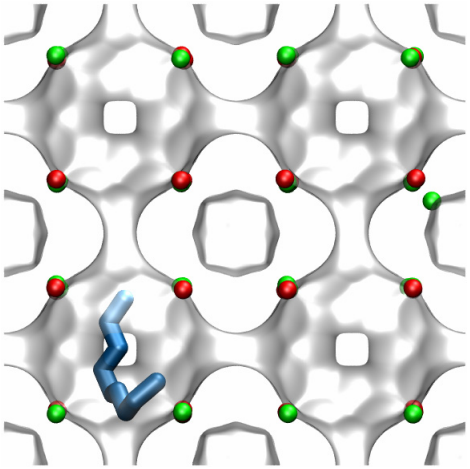

nC10

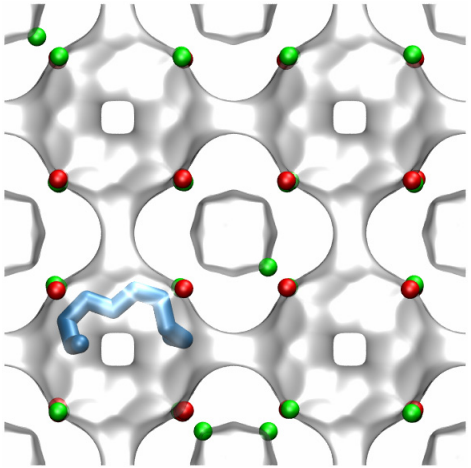

nC11

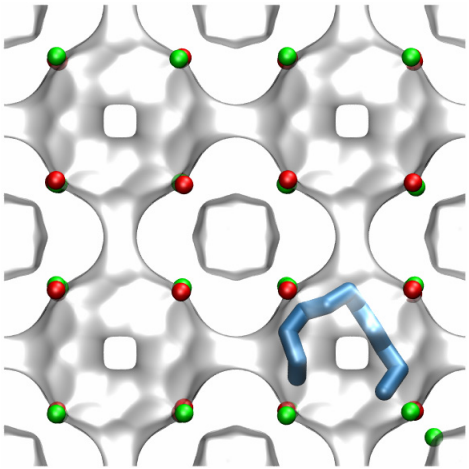

nC12

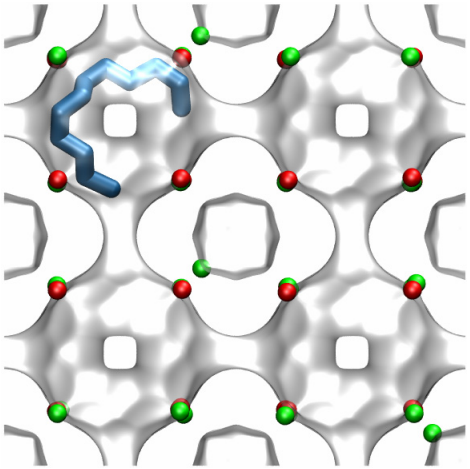

nC13

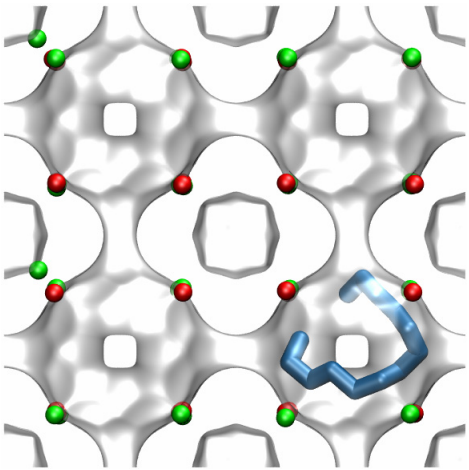

nC14

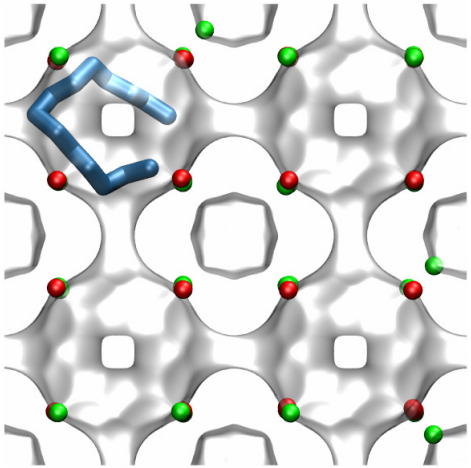

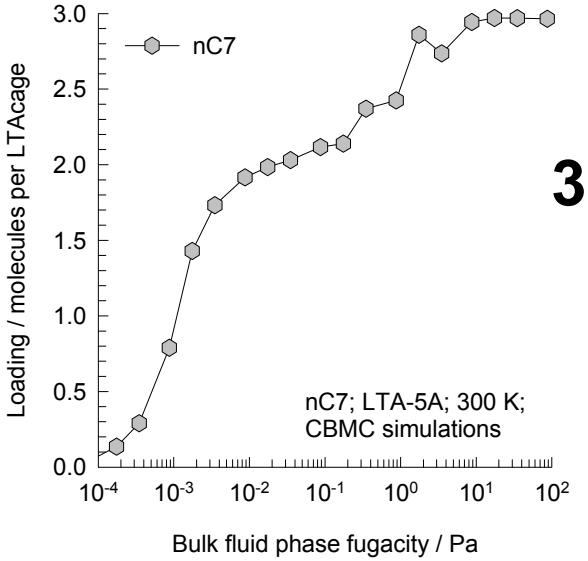

300 K

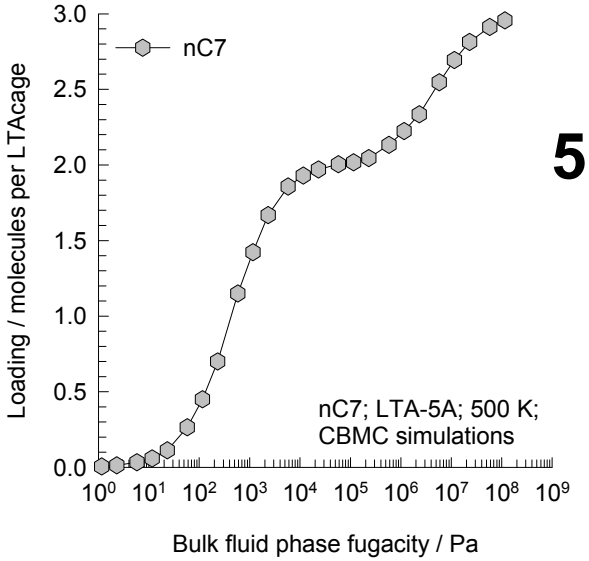

500 K

LTA-5A, nC7
2 molecules/cage

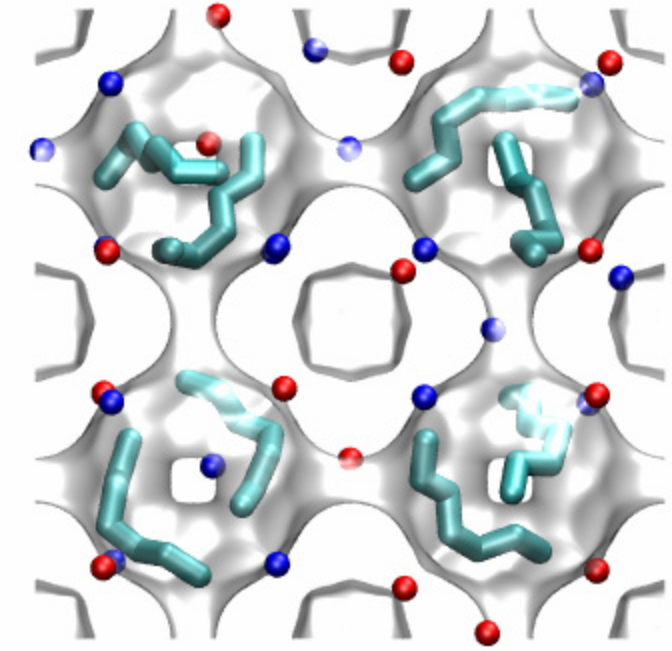

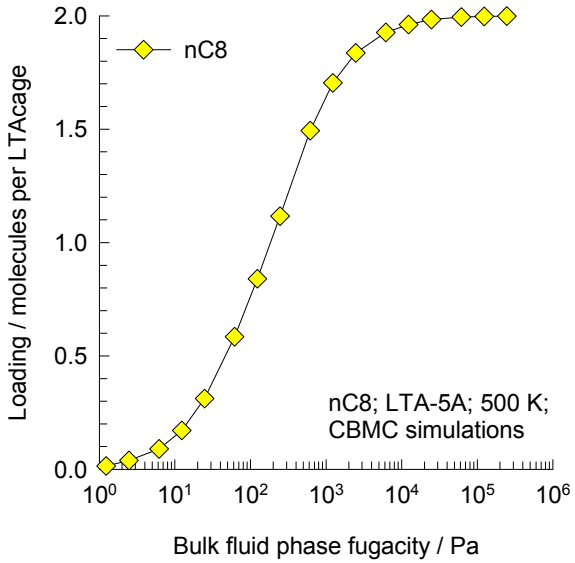

LTA-5A, nC8
2 molecules/cage

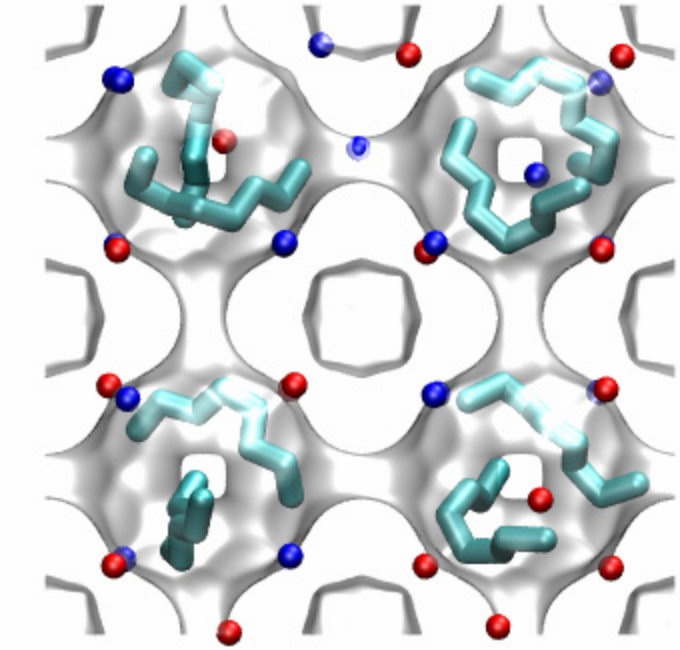

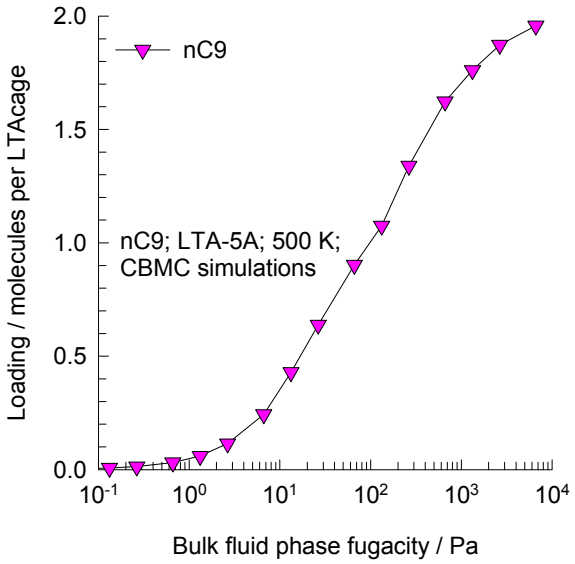

LTA-5A, nC9
2 molecules/cage

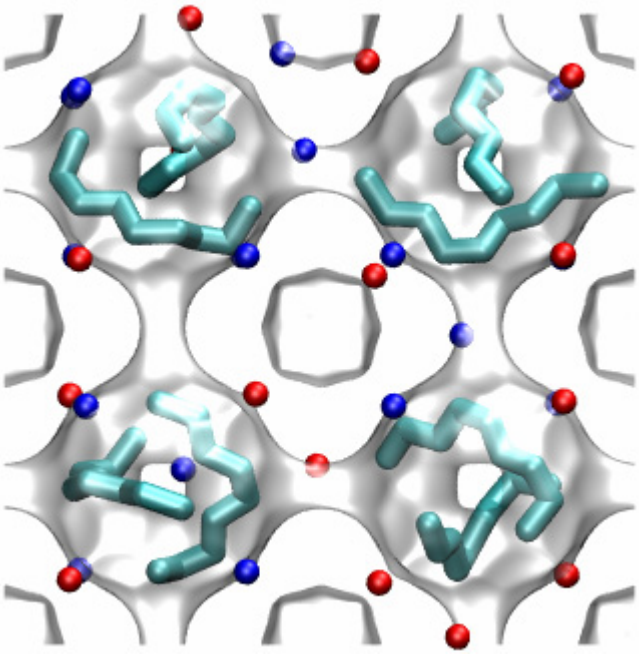

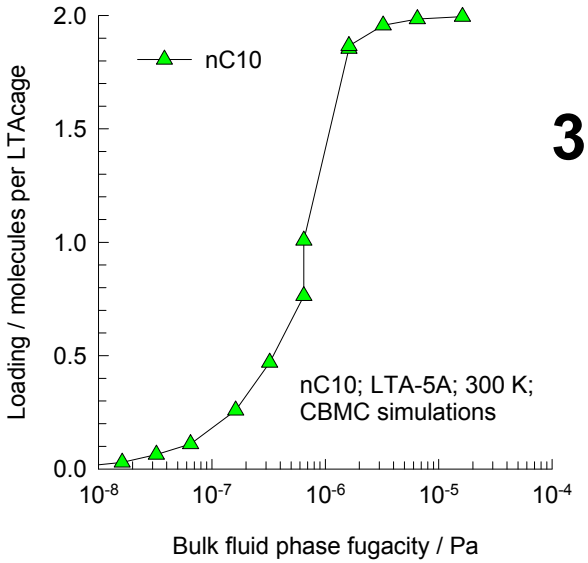

300 K

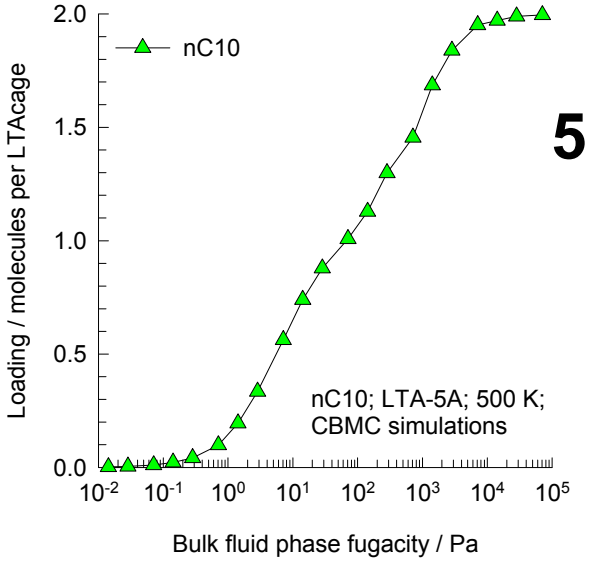

500 K

LTA-5A, nC10
2 molecules/cage

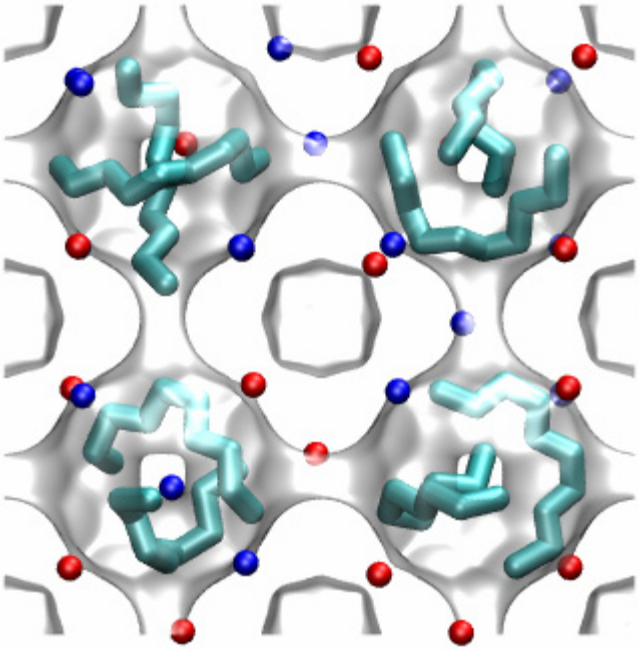

LTA-5A, nC11
2 molecules/cage

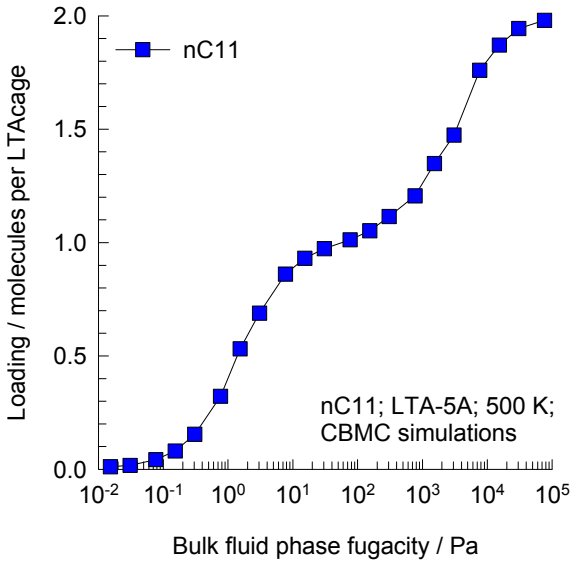

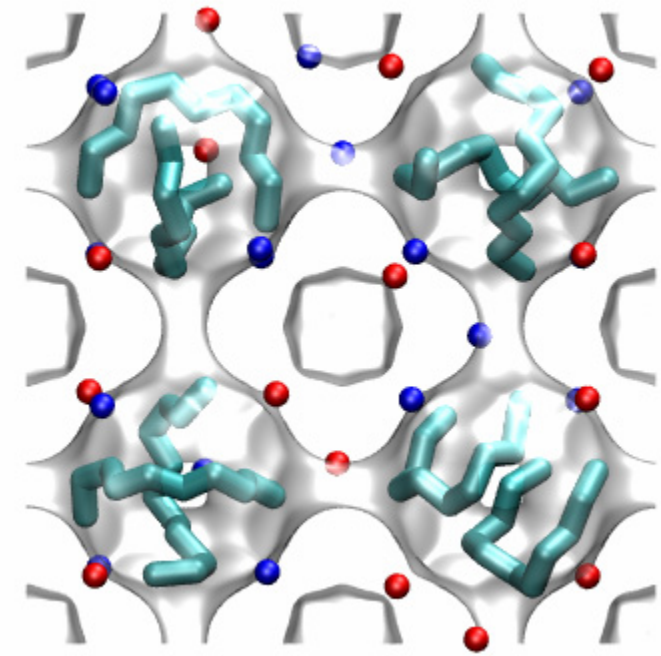

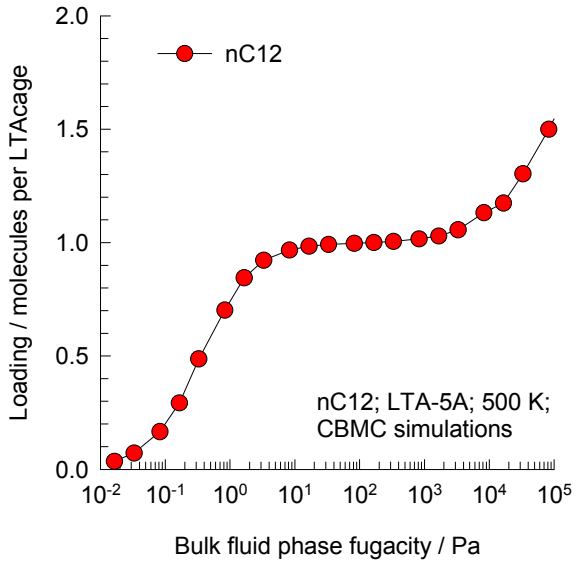

LTA-5A, nC12
2 molecules/cage

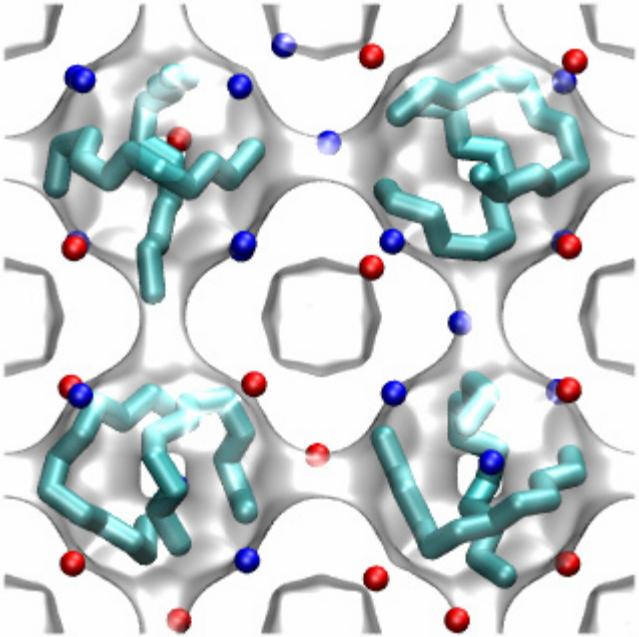

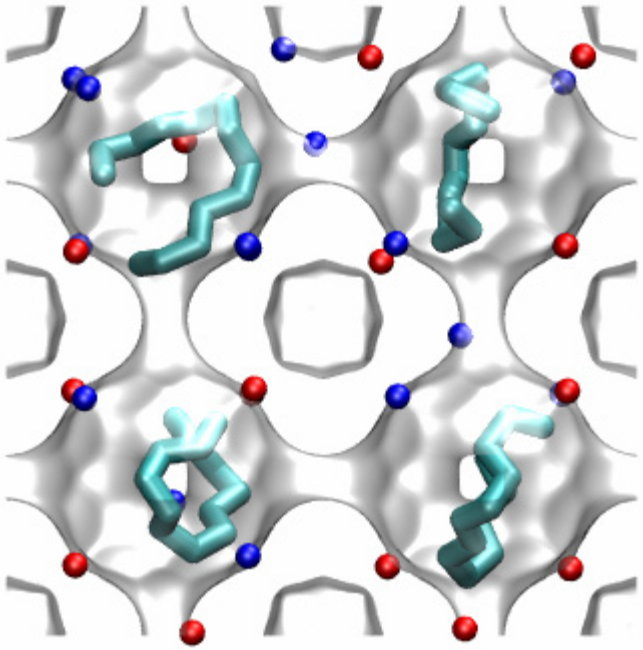

LTA-5A, nC13
10 molecules/uc

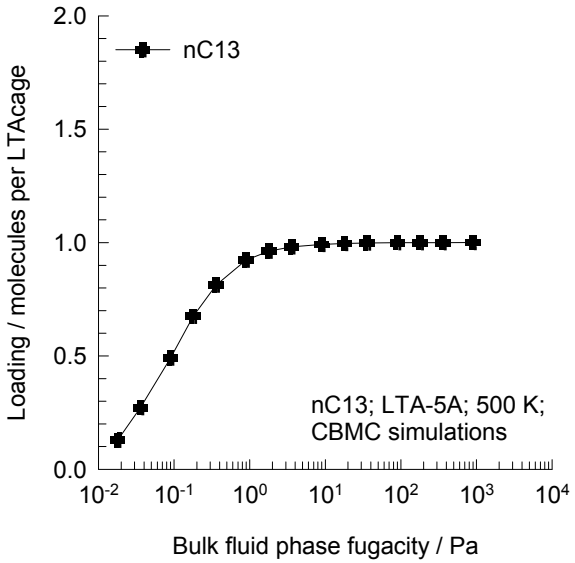

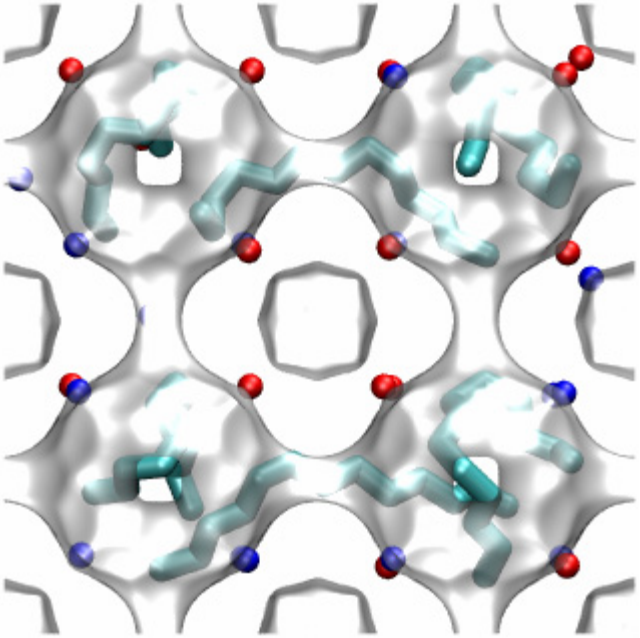

LTA (all-silica), 300 K, nC14, 0.1 kPa

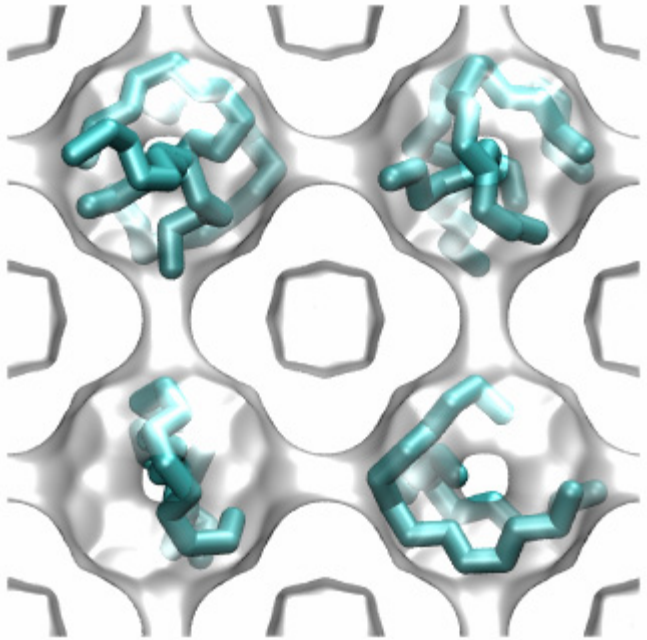

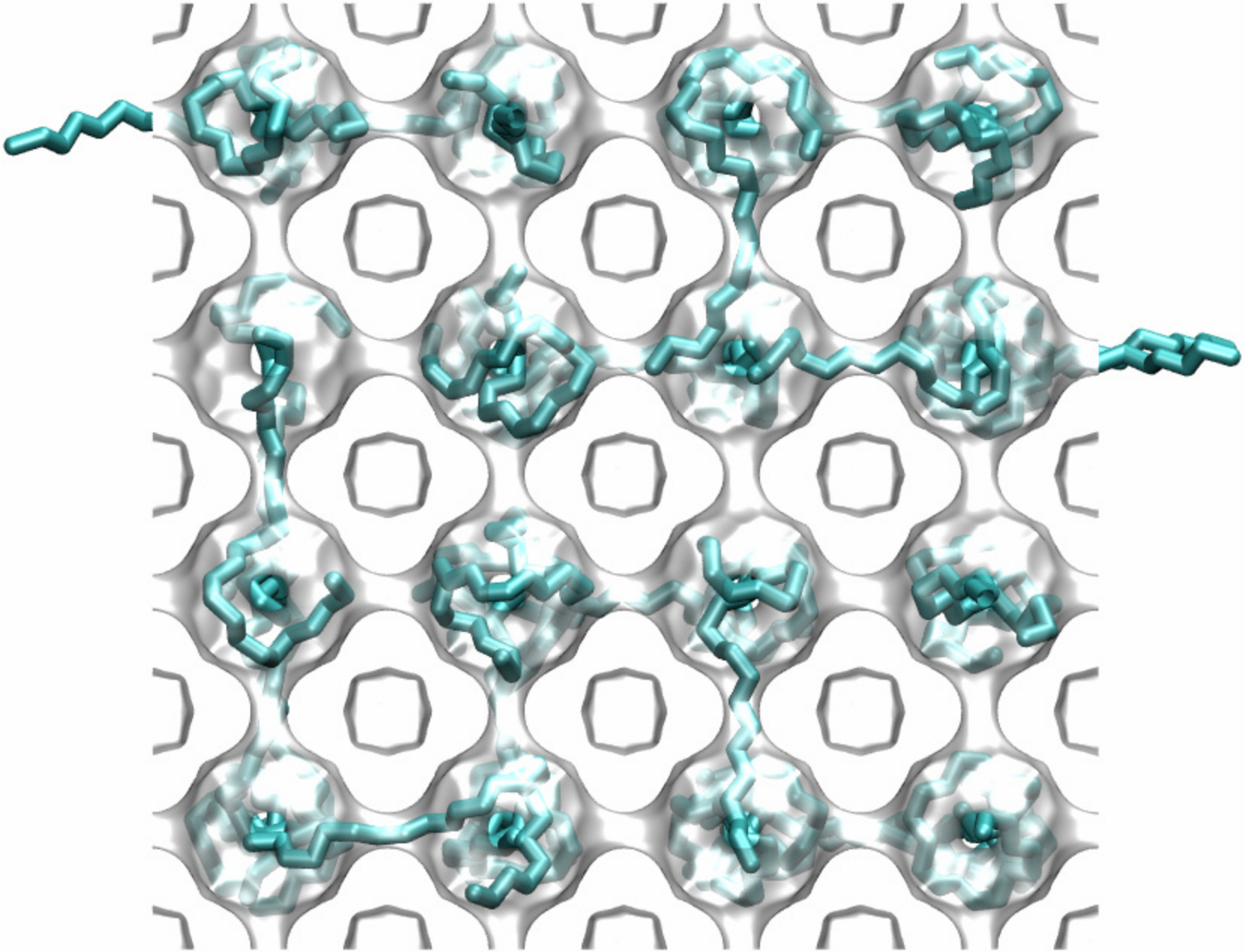

LTA(all-silica), 500 K, nC25, 100 kPa

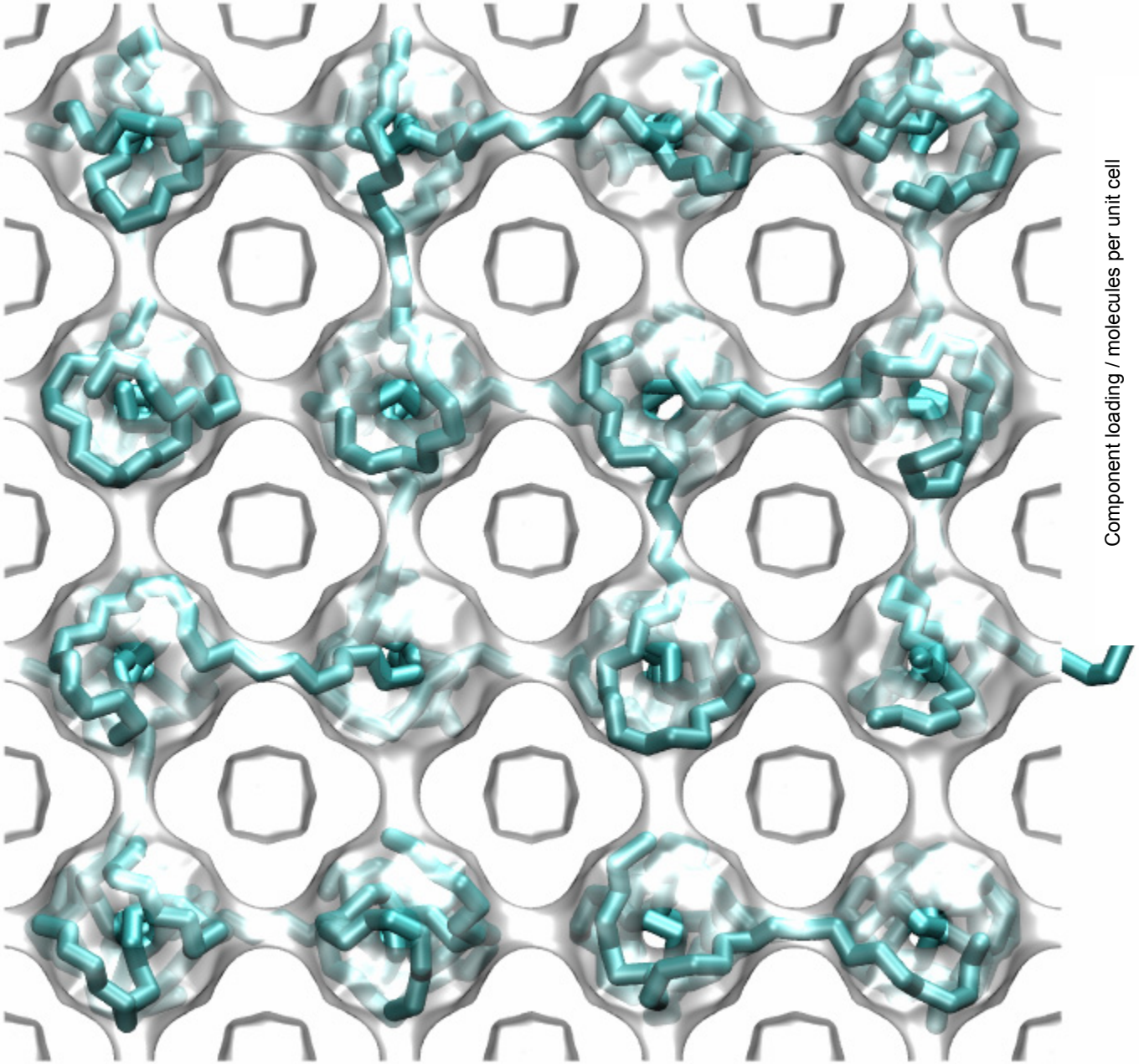

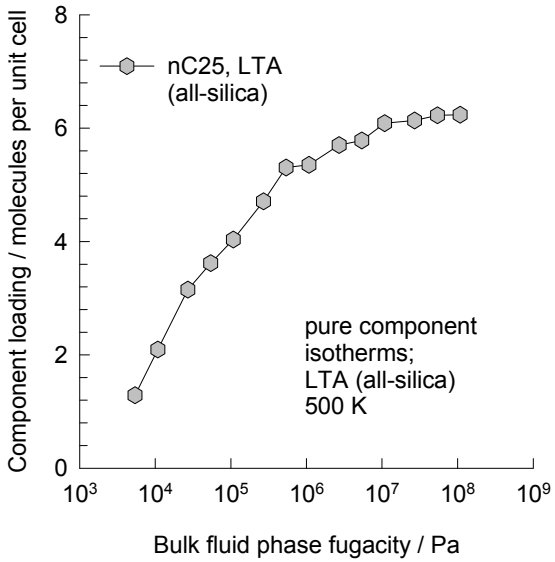

LTA(all-silica), 500 K, nC25, 20000 kPa

LTA-5A CBMC simulations of pure component isotherms at 300 K, and 500 K

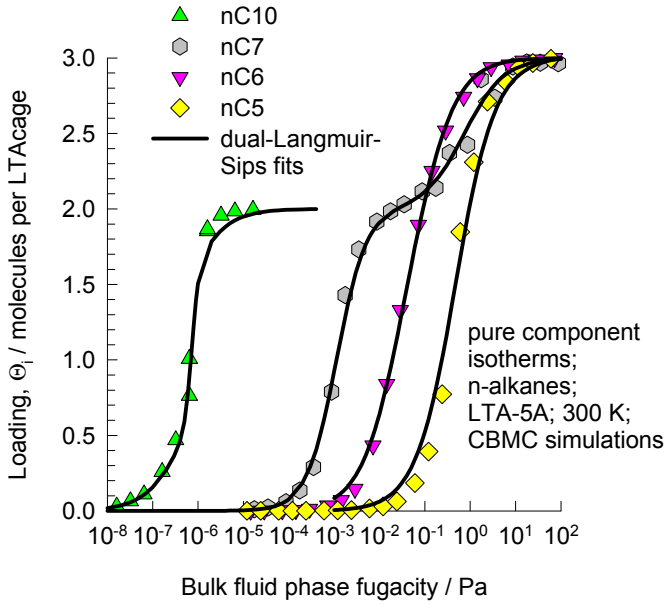

Pure n-alkanes, LTA-5A, 300 K

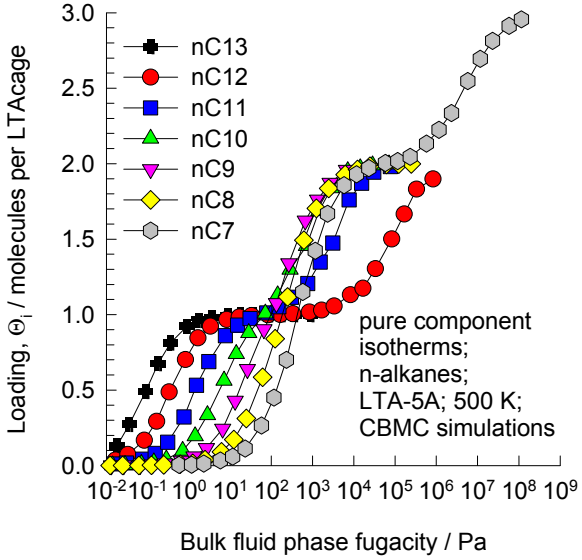

Pure n-alkanes, LTA-5A, 500 K

LTA-5A CBMC simulations of pure component isotherm of nC10 compared with published experimental data at 589 K

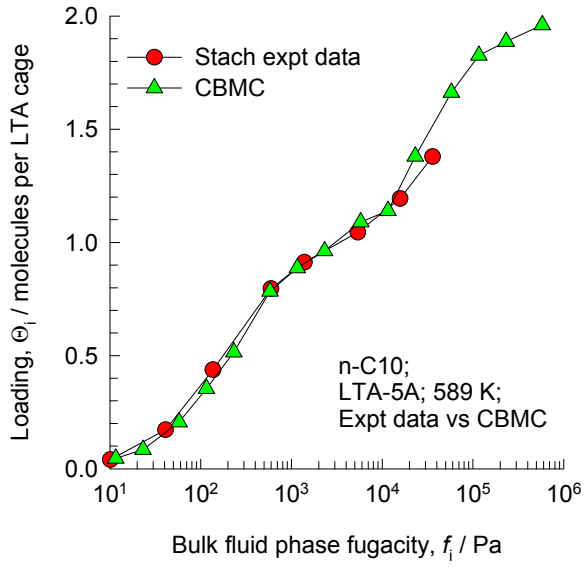

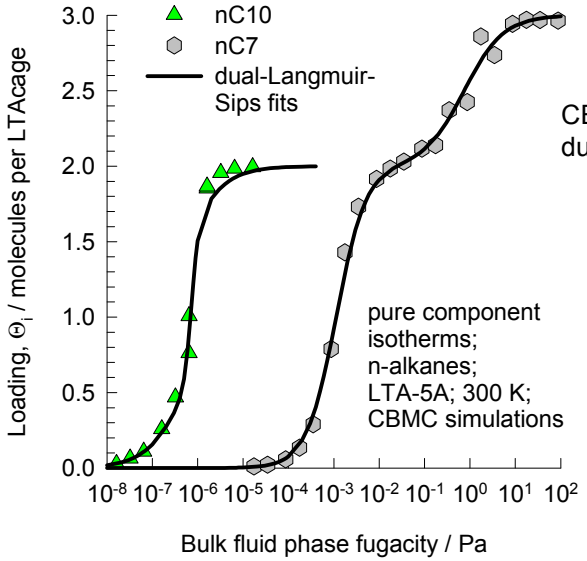

CBMC simulations of pure component isotherms along with dual-Langmuir-Sips fits

IAST predictions are compared with CBMC mixture simulations

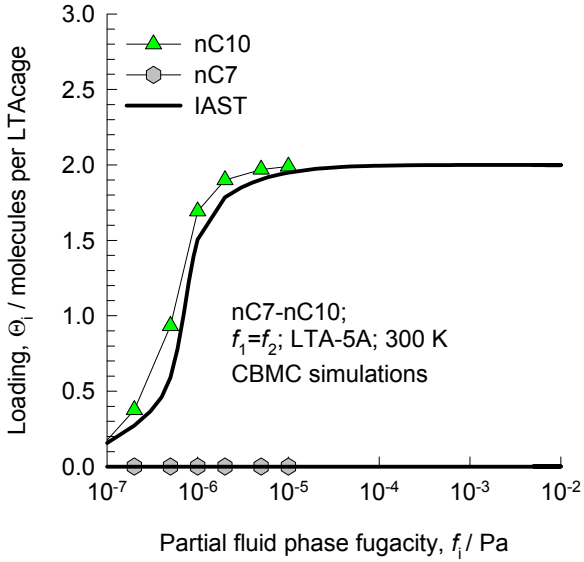

LTA-5A, 300 K, nC7-nC10 mixture

The IAST calculations are on the basis of pure component isotherms;

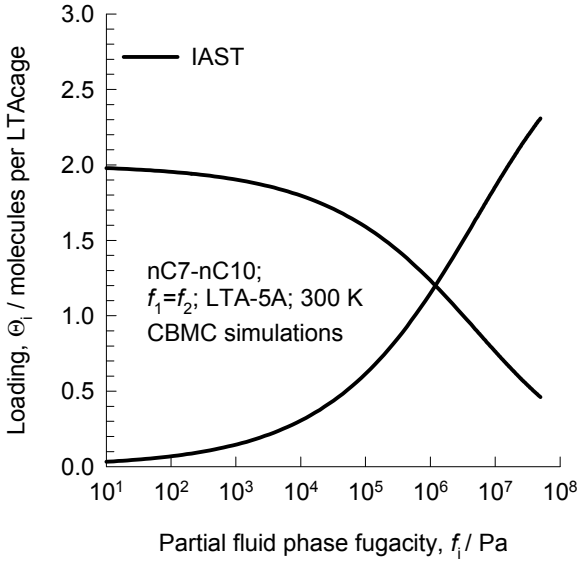

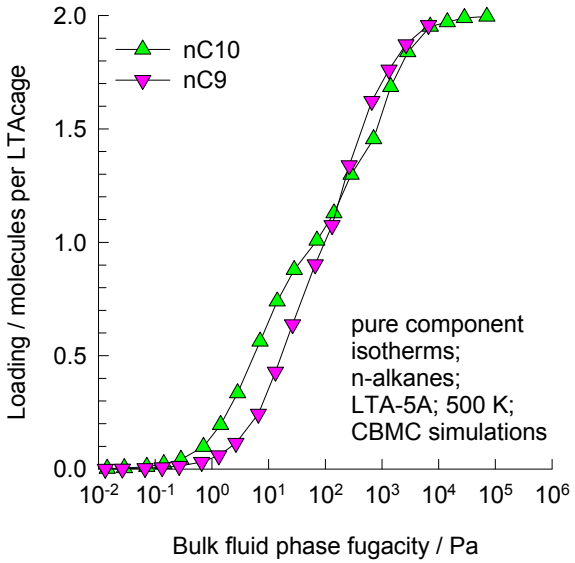

The IAST calculations are on the basis of pure component isotherms; these do not anticipate selectivity reversal

LTA-5A, 500 K, nC9-nC10 mixture

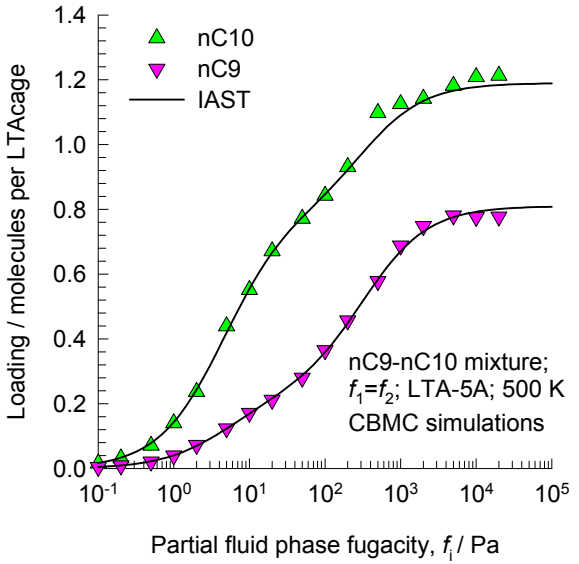

All-silica
TSC

TSC

To convert from molecules per unit cell to mol kg^{-1}, multiply by 0.0433.
The pore volume is 0.344 cm^3/g.

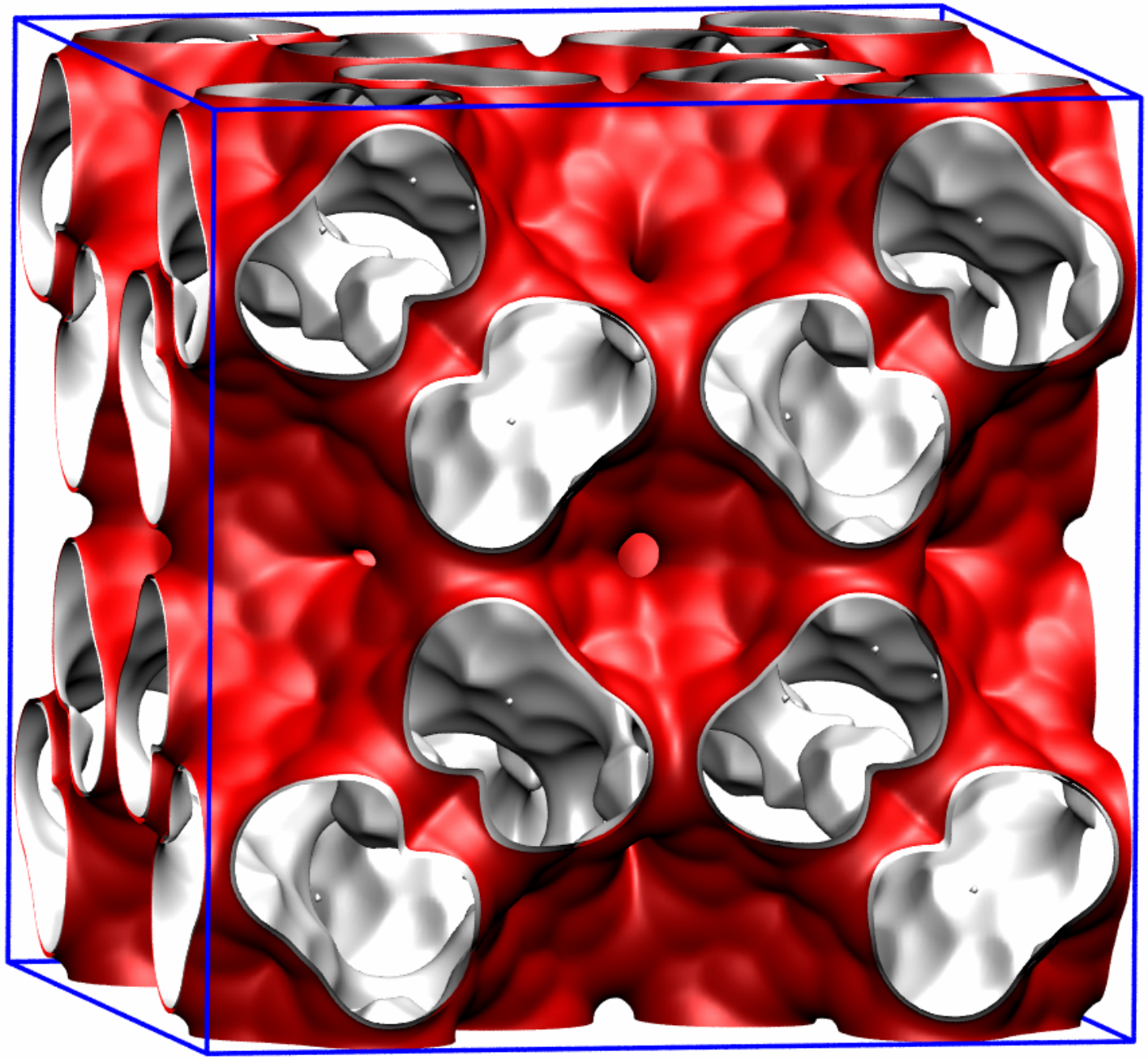

Unit cell of TSC

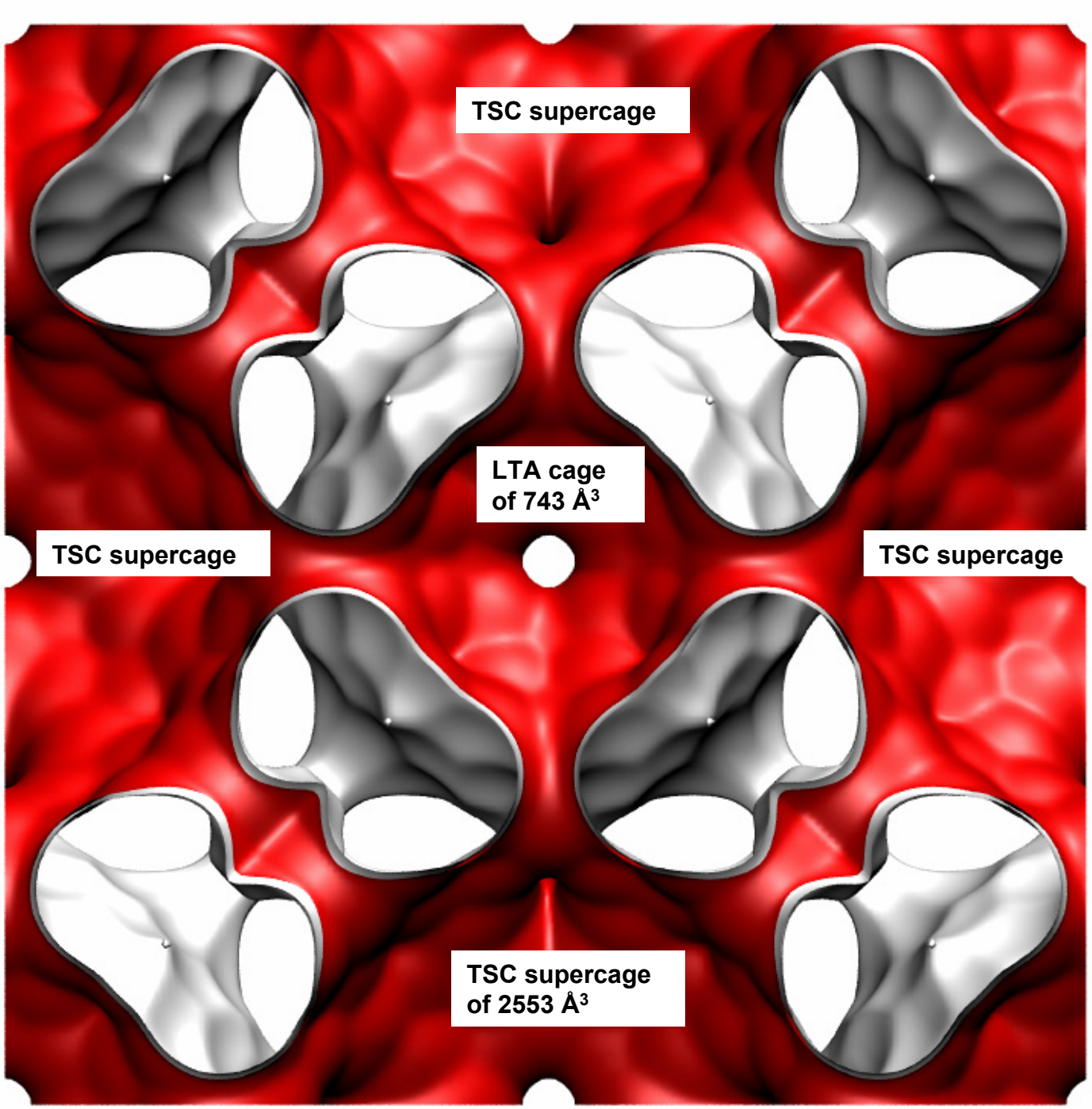

Front plane of unit cell of TSC

TSC window dimensions

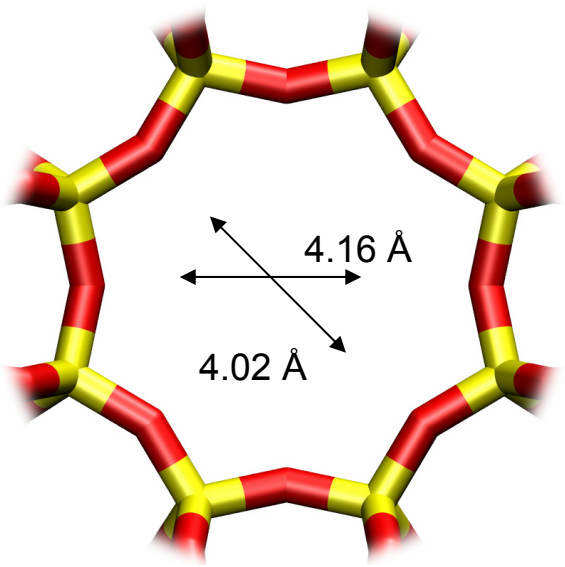

TSC
(supercage - cage)

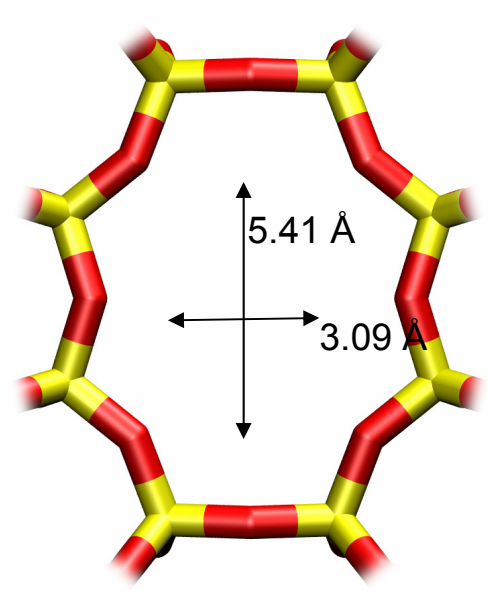

TSC
(supercage - pocket)

The window dimension calculated using the van der Waals diameter of framework atoms = 2.7 Å are indicated above by the arrows. It is likely that the pockets are inaccessible due to the narrow constriction of 3.09 Å.

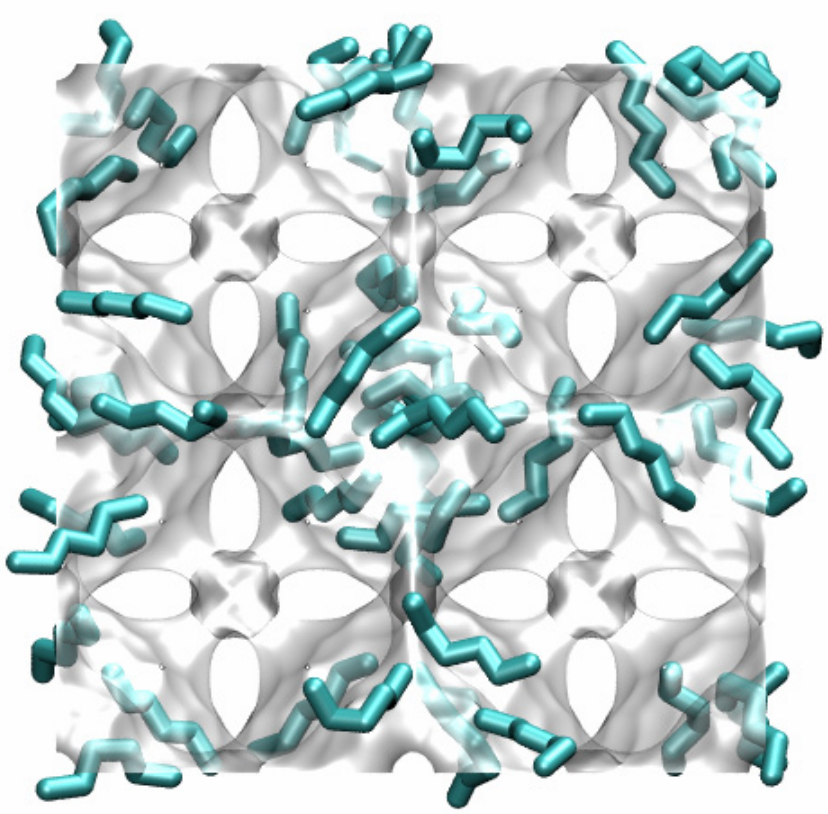

TSC, 300 K,
nC6, 20 kPa

TSC, 300 K,
nC6, 2000 kPa

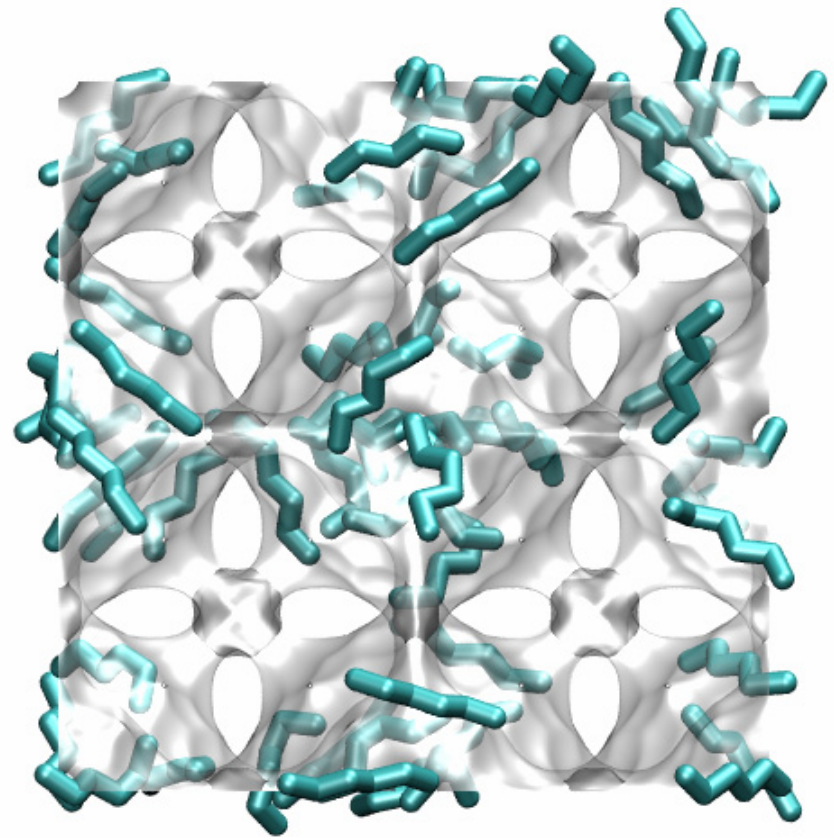

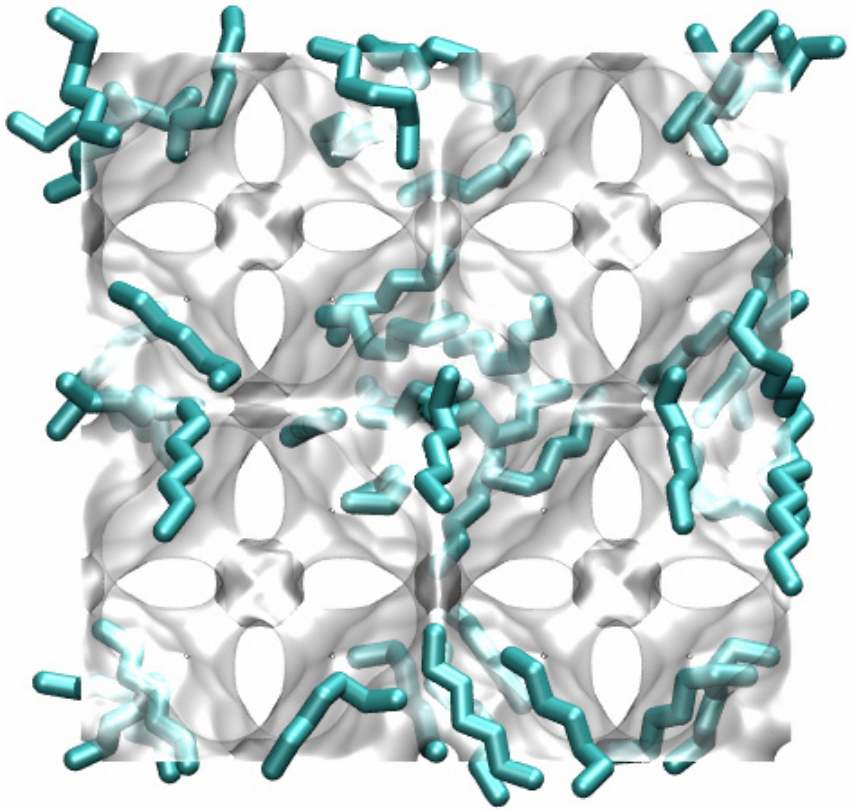

TSC, 300 K,
nC7, 100 kPa

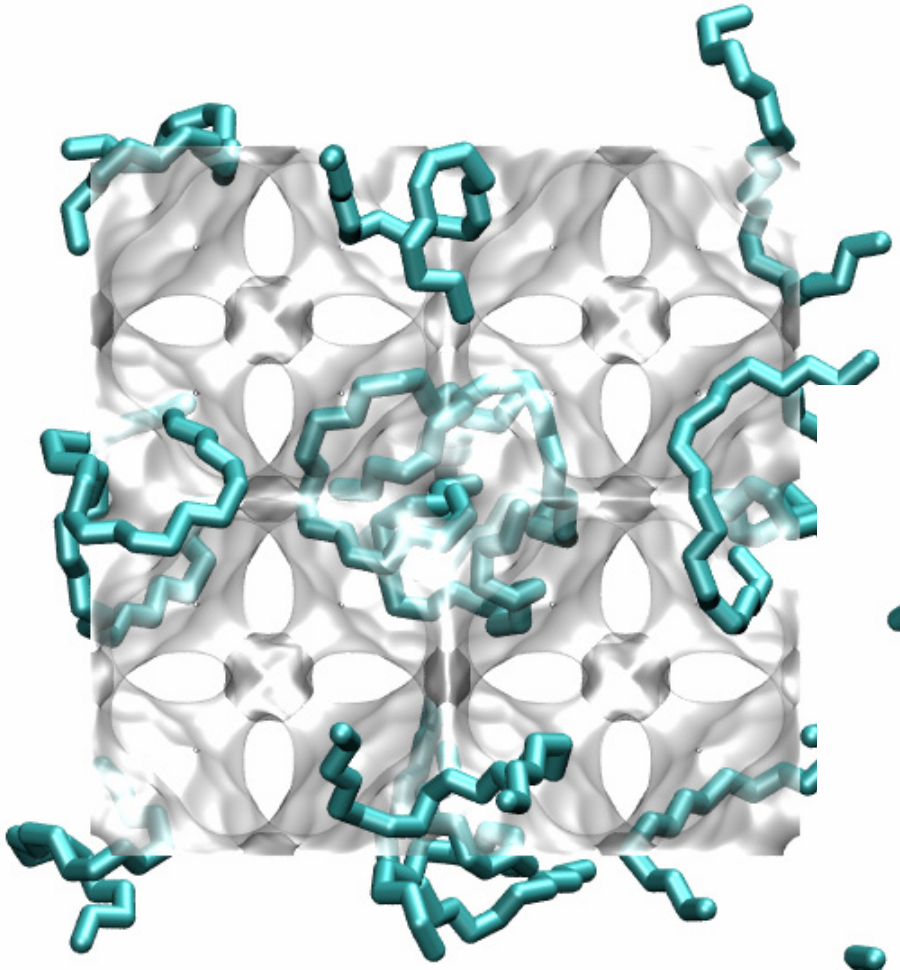

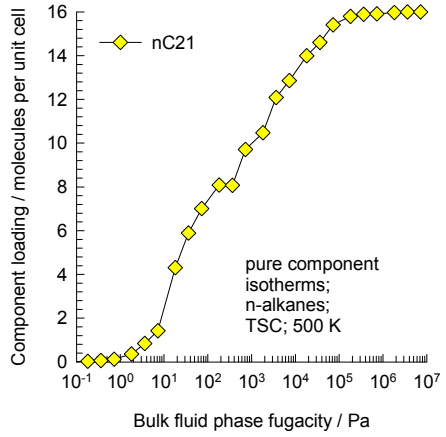

TSC, 500 K,
nC21. 2000 kPa

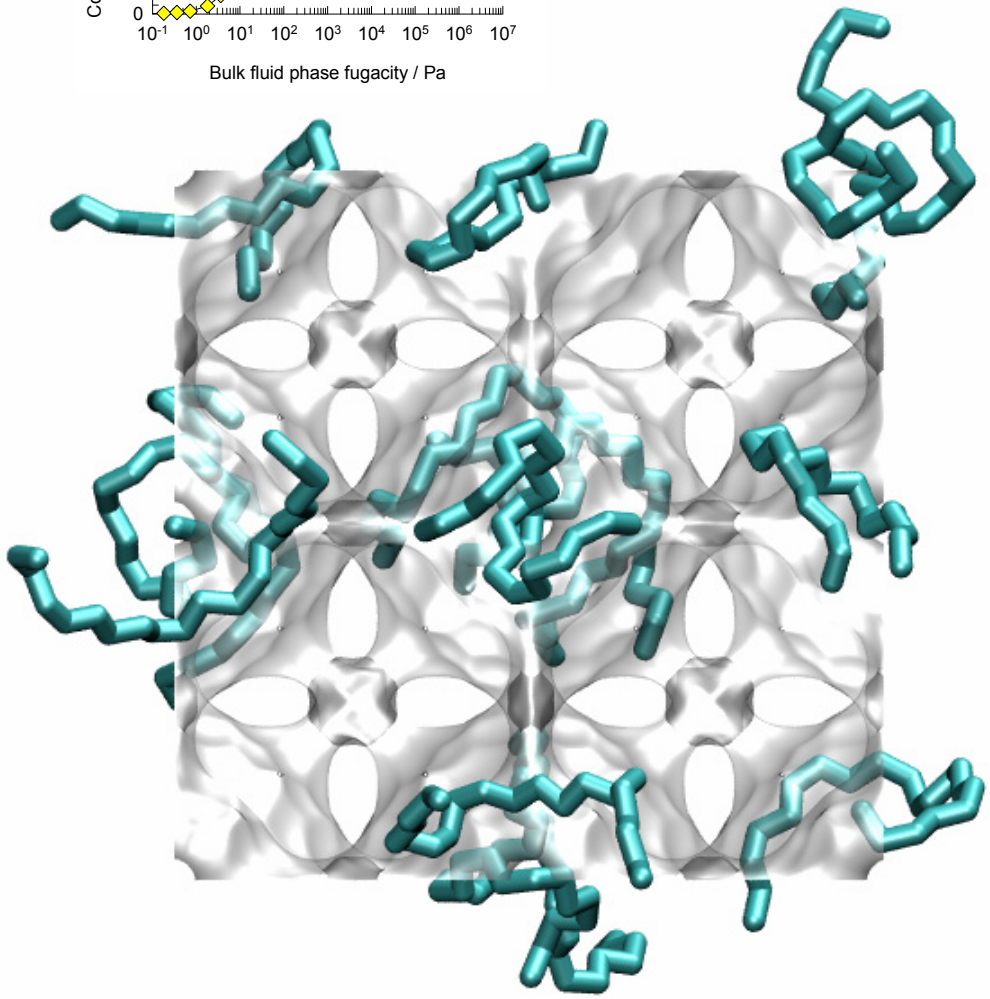

TSC, 500 K,
nC21, 500 kPa

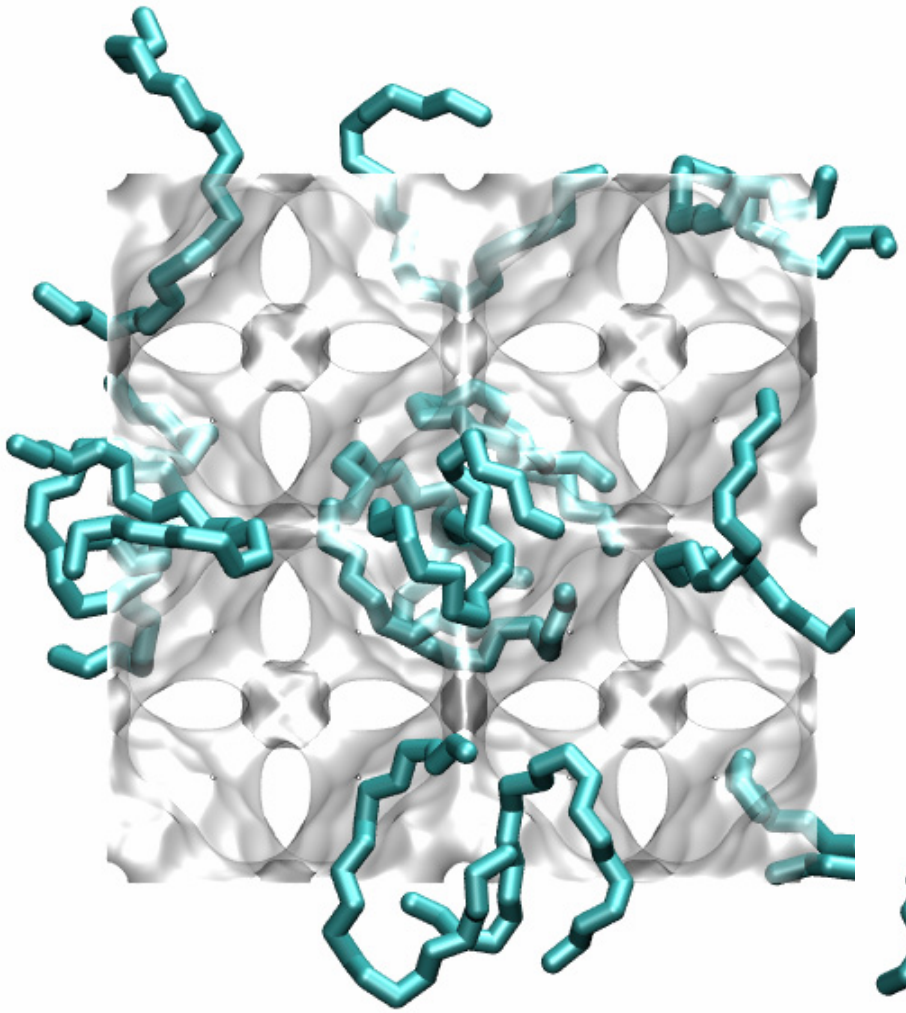

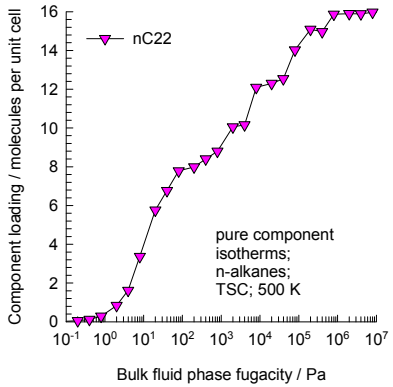

**TSC, 500 K,
nC22, 5000 kPa**

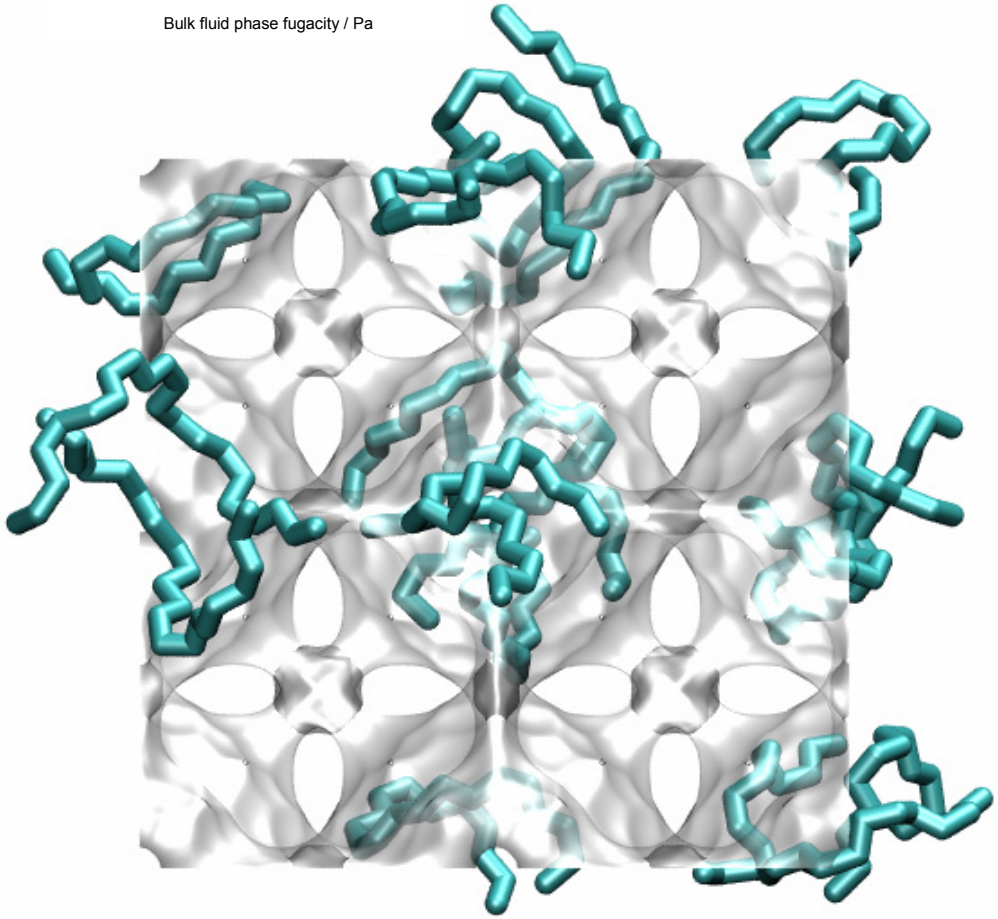

**TSC, 500 K,
nC22, 20 kPa**

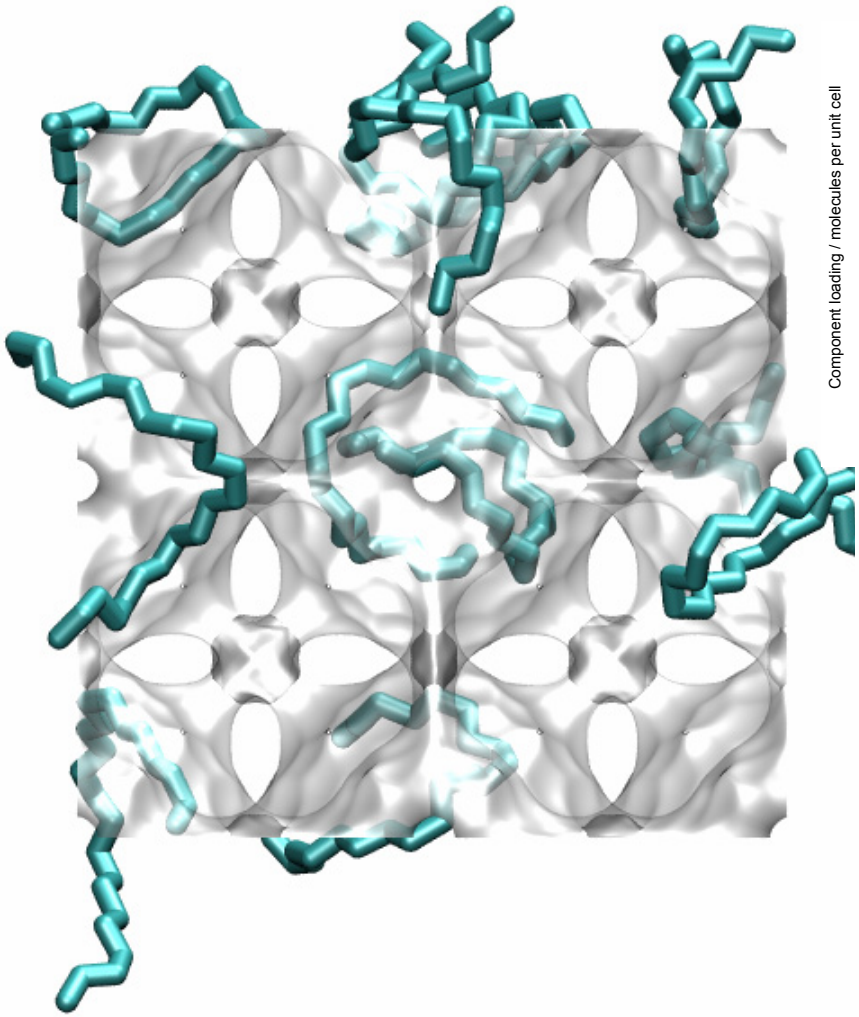

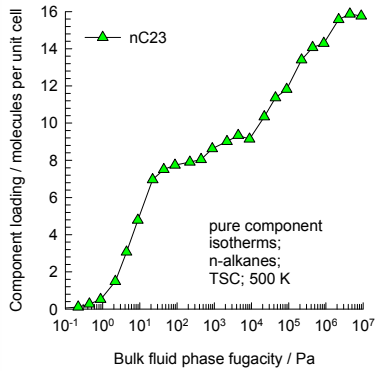

TSC, 500 K,
nC23, 10 kPa

TSC, 500 K,
nC23, 2000 kPa

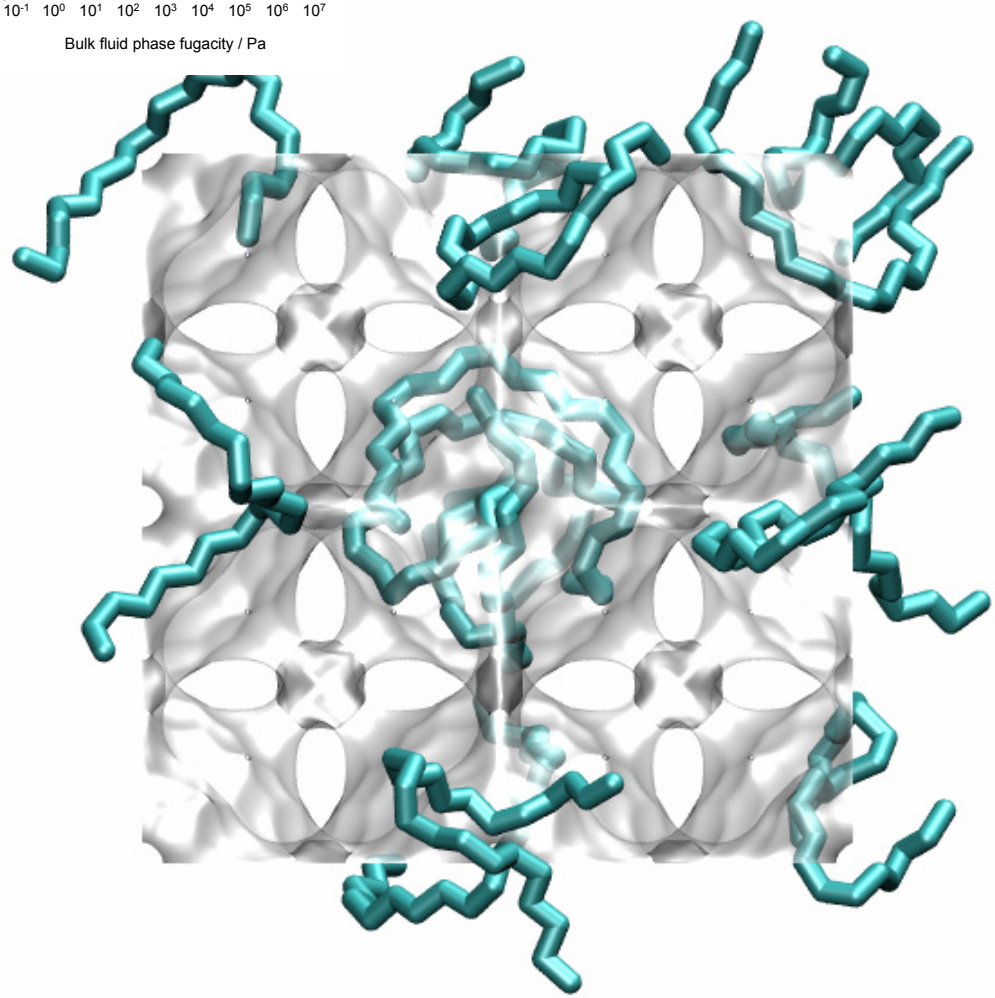

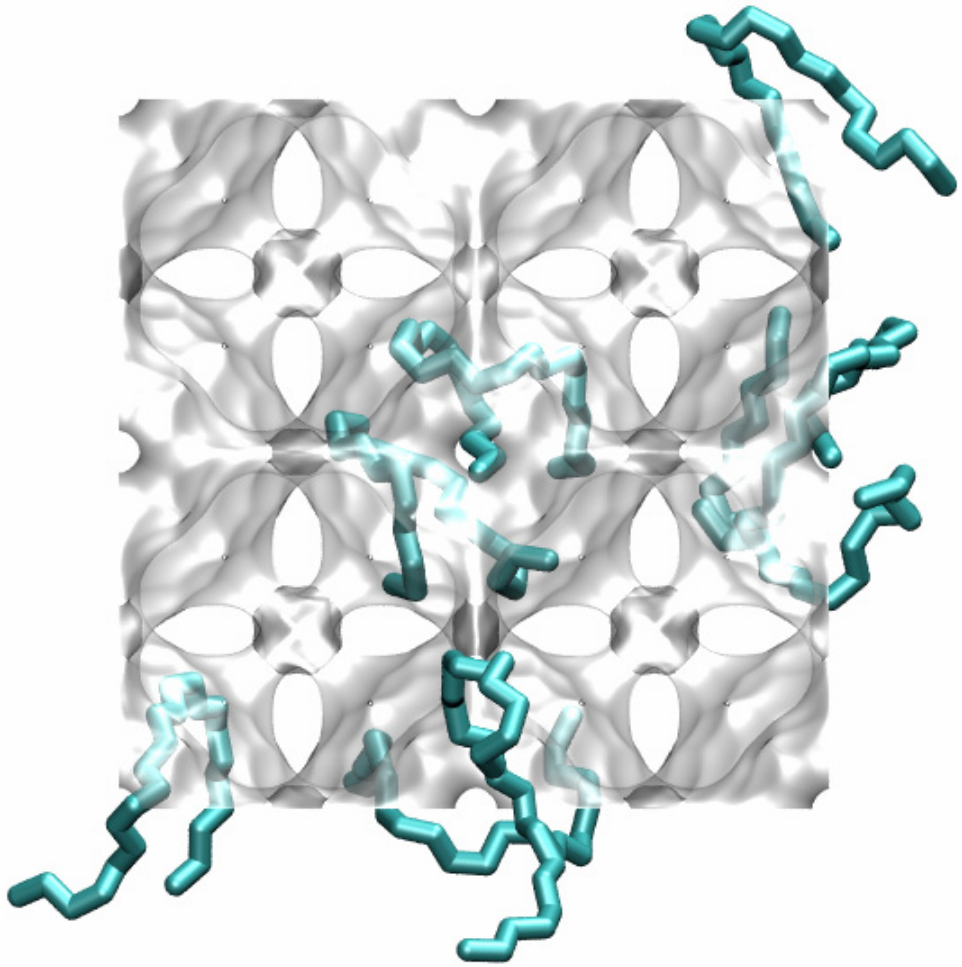

TSC, 500 K,
nC24, 5 kPa

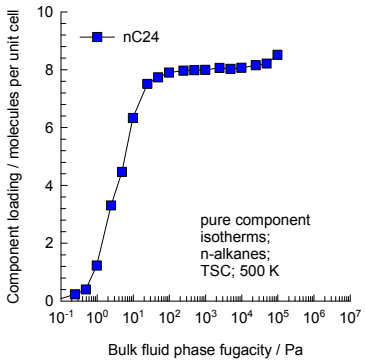

TSC, 500 K,
nC24, 20 kPa

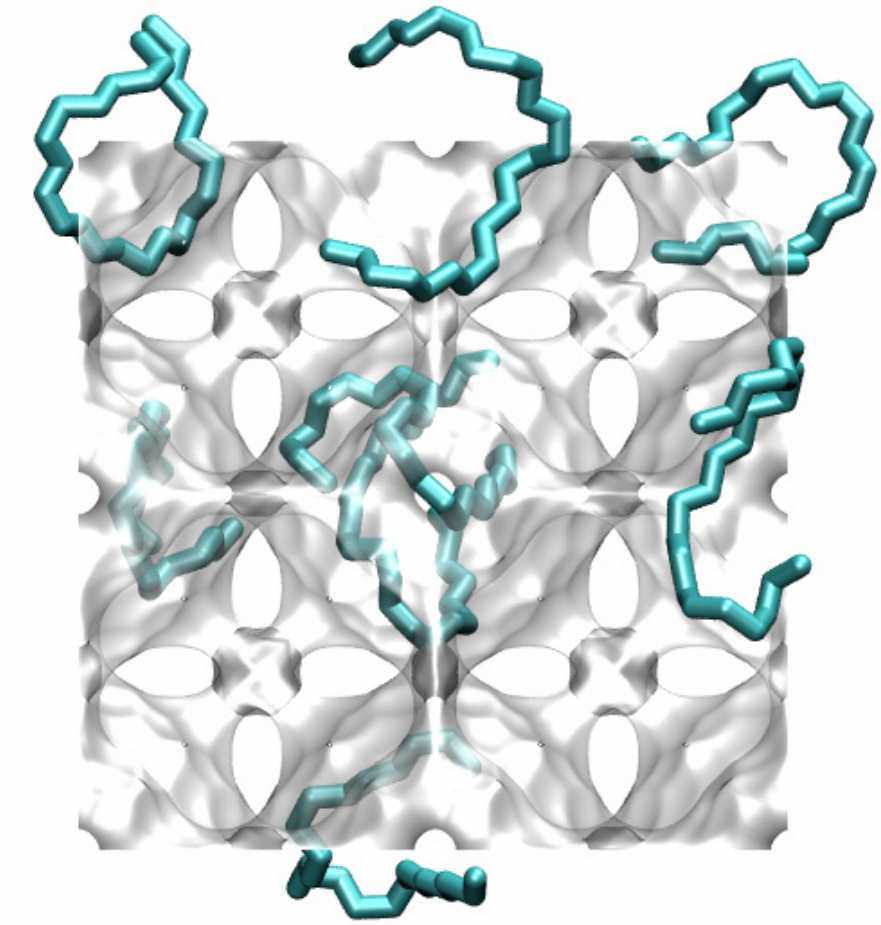

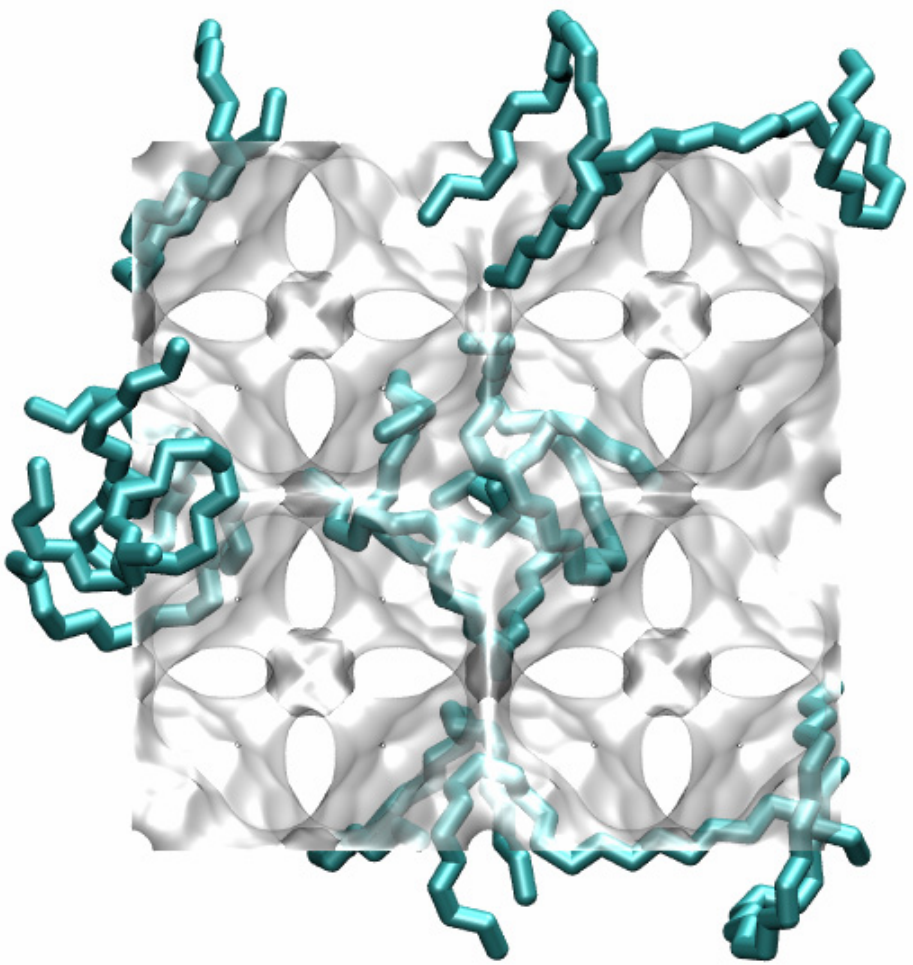

TSC, 300 K,
nC25, 5e-8 kPa

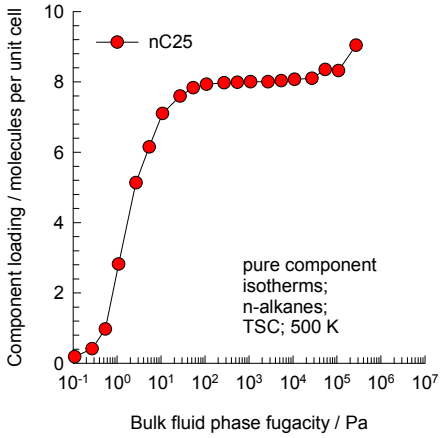

TSC, 500 K,
nC25, 10 kPa

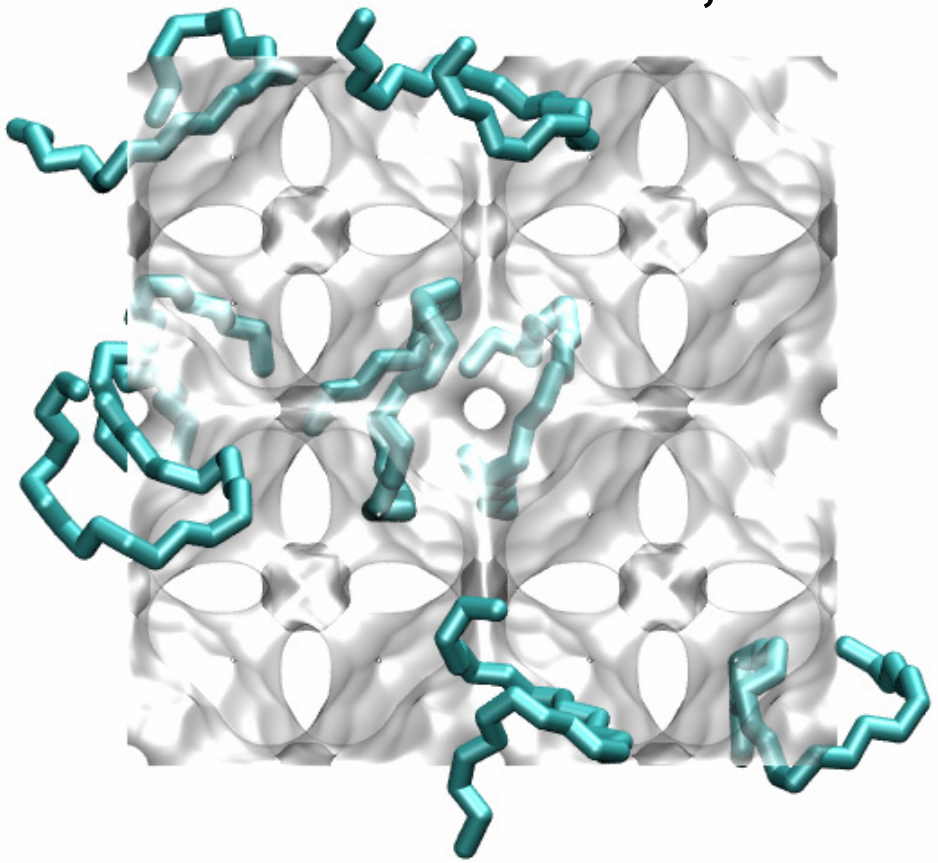

Pure n-alkanes, Henry coefficients in TSC

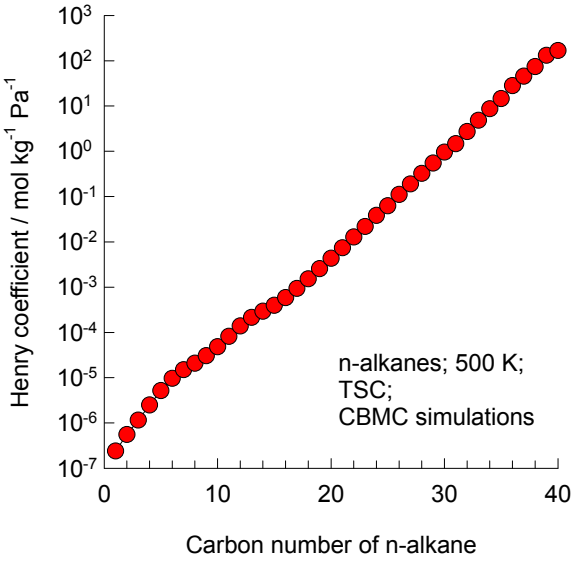

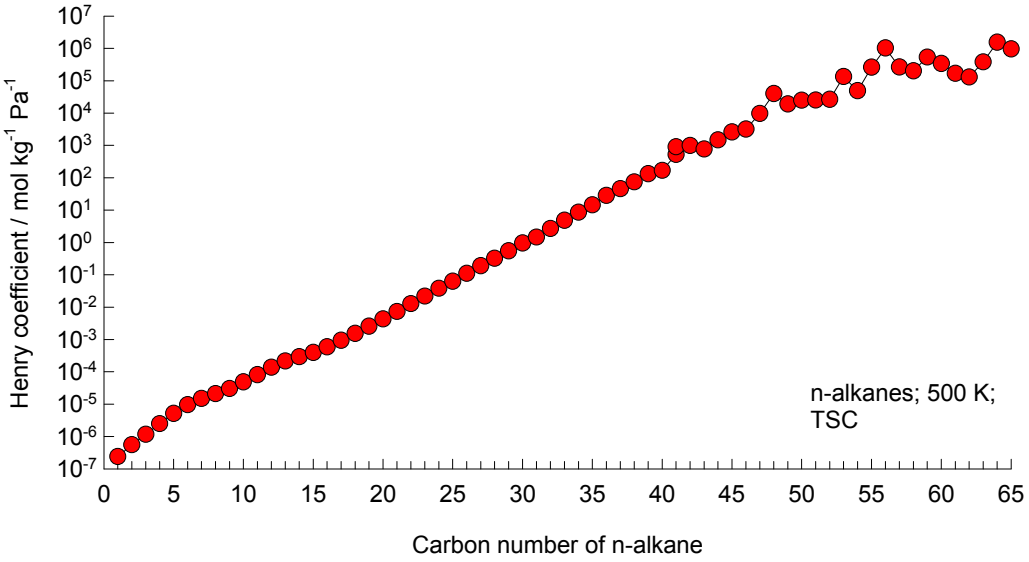

The data shown in Figure 6a of the manuscript only extends to 40 C atoms. The complete simulation data are presented here.

CBMC simulations of isotherms of pure n-alkanes in TSC

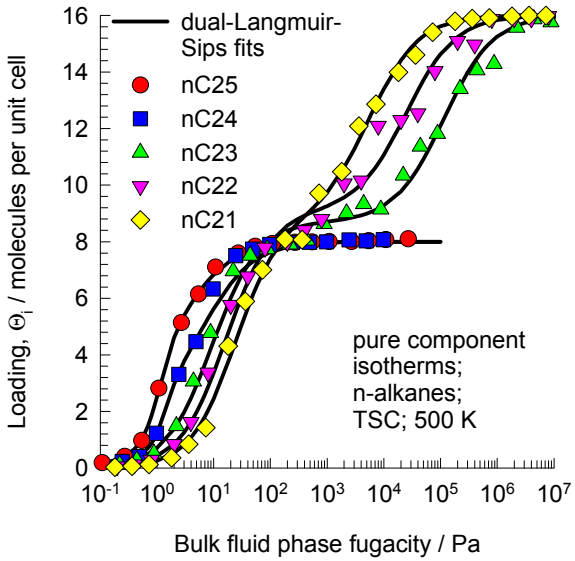

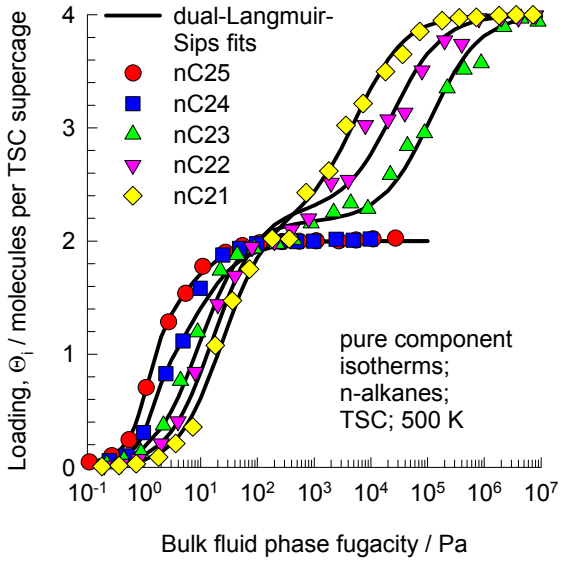

The loadings are expressed both in terms of molecules per unit cell, and molecules per TSC supercage

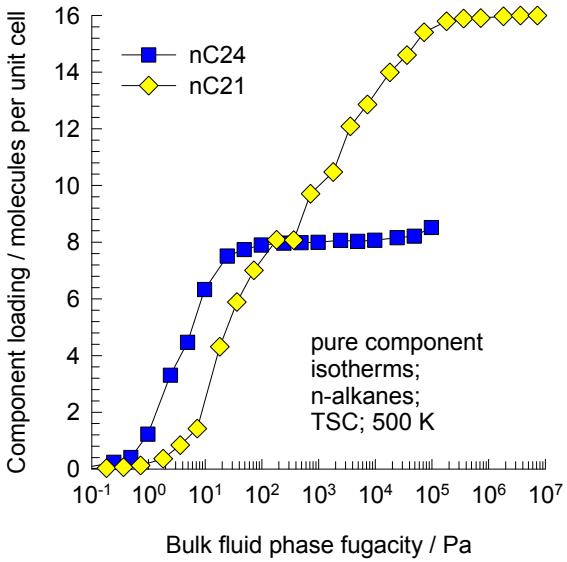

The IAST calculations are on the basis of pure component isotherms

The loadings are expressed both in terms of molecules per unit cell, and molecules per TSC supercage

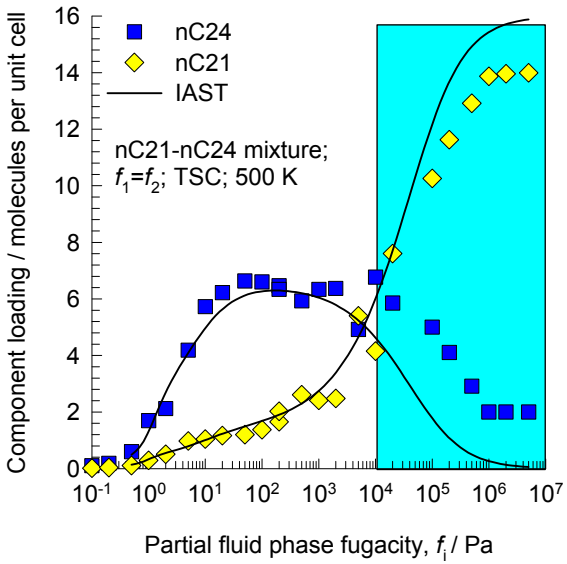

TSC, 500 K, nC21-nC24 mixture

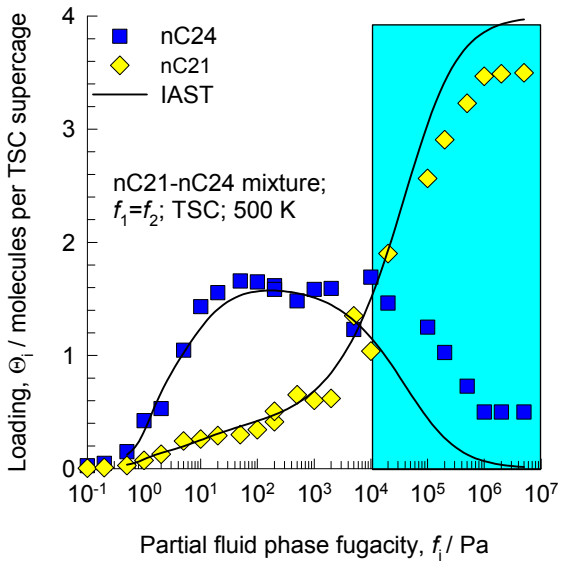

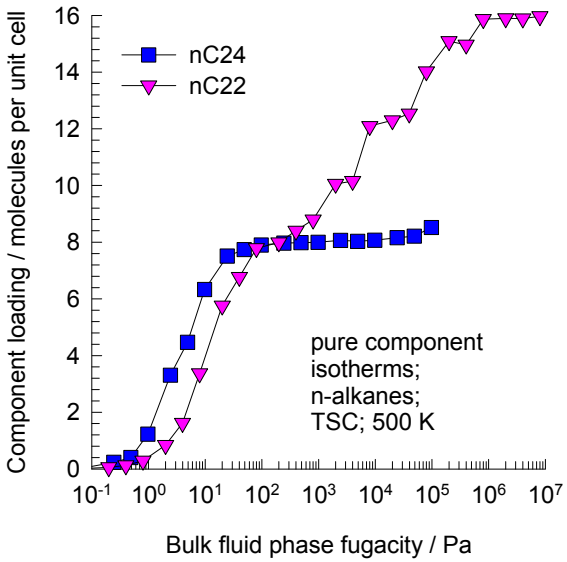

The IAST calculations are on the basis of pure component isotherms

The loadings are expressed both in terms of molecules per unit cell, and molecules per TSC supercage

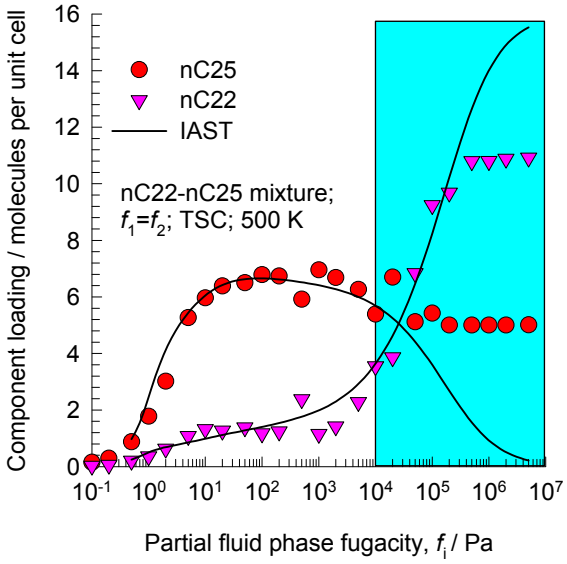

TSC, 500 K, nC22-nC25 mixture

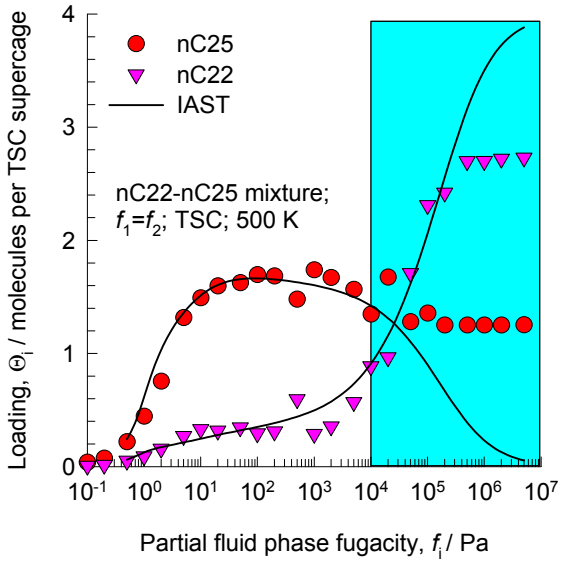

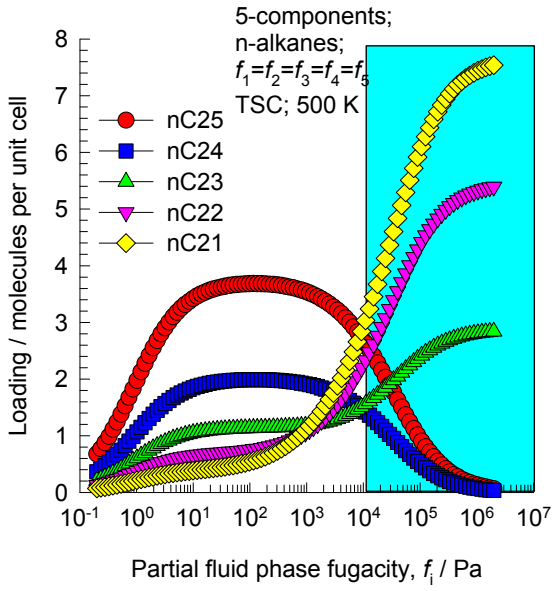

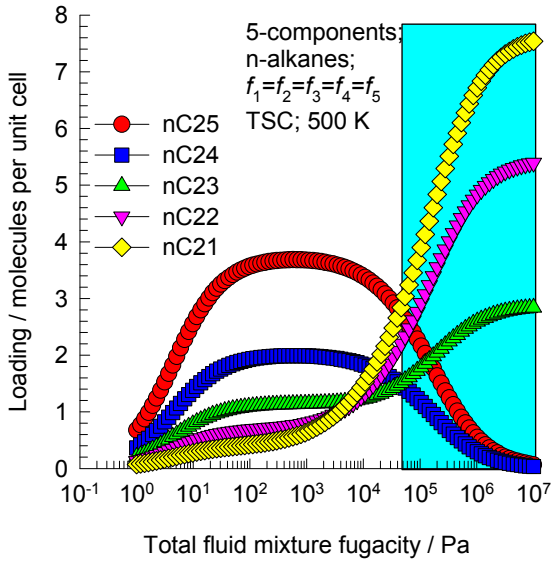

These are IAST predictions of loadings for 5-component mixture

All-silica
LTA-Si

LTA-Si

To convert from molecules per unit cell to mol kg^{-1}, multiply by 0.086683.
The pore volume is 0.310 cm^3/g.

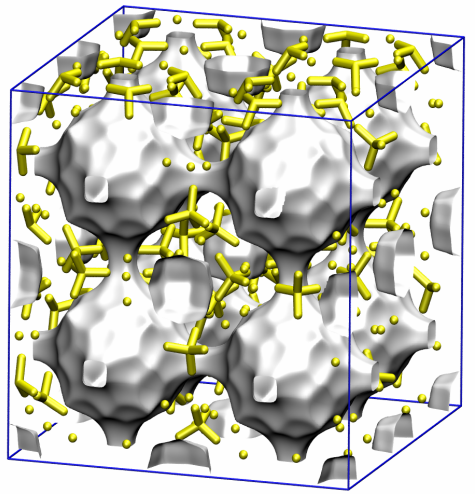

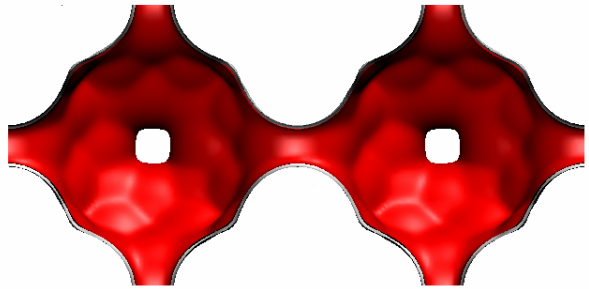

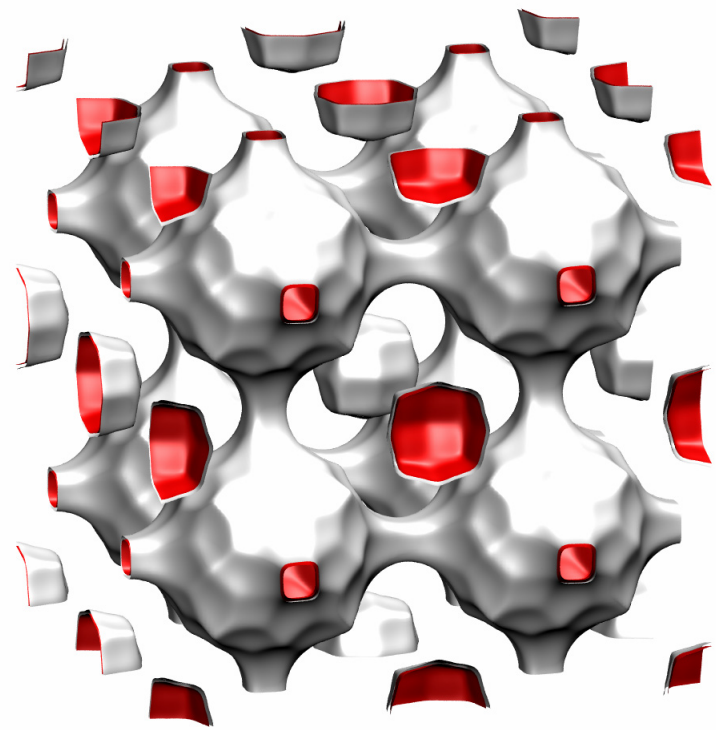

LTA-Si landscapes

If pockets are not blocked guest molecules occupy the inaccessible sodalite cages.
See Krishna, R.; van Baten, J. M. Langmuir 2010, 26, 2975-2978.

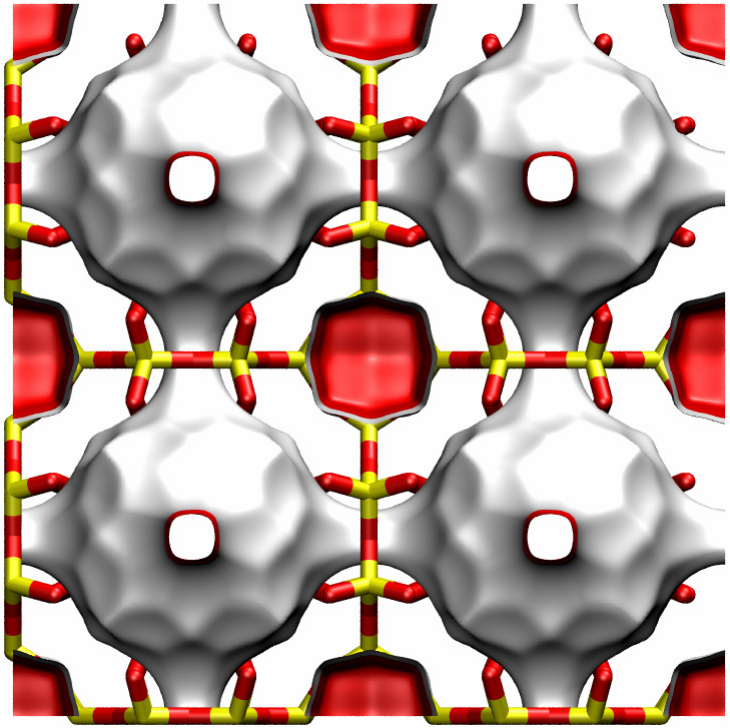

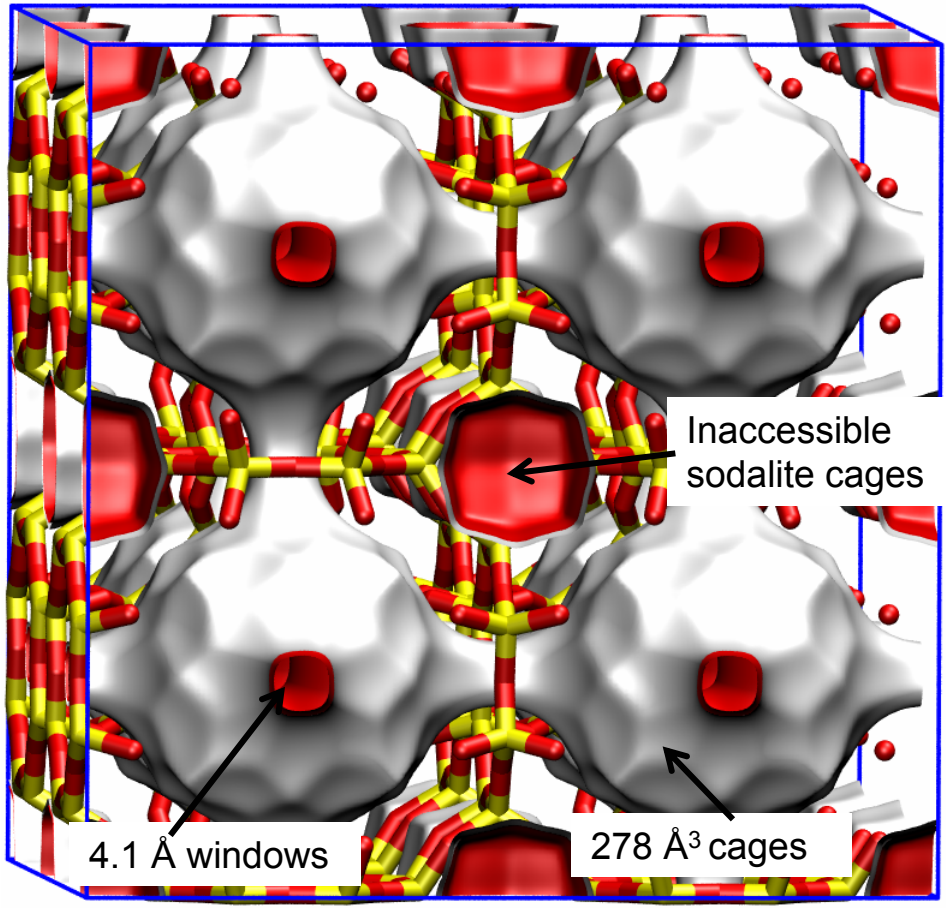

LTA-Si window dimensions

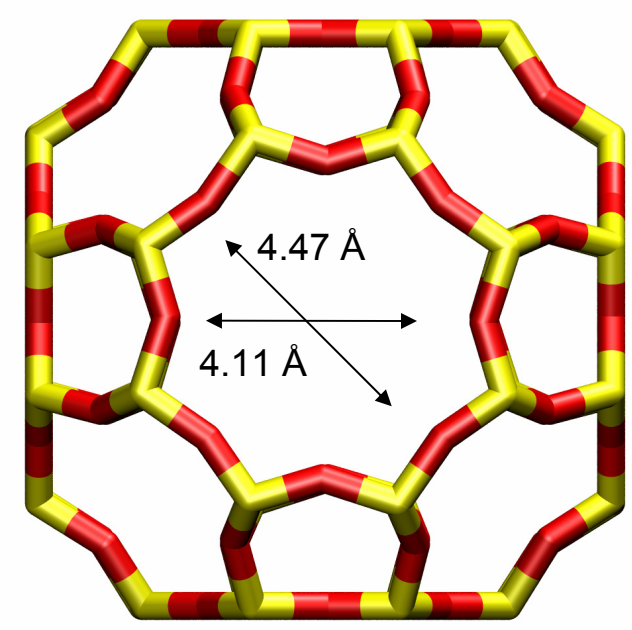

The window dimension calculated using the van der Waals diameter of framework atoms = 2.7 Å is indicated above by the arrows.

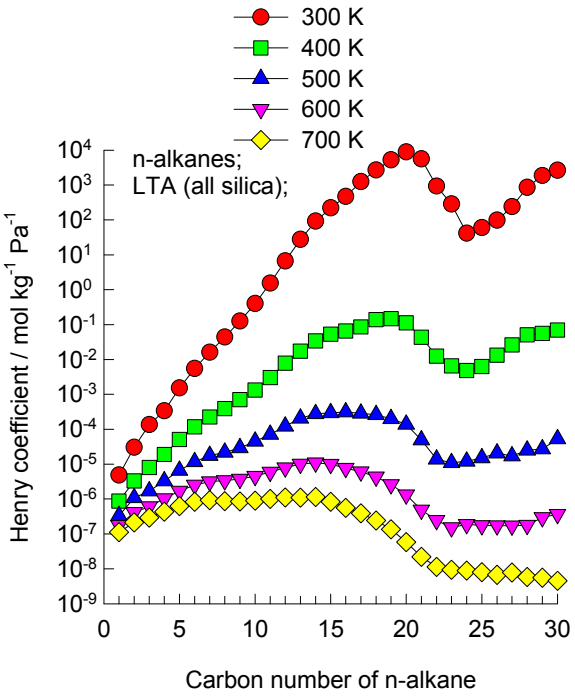

Henry coefficients for linear alkanes in LTA-Si

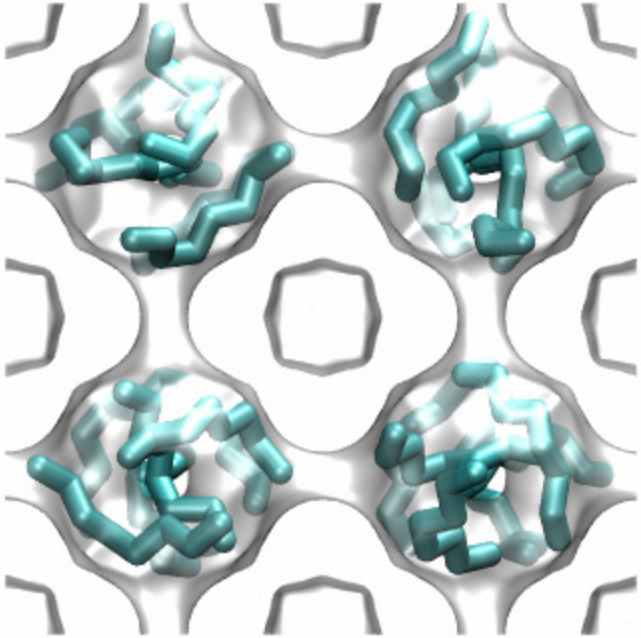

LTA (all-silica),
300 K, nC8, 100000 kPa

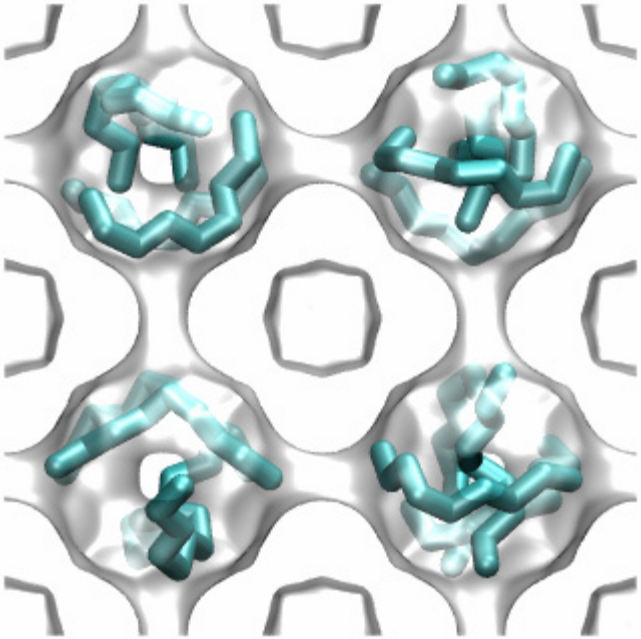

LTA (all-silica), 300 K, nC9, 5000 kPa

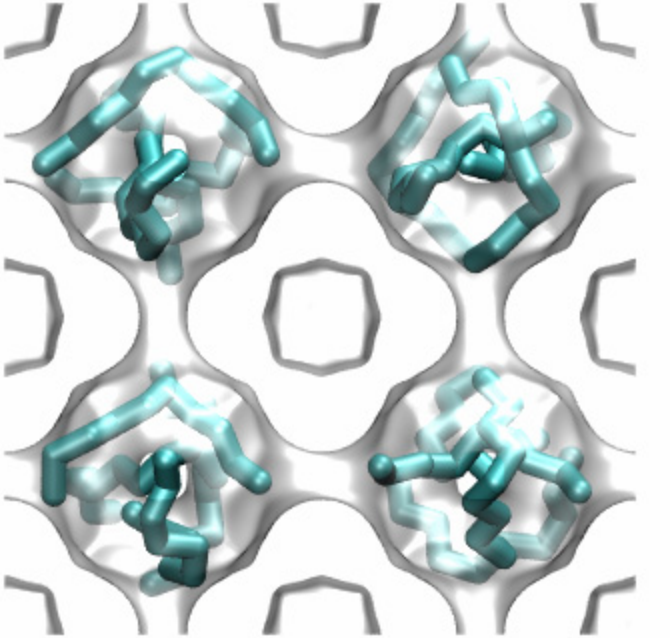

LTA (all-silica), 300 K, nC10, 10000 kPa

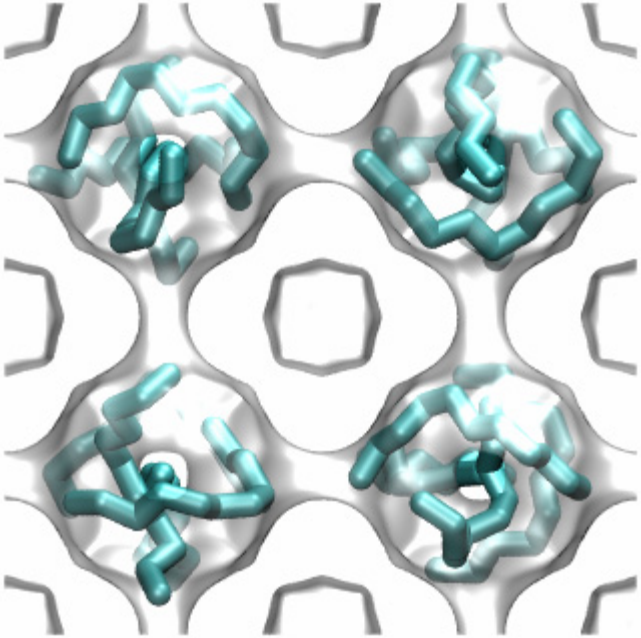

LTA (all-silica), 300 K, nC11, 10 kPa

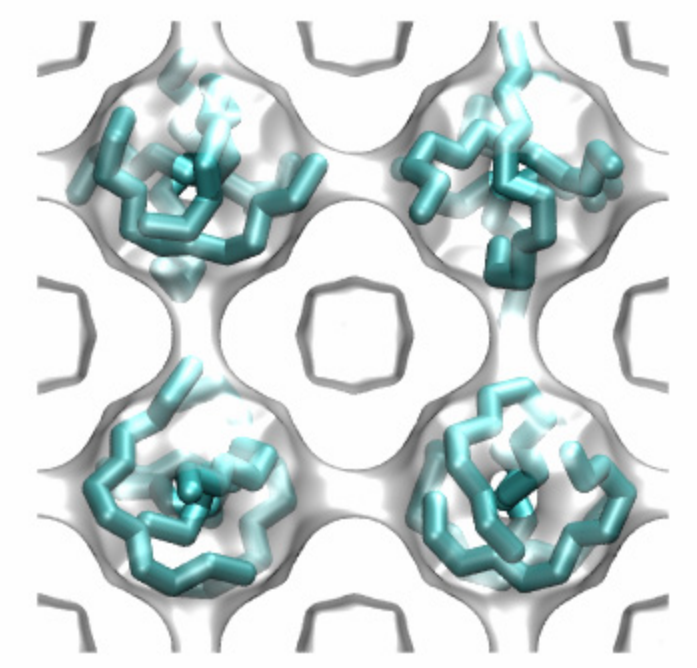

LTA (all-silica), 300 K, nC12, 10 kPa

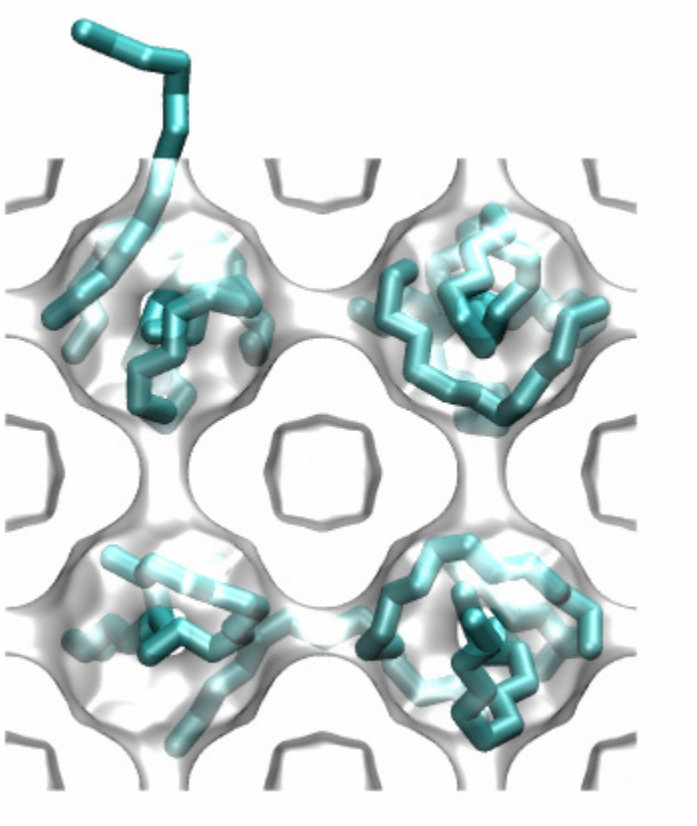

LTA (all-silica), 300 K, nC13, 10 kPa

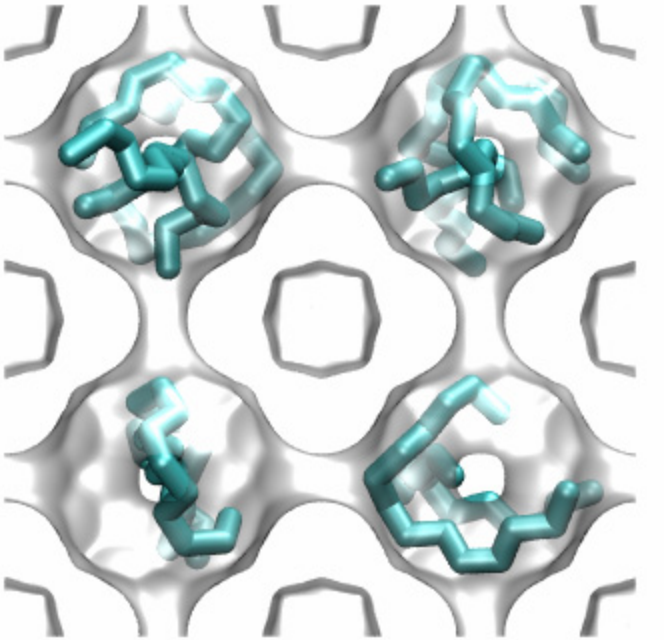

LTA (all-silica), 300 K, nC14, 0.1 kPa

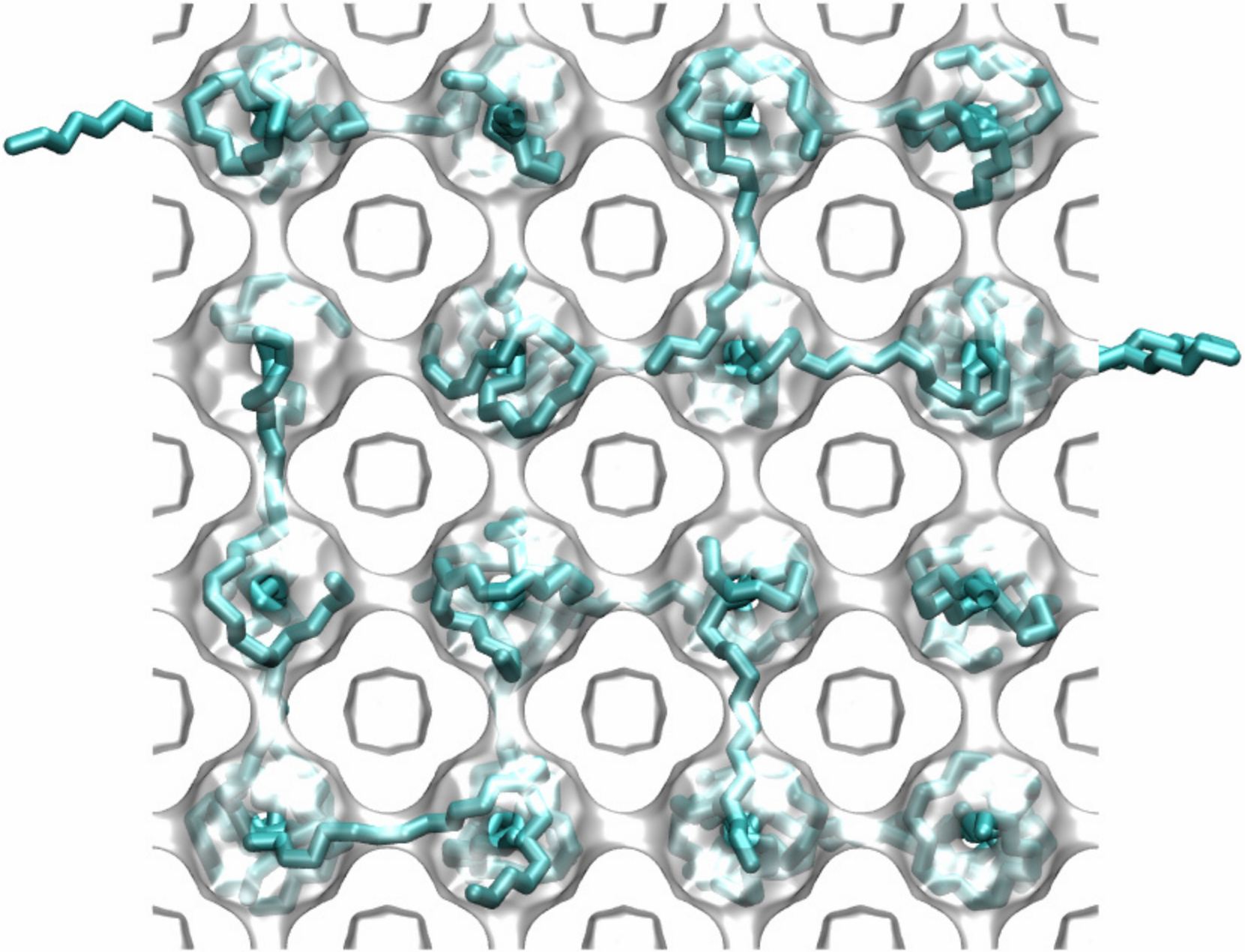

LTA(all-silica), 500 K, nC25, 100 kPa

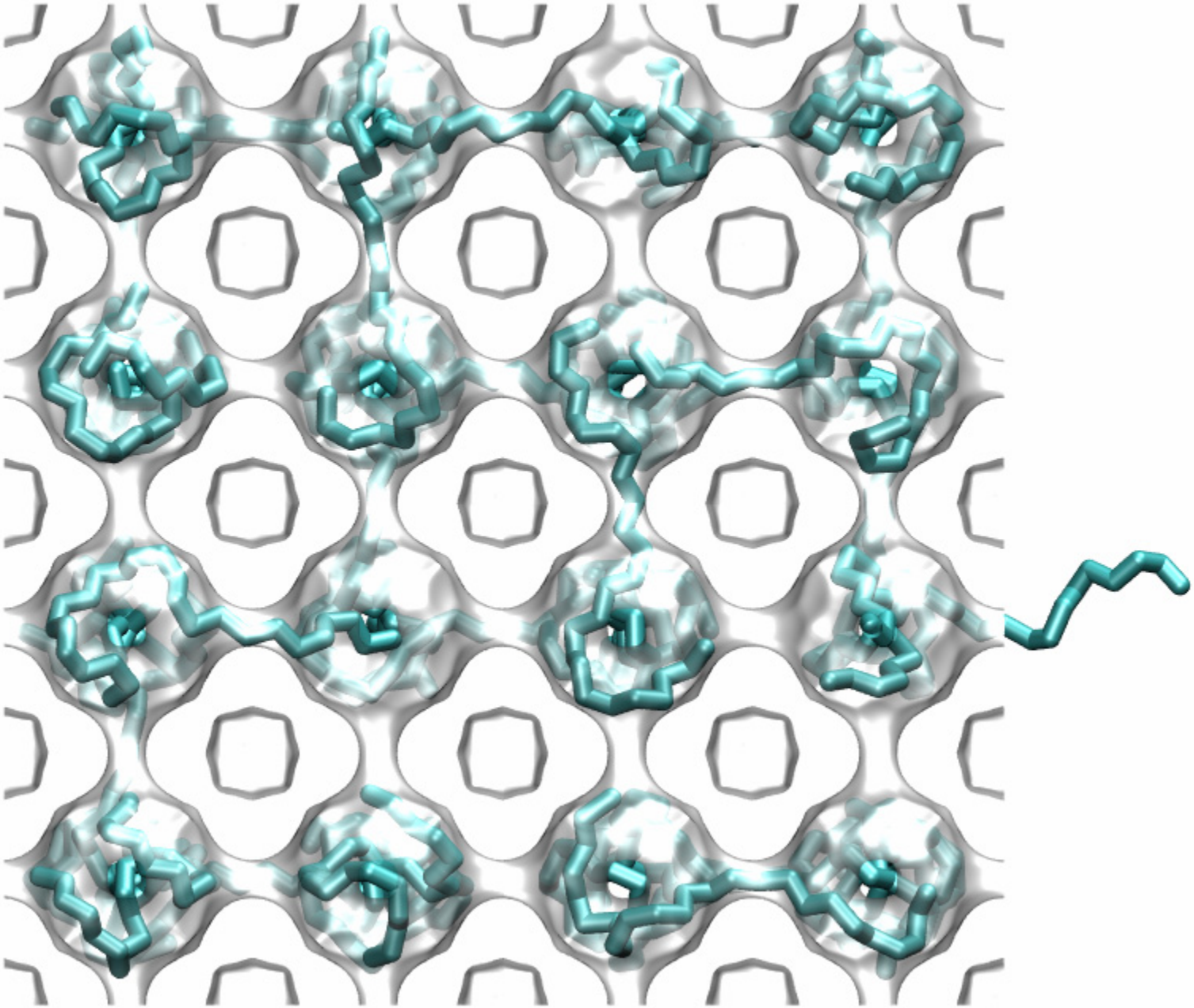

LTA(all-silica), 500 K, nC25, 20000 kPa

ERI

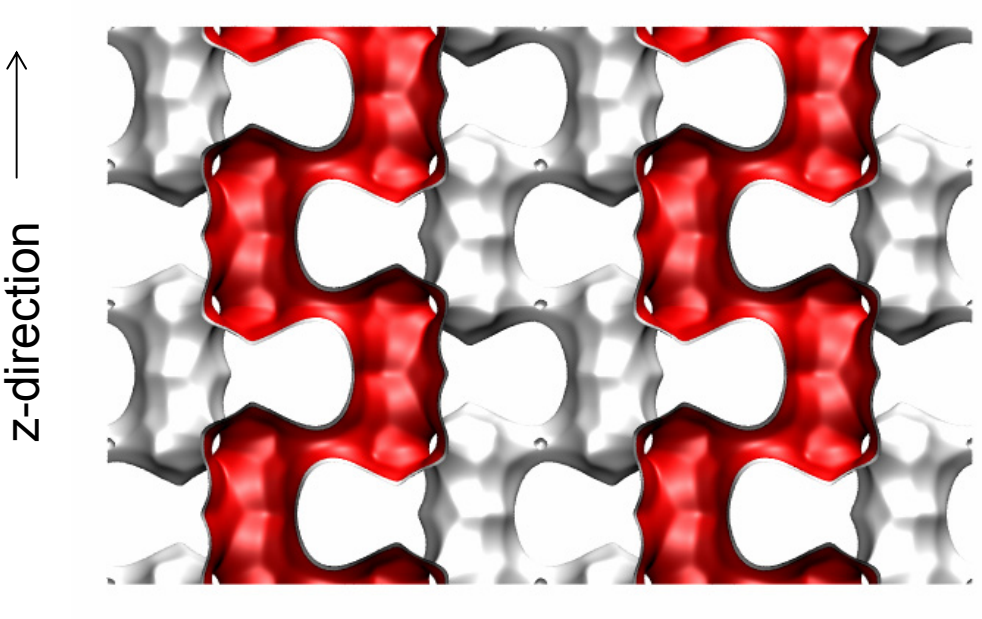

To convert from molecules per unit cell to mol kg^{-1}, multiply by 0.23115.
The pore volume is 0.2275 cm^3/g.

ERI window dimensions

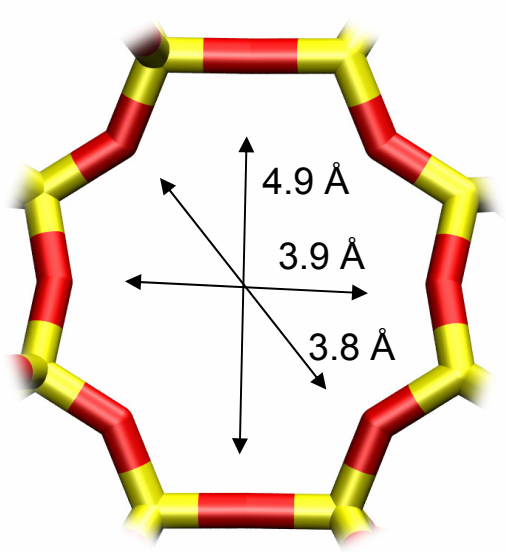

ERI

The window dimensions calculated using the van der Waals diameter of framework atoms = 2.7 Å are indicated above by arrows.

ERI CBMC simulations for pure component isotherms

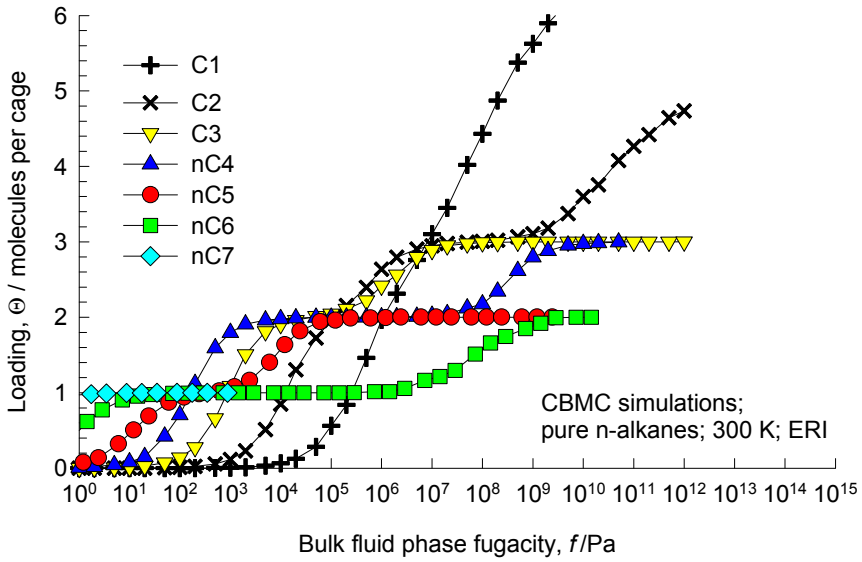

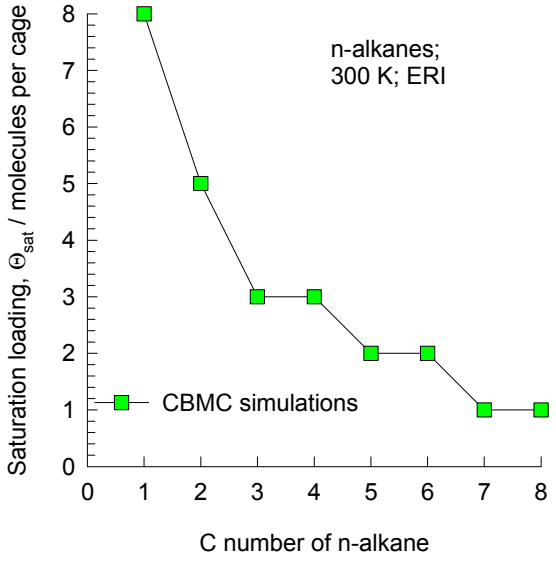

AFX pore landscape

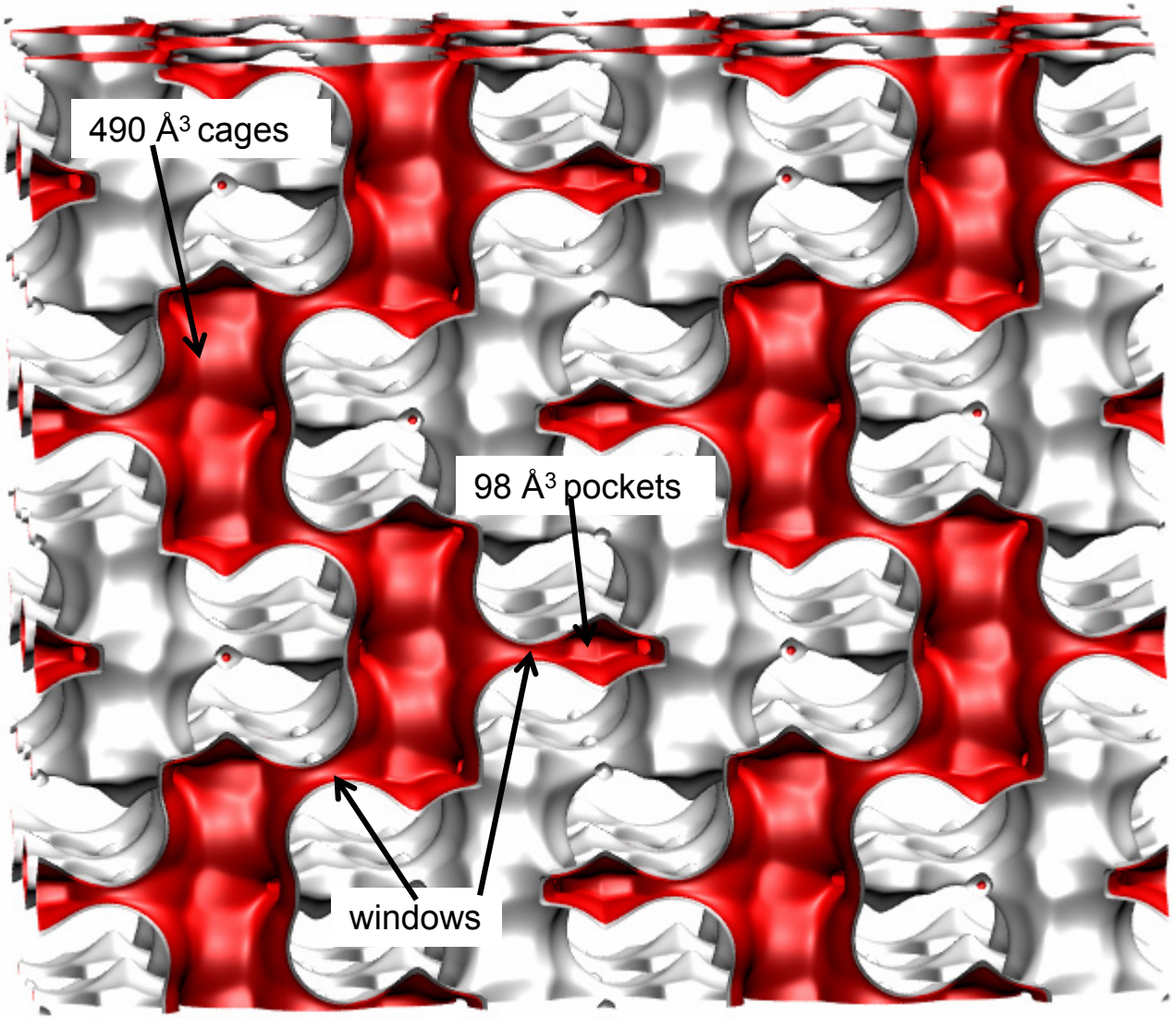

To convert from molecules per unit cell to mol kg^{-1}, multiply by 0.1734.
The pore volume is 0.2456 cm^3/g.

AFX window sizes

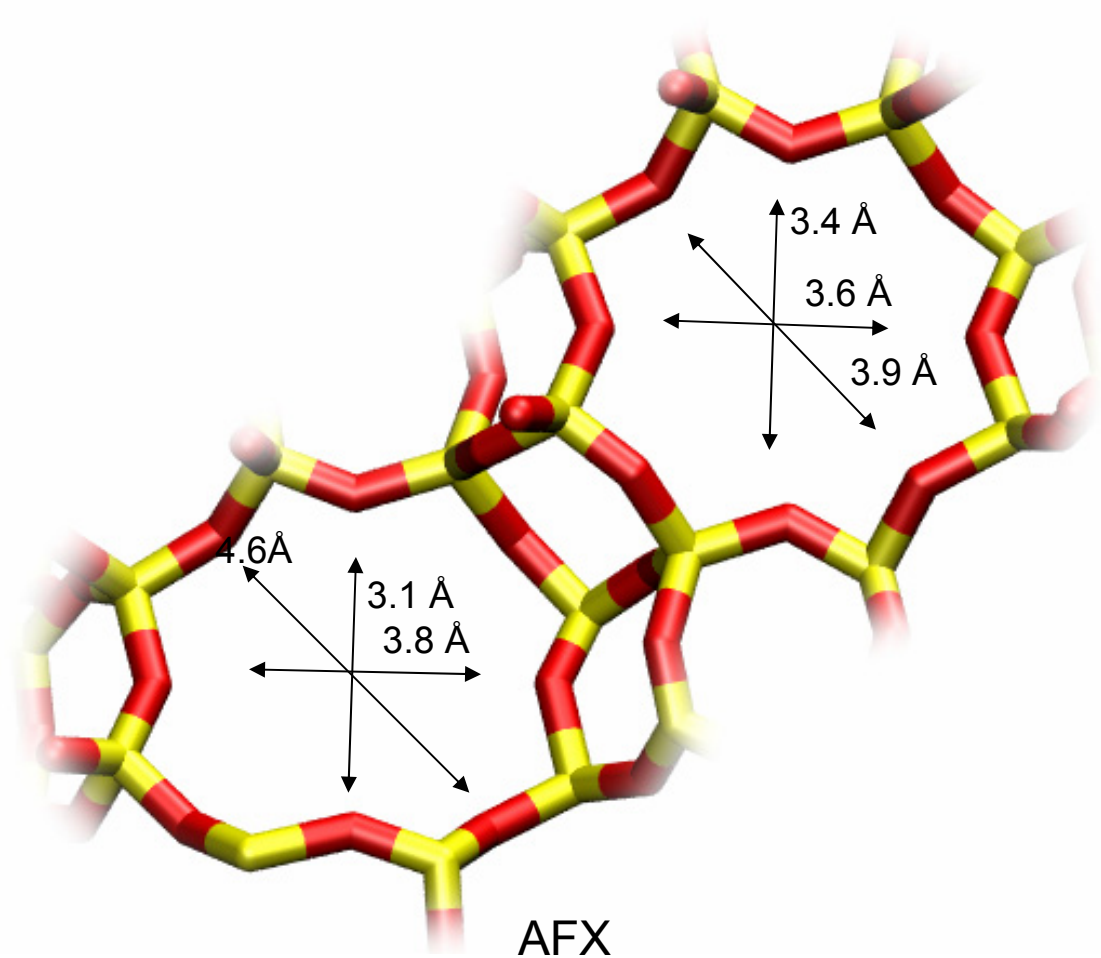

The window dimension calculated using the van der Waals diameter of framework atoms = 2.7 Å are indicated above by the arrows.

AFX CBMC simulations for pure component isotherms